Analytical and numerical results for some classes of nonlinear Schrödinger equations

by

Xiao Liu

A thesis submitted in conformity with the requirements
for the degree of Doctor of Philosophy
Graduate Department of Mathematics
University of Toronto

Abstract

Analytical and numerical results for some classes of nonlinear Schrödinger equations

Xiao Liu
Doctor of Philosophy
Graduate Department of Mathematics
University of Toronto
2013

This thesis is devoted to the study of nonlinear dispersive partial differential equations of Schrödinger type. The main questions we investigate are long-time behavior or occurrence of a finite time singularity, as well as stability properties of solitary wave solutions.

The derivative nonlinear Schrödinger (DNLS) equation is a nonlinear dispersive model that appears in the description of wave propagation in plasmas. The first part of this thesis concerns a DNLS equation with a generalized nonlinearity (gDNLS). We first investigate numerically the possible occurrence of singularities. We show that, in the L^2-supercritical regime, singularities can occur. We obtain a precise description of the local structure of the solution in terms of the blowup rate and asymptotic profile, in a form similar to that of the nonlinear Schrödinger equation (NLS) with supercritical power law nonlinearity. We also show that the gDNLS equation possesses a two-parameter family of solitary wave solutions and study their stability. We fully classify their orbital stability or orbital instability properties according to the strength of the nonlinearity and, in some instances, their velocity.

In linear quantum mechanical scattering theory, the phenomenon of resonant tunneling refers to the situation where incoming waves are fully transmitted through potential barriers at certain energies. In the second part of this thesis, we consider the one-dimensional cubic NLS equation with two classes of external potentials, namely the 'box' potential and a repulsive 2-delta potential. We demonstrate numerically that resonant

tunneling may occur in a nonlinear setting: Taking initial condition as a slightly perturbed, fast moving NLS soliton, we show that, under a certain resonant condition, the incoming soliton is almost fully transmitted. As the velocity of the incoming soliton increases, the transmitted mass of the soliton converges to the total mass.

Acknowledgements

I would like to express my sincere gratitude to my advisor, Professor Catherine Sulem, for her continuous support of my graduate study and research with her motivation, enthusiasm, patience and most of all, her immense knowledge and rich experience. Moreover, Catherine helped me a lot in writing papers, making slides and teaching in large classes. She also invited me to her concerts, which are very enjoyable and remarkable.

I am grateful to Walid Abou Salem and Gideon Simpson, who, as post-doc at the University of Toronto, taught me a tremendous amount of analytical and numerical skills, helped me improve programming techniques and suggested me lots of interesting topics to research.

I thank my thesis committee members, Adrian Nachman and Mary Pugh, for their help during my PhD study, as well as my external examiner, Dmitry Pelinovsky, all of them, provided insightful suggestions and remarks for my thesis. I would like to thank also Almut Burchard, Jim Colliander, Abe Igelfeld, Robert Jerrard, Robert Mccann, Joe Repka, and Israel Michael Sigal for their guidance and support.

I would like to thank the staff of the Department of Mathematics at the University of Toronto. Particularly Ida Bulat, our graduate administrator, without whom the life at the University of Toronto would never be easy and joyful.

I am also grateful to all my friends at the University of Toronto. I deeply cherish my experience in Toronto during the past six years.

I am hugely indebted to my parents, Daqing Liu and Ping Chen, and my girlfriend Zunwei Du for their endless love, concern and support.

Finally, I acknowledge that a refined version of Chapter 3 and 4 have been accepted for publication by Journal of Nonlinear Science, doi:10.1007/s00332-012-9161-2, and Discrete and Continuous Dynamical Systems. Series A, doi:10.3934/dcds.2011.29.1637, respectively.

Contents

Chapter 1

Introduction

1.1 Derivative Nonlinear Schrödinger Equation (DNLS)

In this thesis, we study the derivative nonlinear Schrödinger equation with a general power nonlinearity (gDNLS)

$$i\partial_t\psi + \partial_x^2\psi + i|\psi|^{2\sigma}\psi_x = 0, \quad x \in \mathbb{R}, \quad t \in \mathbb{R}, \tag{1.1.1}$$

where $\sigma > 0$. This equation can be seen as a generalization of

$$i\partial_t\psi + \partial_x^2\psi + i|\psi|^{2}\psi_x = 0, \quad x \in \mathbb{R}, \quad t \in \mathbb{R} \tag{1.1.2}$$

which is equivalent to the derivative nonlinear Schrödinger equation (DNLS)

$$i\partial_t u + \partial_x^2 u + i(|u|^2 u)_x = 0, \quad x \in \mathbb{R}, \quad t \in \mathbb{R}, \tag{1.1.3}$$

under the Gauge transformation

$$\psi(x) = u(x)\exp\left\{\frac{i}{2}\int_{-\infty}^{x}|u(\eta)|^2 d\eta\right\}.$$

Under a long wavelength approximation,the DNLS equation (1.1.3) is a model for Alfvén waves in plasma physics, [53, 54, 58, 62]. An Alfvén wave, named after Hannes Alfvén, is a type of magnetohydrodynamic wave. It is a low-frequency traveling oscillation of the ions and the magnetic field. We briefly present the derivation of the DNLS equation following references [11, 54], using the reductive perturbation method. When the plasma is quasineutral and consists of electrons and one kind of ions, waves propagating in the

x direction are described by equations in the form of

$$\frac{\partial \rho}{\partial t} + \frac{\partial}{\partial x}(\rho u_1) = 0, \tag{1.1.4a}$$

$$\frac{\partial u_1}{\partial t} + u_1 \frac{\partial u_1}{\partial x} = -\frac{1}{\rho}\frac{\partial}{\partial x}\left(\frac{\beta}{\gamma}\rho^\gamma + \frac{1}{2}|b|^2\right), \tag{1.1.4b}$$

$$\rho\left(\frac{\partial v}{\partial t} + u_1 \frac{\partial v}{\partial x}\right) = \frac{\partial b}{\partial x}, \tag{1.1.4c}$$

$$\frac{\partial b}{\partial t} + \frac{\partial}{\partial x}(u_1 b - v) = i\frac{1}{R}\frac{\partial}{\partial x}\left(\frac{1}{\rho}\frac{\partial b}{\partial x}\right), \tag{1.1.4d}$$

where ρ, (b_1, b_2, b_3) and (u_1, u_2, u_3) are the normalized mass density, magnetic field and fluid velocity, respectively. R, γ, β and the magnetic field along x-axis b_1 are constants. The transverse components of velocity and magnetic field are synthesized in the complex-valued quantities,

$$v = u_2 + iu_3, \quad b = b_2 + ib_3 \tag{1.1.5}$$

By introducing the following stretched space and time variables,

$$\xi = \epsilon(x - t), \quad \tau = \epsilon^2 t, \tag{1.1.6}$$

where $0 < \epsilon < 1$ is a small parameter, the functions have the power expansions in ϵ,

$$v = \epsilon^{1/2}(v^{(1)} + \epsilon v^{(2)} + \cdots),$$

$$b = \epsilon^{1/2}(b^{(1)} + \epsilon b^{(2)} + \cdots),$$

$$\rho = 1 + \epsilon\rho^{(1)} + \epsilon^2\rho^{(2)} + \cdots,$$

$$u_x = \epsilon u^{(1)} + \epsilon^2 u^{(2)} + \cdots.$$

Inserting (1.1.6) and (1.1.7) into (1.1.4), we obtain, at the order $O(\epsilon^{3/2})$,

$$b^{(1)} = -v^{(1)}, \tag{1.1.8}$$

at the order $O(\epsilon^2)$,

$$\rho^{(1)} = u^{(1)} = \frac{|b^{(1)}|^2}{2(1-\beta)},$$

and at the order $O(\epsilon^{5/2})$, one find the DNLS equation (1.1.3) using (1.1.4c), (1.1.4d) and (1.1.8), where $b^{(1)}, \xi$ and τ are replaced by u, x and t, respectively.

As we mentioned earlier, there are several equivalent forms for the DNLS equation (1.1.3). Let u be the solution of (1.1.3). Multiplying (1.1.3) by $\bar{u}$ and taking the real part, we obtain

$$\partial_t |u|^2 + \partial_x \left\{ 2\Im(\bar{u}u_x) + \frac{3}{2}|u|^4 \right\} = 0. \tag{1.1.9}$$

Using a Gauge transformation,

$$\psi = u(x) \exp\left\{ i\nu \int_{-\infty}^{x} |u(\eta)|^2 d\eta \right\}, \quad \nu \in \mathbb{R}, \tag{1.1.10}$$

and (1.1.9), DNLS equation (1.1.3) takes the form

$$i\partial_t \psi + \psi_{xx} + 2i(1-\nu)|\psi|^2\psi_x + i(1-2\nu)\psi^2\bar{\psi}_x + \nu(\nu - \frac{1}{2})|\psi|^4\psi = 0. \tag{1.1.11}$$

When $\nu = \frac{1}{2}$, (1.1.11) simplifies to (1.1.2). Equation (1.1.2) and some of its generalizations, also appear in the modeling of ultrashort optical pulses [5, 55]. There is a Hamiltonian form for (1.1.2)

$$\partial_t \psi = -2i \frac{\delta E}{\delta \bar{\psi}} \tag{1.1.12}$$

with the Hamiltonian

$$E = \frac{1}{2}\int_{-\infty}^{\infty} |\psi_x|^2 dx + \frac{1}{4}\Im \int_{-\infty}^{\infty} |\psi|^2 \bar{\psi}\psi_x dx. \tag{1.1.13}$$

Equation (1.1.2) also has the mass and momentum invariants:

$$M = \frac{1}{2}\int_{-\infty}^{\infty} |\psi|^2 dx, \tag{1.1.14}$$

$$P = \frac{1}{2}\Im \int_{\infty}^{\infty} \psi\bar{\psi}_x dx. \tag{1.1.15}$$

Furthermore, the DNLS equation (1.1.3) has remarkable property of being integrable by inverse scattering [38], which implies that there exist infinitely many conservation laws.

The initial value problem of the DNLS equation (1.1.3) has been studied in the Sobolev space $H^k, k \geq 1$, with results for both local and global well-posedness. The Sobolev space

$$H^k \equiv \{ f \in L^2(\mathbb{R}) : \mathcal{F}^{-1}(1 + |\xi|^2)^{k/2}\mathcal{F}f \in L^2(\mathbb{R}) \}$$

is equipped with the norm

$$\|f\|_{H^k} \equiv \|\mathcal{F}^{-1}(1 + |\xi|^2)^{k/2}\mathcal{F}f\|_{L^2(\mathbb{R})},$$

where $\mathcal{F}$ and $\mathcal{F}^{-1}$ are the Fourier transform and inverse Fourier transform on the real line respectively. Much of the well-posedness analysis relies on a transformation related to (1.1.10) that turns the equation into two coupled semilinear Schrödinger equations with no derivative. One of the earliest results is due to Tsutsumi and Fukuda [64], who proved local well-posedness on both the real line $\mathbb{R}$ and the unit torus $\mathbb{T}$ in the Sobolev space H^s, provided $s > 3/2$ and the data is sufficiently small. This was subsequently refined by Hayashi and Ozawa [29], who found that for initial conditions satisfying

$$\|u_0\|_{L^2} < \sqrt{2\pi}, \tag{1.1.16}$$

the solution exists for all time in H^s for $s \in \mathbb{Z}^+$. More recently, the global in time result for data satisfying (1.1.16) was extended to all H^s spaces with $s > 1/2$ by Colliander et al. [13]. Working in the Schwartz space, Lee [44] used the framework of inverse scattering to show that DNLS is globally well-posed for a dense subset of initial conditions, excluding certain non generic ones. There has also been progress beyond the cubic equation in the aforementioned results. Some studies, such as [17, 57, 63], include additive terms to the cubic nonlinearity with derivative. However, an outstanding problem for DNLS is to determine the fate of large data. At present, there is neither a result on global well posedness, nor is there a known finite time singularity.

The DNLS equation (1.1.3) admits a two-parameter family of solitary wave solutions of the form:

$$u_{\omega,c}(x,t) = \varphi_{\omega,c}(x-ct)\exp\left\{i\left(\omega t + \frac{c}{2}(x-ct) - \frac{3}{4}\int_{-\infty}^{x-ct}\varphi_{\omega,c}^2(\eta)d\eta\right)\right\}, \tag{1.1.17}$$

where $\omega > c^2/4$ and

$$\varphi_{\omega,c}(y) = \sqrt{\frac{(4\omega - c^2)}{\sqrt{\omega}(\cosh(\sigma\sqrt{4\omega - c^2}y) - \frac{c}{2\sqrt{\omega}})}} \tag{1.1.18}$$

is the positive solution to

$$-\partial_y^2\varphi_{\omega,c} + (\omega - \frac{c^2}{4})\varphi_{\omega,c} + \frac{c}{2}|\varphi_{\omega,c}|^2\varphi_{\omega,c} - \frac{3}{16}|\varphi_{\omega,c}|^4\varphi_{\omega,c} = 0. \tag{1.1.19}$$

Guo and Wu [26] showed that these solitary waves are *orbitally stable* if $c < 0$ and $c^2 < 4\omega$. Colin and Ohta [12] subsequently extended the result, proving orbital stability for all $c, c^2 < 4\omega$. We will present more details about those two results in Section 1.3.2.

Definition 1.1.1. Let $u_{\omega,c}$ be the solitary wave solution of (1.1.3). The solitary wave

$u_{\omega,c}$ is *orbitally stable* if, for all $\epsilon > 0$, there exists $\delta > 0$ such that if $\|u_0 - u_{\omega,c}\|_{H^1} < \delta$, then the solution $u(t)$ of (1.1.3) with initial data $u(0) = u_0$, exists globally in time and satisfies

$$\sup_{t\geq 0} \inf_{(\theta,y)\in\mathbb{R}^2} \|u(t) - e^{i\theta}u_{\omega,c}(t, \cdot - y)\|_{H^1} < \epsilon.$$

Otherwise, $u_{\omega,c}$ is said to be *orbitally unstable*.

1.2 DNLS with General Power Nonlinearity (gDNLS)

In an effort to better understand the properties of DNLS, we study an extension of (1.1.2) with general power nonlinearity (1.1.1). The gDNLS equation (1.1.1) also has a Hamiltonian structure with generalized energy:

$$E = \frac{1}{2}\int_{-\infty}^{\infty} |\psi_x|^2 dx + \frac{1}{2(\sigma+1)}\Im\int_{-\infty}^{\infty} |\psi|^{2\sigma}\bar{\psi}\psi_x dx, \quad \text{(Energy)}. \tag{1.2.1}$$

The mass and momentum invariants are the same as (1.1.14) and (1.1.15). Please note that we can not transform (1.1.1) into

$$i\partial_t u + \partial_x^2 u + i(|u|^{2\sigma}u)_x = 0.$$

via a Gauge transformation.

For all values of σ, we have the scaling property that if $\psi(x,t)$ is a solution of (1.1.1), then so is

$$\psi_\lambda(x,t) = \lambda^{-\frac{1}{2\sigma}}\psi\left(\lambda^{-1}x, \lambda^{-2}t\right). \tag{1.2.2}$$

It follows that the L^2 norm

$$\|\psi_\lambda\|_{L^2} = \lambda^{-\frac{1}{2\sigma}+\frac{1}{2}}\|\psi\|_{L^2}.$$

Hence, (1.1.1) is L^2-critical for $\sigma = 1$ and L^2-supercritical for $\sigma > 1$.

For general quasilinear Schrödinger equation with polynomial nonlinearities, local well-posedness holds in Sobolev spaces of high enough index [39,40,47]. In dimension one, Hayashi and Ozawa [30] considered the initial value problem for nonlinear Schrödinger equation,

$$\begin{aligned} i\partial_t u + \frac{1}{2}\partial_x^2 u =& F(u, \partial_x u, \bar{u}, \partial_x\bar{u}), \quad (x,t) \in \mathbb{R}\times\mathbb{R}^+, \\ u(x,0) =& u_0(x), \quad x \in \mathbb{R}, \end{aligned} \tag{1.2.3}$$

where F denotes a complex valued polynomial defined on $\mathbb{C}^4$ such that

$$F(z) = F(z_1, z_2, z_3, z_4) = \sum_{\substack{\nu \le |\alpha| < \rho \\ \alpha \in \mathbb{Z}_+^4}} a_\alpha z^\alpha, \tag{1.2.4}$$

and the standard notation for multi-indices is used. They had the following local existence result,

Theorem 1.2.1 ([30]). *If the lowest power in the nonlinear term F (1.2.4) is cubic ($\nu = 3$), then for any $u_0 \in H^3$, there exists a unique solution $u(\cdot)$ for (1.2.3) defined in the interval $[0, T]$, $T = T(\|u_0\|_{H^3}) > 0$ with $T(\theta) \to \infty$, as $\theta \to 0$, satisfying*

$$u \in C([0, T]; H^2) \cap C_w(0, T; H^3),$$

where, for any interval I of $\mathbb{R}$, $C(I; B)$ and $C_w(I; B)$ denote the space of continuous and weakly continuous functions from I to B, respectively.

In [28], Hao proved that (1.1.1) is locally well-posed in $H^{1/2}$ intersected with an appropriate Strichartz space for $\sigma \ge 5/2$.

As the DNLS equation (1.1.3), (1.1.1) admits a two-parameter family of solitary wave solutions,

$$\psi_{\omega,c}(x,t) = \varphi_{\omega,c}(x - ct) \exp\left\{ i \left(\omega t + \frac{c}{2}(x - ct) - \frac{1}{2\sigma + 2} \int_{-\infty}^{x-ct} \varphi_{\omega,c}^{2\sigma}(\eta) d\eta \right) \right\}, \tag{1.2.5}$$

where $\omega > c^2/4$ and

$$\varphi_{\omega,c}(y)^{2\sigma} = \frac{(\sigma + 1)(4\omega - c^2)}{2\sqrt{\omega}(\cosh(\sigma\sqrt{4\omega - c^2}y) - \frac{c}{2\sqrt{\omega}})} \tag{1.2.6}$$

is the positive solution of

$$-\partial_y^2 \varphi_{\omega,c} + (\omega - \frac{c^2}{4})\varphi_{\omega,c} + \frac{c}{2}|\varphi_{\omega,c}|^{2\sigma}\varphi_{\omega,c} - \frac{2\sigma + 1}{(2\sigma + 2)^2}|\varphi_{\omega,c}|^{4\sigma}\varphi_{\omega,c} = 0. \tag{1.2.7}$$

It is convenient to define

$$\phi_{\omega,c}(y) = \varphi_{\omega,c}(y) e^{i\theta_{\omega,c}(y)}, \tag{1.2.8}$$

with the traveling phase

$$\theta_{\omega,c}(y) \equiv \frac{c}{2} y - \frac{1}{2\sigma + 2} \int_{-\infty}^{y} \varphi_{\omega,c}^{2\sigma}(\eta) d\eta. \tag{1.2.9}$$

Clearly,

$$\psi_{\omega,c}(x,t) = e^{i\omega t}\phi_{\omega,c}(x-ct), \tag{1.2.10}$$

and the complex function $\phi_{\omega,c}(y)$ satisfies

$$-\partial_y^2\phi_{\omega,c} + \omega\phi_{\omega,c} + ic\partial_y\phi_{\omega,c} - i|\phi_{\omega,c}|^{2\sigma}\partial_y\phi_{\omega,c} = 0, y \in \mathbb{R}. \tag{1.2.11}$$

1.3 Main Results

1.3.1 Singularity Formation

We will first recall the focusing nonlinear Schrödinger equation with power law nonlinearity (NLS), and then present our results about gDNLS equation. The NLS equation with an attracting nonlinearity in $\mathbb{R}^d$ is

$$i\partial_t u + \Delta u + |u|^{2\sigma}u = 0, t \in [0,T], \tag{1.3.1}$$

where $u : \mathbb{R}^d \times [0,T] \to \mathbb{C}$. It has a scaling property that if $u(\mathbf{x},t)$ is a solution of (1.3.1) with initial condition u_0 for $t \in [0,T]$, then for any $\lambda > 0$,

$$u_\lambda(t,\mathbf{x}) \equiv \lambda^{-\frac{1}{\sigma}}u(\lambda^{-1}\mathbf{x}, \lambda^{-2}t)$$

also solves (1.3.1) with initial condition $u_{0,\lambda} \equiv \lambda^{-\frac{1}{\sigma}}u_0(\lambda\mathbf{x})$ for $t \in [0, T/\lambda^2]$. we also have the L^2 norm

$$\|u_{0,\lambda}\|_{L^2} = \lambda^{\frac{d}{2}-\frac{1}{\sigma}}\|u_0\|_{L^2}.$$

It follows that three cases arise according to values of the dimension d and the exponent σ.

- $\sigma d < 2$, L^2-subcritical case. Wave dispersion dominates over nonlinear focusing, the solution exists for all time [10, 21, 46, 65].
- $\sigma d \geq 2$, L^2-critical and super-critical case. Solution may blow up in finite time [22, 67, 71]. When the initial condition has a negative energy

  $$H = \int |\nabla u|^2 - \frac{1}{\sigma+1}|u|^{2\sigma+2}d\mathbf{x}$$

  and a finite variance

  $$V(t) = \int |\mathbf{x}|^2|u|^2 d\mathbf{x},$$

a singularity occurs at a finite time. This result is based on the variance identity,

$$\frac{d^2}{dt^2}V(t) = 8\left(H - \frac{d\sigma - 2}{2\sigma + 2}\int |u|^{2\sigma+2}d\mathbf{x}\right).$$

When $\sigma d = 2$, the problem is well posed globally in time for initial conditions u_0 with sufficiently small mass [68], namely $\|u_0\|_{L^2}^2 < \|R\|_{L^2}^2$, where R is the ground state of

$$-\Delta R + R - R^{2\sigma+1} = 0, \quad \lim_{|\mathbf{x}|\to\infty} |R(\mathbf{x})| = 0.$$

At the critical mass $\|u_0\|_{L^2} = \|R\|_{L^2}$, there are exact self-similar solutions [51]. More precisely, let $u_0 \in H^1(\mathbb{R}^d)$ and $|\mathbf{x}u_0| \in L^2(\mathbb{R}^d)$ (finite variance). Suppose in addition that $\|u_0\|_{L^2} = \|R\|_{L^2}$ and $u(t)$ blows up in a finite time t^*, then there exist constants θ, ω, and $\mathbf{x_1} \in \mathbb{R}^d$ such that the solution is expressed in the form

$$u(\mathbf{x},t) = \frac{\omega^{d/2}}{(t^*-t)^{d/2}} R_0\left(\omega\left(\frac{\mathbf{x}-\mathbf{x}_1}{t^*-t} - \xi\right)\right) e^{i\left(\theta + \frac{\omega^2}{t^*-t} - \frac{|\mathbf{x}-\mathbf{x}_1|^2}{4(t^*-t)}\right)}.$$

On the other hand, the blow up rate for generic initial data has the form $(\ln|\ln(t_*-t)|/(t_*-t))^{1/2}$, where t_* is the blowup time [18, 42, 45, 52].

When $\sigma d > 2$ and in the case of radially symmetric, the local structure of the singularity is self-similar and has the form [23, 50, 62]

$$u(\mathbf{x},t) \sim \frac{1}{(2a(t^*-t))^{1/2\sigma}} Q\left(\frac{|\mathbf{x}-\mathbf{x}^*|}{(2a(t^*-t))^{1/2}}\right) e^{i\left(\theta + \frac{1}{2a}\ln\frac{t^*}{t^*-t}\right)}, a \in \mathbb{R}$$

where $\mathbf{x}^*$ and t^* are the location and the time of the blowup. The profile Q satisfies

$$\begin{aligned} Q_{\eta\eta} + \frac{d-1}{\eta}Q_\eta - Q + ia\left(\eta Q_\eta + \frac{Q}{\sigma}\right) + |Q|^{2\sigma}Q = 0, \eta > 0 \\ Q_\eta(0) = 0, Q(\infty) = 0. \end{aligned} \tag{1.3.2}$$

When $\sigma = 1, d = 3$, the constant a in (1.3.2) is observed to be independent of the initial data and has the value $a \sim 0.917$. This precise description of the nature of the focusing singularity is achieved by using an adaptive grid numerical method, called *dynamic rescaling*. This method is motivated by the scaling invariance of the equation. The dependent and independent variables are rescaled by factors related to a norm of the solution which blows up at the singularity. The rescaled solution exists for all time. The solution of the primitive equation can be in principle computed up to time very close to blow up.

Comparing the gDNLS equation (1.1.1) to the NLS equation, a natural question is whether the solutions to gDNLS may blow up in finite time in the L^2-supercritical regime ($\sigma > 1$). The first result, presented in Chapter 2, is to numerically explore the possibility for singularity formation in (1.1.1), and our simulations and asymptotics indicate that there is indeed collapse when $\sigma > 1$. We then give an accurate description of the nature of the focusing singularity with generic "large" data by using the *dynamic rescaling* method. Up to a rescaling, we observe numerically for $\sigma > 1$, the solutions locally blow up like

$$\psi(x,t) \sim \left(\frac{1}{2\alpha(t^*-t)}\right)^{\frac{1}{4\sigma}} Q\left(\frac{x-x^*}{\sqrt{2\alpha(t^*-t)}} + \frac{\beta}{\alpha}\right) e^{i(\theta+\frac{1}{2\alpha}\ln\frac{t^*}{t^*-t})}, \tag{1.3.3}$$

where t^* is the singularity time and x^* is the position of $\max_x |\psi(x,t^*)|$. The function $Q(\xi)$ is a complex-valued solution of the equation

$$Q_{\xi\xi} - Q + i\alpha(\tfrac{1}{2\sigma}Q + \xi Q_\xi) - i\beta Q_\xi + i|Q|^{2\sigma}Q_\xi = 0, \tag{1.3.4}$$

with amplitude that decays monotonically as $\xi \to \pm\infty$. The coefficients α and β are real numbers, and our simulations show that they depend on σ but not on the initial condition. We also observe that α decreases monotonically as $\sigma \to 1$ (Figure 2.19). This observed blowup is analogous to that of NLS with supercritical power nonlinearity in terms of the blowup speed and asymptotic profile [50].

1.3.2 Orbital Stability/Instability of Solitary Waves

The second result of this thesis is about stability of solitary wave solutions (1.2.5) to the gDNLS equation (1.1.1). Before we present our results, we briefly recall the orbital stability properties of the solitary wave solution in the case of $\sigma = 1$ (DNLS). In [26], Guo and Wu considered a nonlinear quintic derivative Schrödinger equation,

$$u_t = iu_{xx} + i(c_3|u|^2 + c_5|u|^4)u + [(s_0 + s_2|u|^2)u]_x, \quad x \in \mathbb{R}, \tag{1.3.5}$$

where s_0, s_2, c_3 and c_5 are real constants. It is shown in [66] that there exists a solitary waves solution

$$u(x,t) = \phi(x-vt)\exp\left(-i\lambda t + \frac{v\xi}{2} + \frac{3}{4}s_2\int_{-\infty}^{x-vt}\phi^2(\xi)d\xi\right), \quad (\lambda, v) \in \mathbb{R}^2. \tag{1.3.6}$$

Here $\phi(\xi)$ is a real function,

$$\phi(\xi) = \sqrt{2\alpha}\left[\beta + \left(\beta^2 + \frac{4}{3}\alpha c_5 + \frac{1}{4}\alpha s_2^2\right)^{1/2}\cosh(2\sqrt{\alpha}\xi)\right]^{-1/2},$$

where

$$\alpha = -\lambda - \frac{v^2}{4} > 0, \quad \beta = \frac{1}{2}c_3 + \frac{1}{4}s_2 v > 0, \tag{1.3.7}$$

and

$$\beta^2 + \frac{4}{3}\alpha c_5 + \frac{1}{4}\alpha s_2^2 > 0. \tag{1.3.8}$$

Using a detailed spectral analysis in the spirit of Grillakis, Shatah and Strauss [24, 25], Guo and Wu obtained the following stability result:

Theorem 1.3.1 ([26]). *For any real fixed constants c_3, c_5 and s_2, if λ and v satisfy* (1.3.7) *and* (1.3.8)*, then the solitary wave* (1.3.6) *is orbitally stable.*

When $c_3 = c_5 = s_0 = 0, s_2 = -1$, (1.3.5) becomes DNLS (1.1.3), and $(-\lambda, v)$ play the role of (ω, c) in the solitary wave solution (1.1.17). From the condition (1.3.7) and Theorem 1.3.1, the solitary wave solution of the DNLS equation is orbitally stable when $\omega \geq \frac{c^2}{4}$ and $c < 0$.

Colin and Ohta [12] subsequently prove the orbital stability of the DNLS equation for all $c, c^2 < 4\omega$, using variational methods. Their analysis is based on the second form of the DNLS equation (1.1.2). Using the three invariants (1.1.13), (1.1.14) and (1.1.15) of (1.1.2), they obtain that the set of all the solitary waves is the same as the set of all the minimizer of the minimization problem

$$\mu(\omega, c) = \inf\{S_{\omega,c}(u) : u \in H^1(\mathbb{R})\backslash\{0\}, K_{\omega,c}(u) = 0\},$$

where

$$S_{\omega,c}(u) = \frac{1}{2}\|\partial u\|_2^2 + \frac{\omega}{2}\|u\|_2^2 - \frac{c}{2}\Im\int_{\mathbb{R}}\bar{u}\partial_x u dx + \frac{1}{4}\Im\int_{\mathbb{R}}|u|^2\bar{u}\partial_x u dx$$

and

$$K_{\omega,c}(u) = \|\partial_x u\|_2^2 + \omega\|u\|_2^2 - c\Im\int_{\mathbb{R}}\bar{u}\partial_x u dx + \Im\int_{\mathbb{R}}|u|^2\bar{u}\partial_x u dx.$$

From this variational characterization of solitary wave solution, they prove the following result:

Theorem 1.3.2 ([12]). *For any $(\omega, c) \in \mathbb{R}^2$ satisfying $c^2 < 4\omega$, the solitary wave solution* (1.1.17) *of the DNLS equation* (1.1.3) *is orbitally stable.*

In Chapter 3, we prove that the orbital stability/ instability of the gDNLS equation (1.1.1) is determined by both the strength of the nonlinearity σ and the choice of the soliton parameters, c and ω. These results are *conditional* in the sense that for $\sigma \neq 1$, we lack a suitable local well-posedness theory. Throughout our study, we assume that given $\sigma > 0$, and $\psi_0 \in H^1(\mathbb{R})$, there exists a weak solution $\psi \in C([0,T); H^1(\mathbb{R}))$ of (1.1.1), for $T > 0$, which satisfies

$$\frac{d}{dt}\langle \psi(\cdot,t), f\rangle = \langle E'(\psi(\cdot,t)), -Jf\rangle \tag{1.3.9}$$

for appropriate test functions f. E is the energy functional, and J is the symplectic operator. These are defined in Section 3.1.

Subject to this assumption, we have the following results:

Theorem 1.3.3. *For any admissible (ω, c) and $\sigma \geq 2$, the solitary wave solution $\psi_{\omega,c}(x,t)$ of (1.1.1) is orbitally unstable.*

For σ between 1 and 2, slow solitons, those with sufficiently low c, are stable, while fast right-moving solitons are unstable.

Theorem 1.3.4. *For $\sigma \in (1,2)$, there exists $z_0 = z_0(\sigma) \in (-1,1)$ such that:*

(i) the solitary wave solution $\psi_{\omega,c}(x,t)$ of (1.1.1) is orbitally stable for admissible (ω, c) satisfying $c < 2z_0\sqrt{\omega}$.

(ii) the solitary wave solution $\psi_{\omega,c}(x,t)$ of (1.1.1) is orbitally unstable for admissible (ω, c) satisfying $c > 2z_0\sqrt{\omega}$.

Our last result concerns $\sigma < 1$, where all solitons are stable:

Theorem 1.3.5. *For admissible (ω, c) and $0 < \sigma < 1$, the solitary wave solution $\psi_{\omega,c}(x,t)$ of (1.1.1) is orbitally stable.*

Theorems 1.3.4 and 1.3.5 are fully rigorous up to the determination of the sign of a function of one variable, which is parametrized by σ. The number z_0 in Theorem 1.3.4 corresponds to a zero crossing. This function, defined in (3.3.14), includes improper integrals of transcendental functions.

Theorem 1.3.4 is particularly noteworthy for distinguishing gDNLS from the focusing NLS equation (1.3.1). As we mentioned before, (1.1.1) is L^2-critical for $\sigma = 1$, and it is L^2-supercritical for $\sigma > 1$. While NLS only admits stable solitons in the L^2-subcritical regime, gDNLS admits stable solitons not only in the critical regime, but also in the supercritical one.

Our results are proven using the abstract functional analysis framework of Grillakis, Shatah and Strauss, [24, 25]; see [8, 69, 70] for related results and [62] for a survey. The test for stability involves two parts: (i) Counting the number of negative eigenvalues of the linearized evolution operator H_ϕ near the solitary solution of (1.1.1), denoted $n(H_\phi)$; (ii) Counting the number of positive eigenvalues of the Hessian of the scalar function $d(\omega, c)$ built out of the action functional evaluated at the soliton, denoted $p(d'')$. We give explicit characterizations of H_ϕ and $d(\omega, c)$ in Section 3.1. We then apply:

Theorem 1.3.6 ([24, 25])**.**

$$p(d'') \leq n(H_\phi) \tag{1.3.10}$$

Furthermore, under the condition that d is non-degenerate at (ω, c):

(i) If $p(d'') = n(H_\phi)$, the solitary wave is orbitally stable;

(ii) If $n(H_\phi) - p(d'')$ is odd, the solitary wave is orbitally unstable.

1.4 Nonlinear Schrödinger Equation with External Potential

It is well known that the one dimensional cubic NLS equation (equation (1.3.1) with $d = \sigma = 1$) admits solitary wave solutions of the form

$$u_{\phi_0}(x,t) = Ae^{i\phi_0 + ivx + i\frac{A^2 - v^2}{2}t}\text{sech}(A(x - a_0 - vt)), \tag{1.4.1}$$

where $a_0 \in \mathbb{R}$ is the initial center of mass position of the soliton, $v \in \mathbb{R}$ is its velocity, $\phi_0 \in [0, 2\pi)$ is the phase, and $A \in \mathbb{R}^+$. In the last part of this thesis, we study the effect of an external potential on the long time behavior of solitary waves $u_{\phi_0}(x,t)$. More precisely, we consider the one dimensional cubic NLS equation,

$$\begin{cases} i\partial_t u = -\frac{1}{2}\partial_x^2 u + |u|^2 u + Vu \\ u(x,0) = u_0(x), \end{cases} \tag{1.4.2}$$

where the external potential $V(x)$ is a double delta potential of height $q > 0$ and located at points $\pm l$,

$$V(x) = q(\delta(x + l) + \delta(x - l)) \tag{1.4.3}$$

or it is a box potential, of height q and width $2l$,

$$V(x) = q(\Theta(x + l) - \Theta(x - l)) \tag{1.4.4}$$

where Θ is the Heaviside step function. We investigate the evolution of the solution $u(x,t)$ of equation (1.4.2) with initial condition $u_0 = u_{\phi_0}$.

The effective dynamics of coherent structures for NLS equations with or without external potential has been the object of numerous studies in the last twenty years. Typically, in the neighborhood of stable states, the dynamics reduces to the coupling of two systems: a finite-dimensional system for the evolution of parameters characterizing the soliton, and an infinite-dimensional one governing the radiation of energy to spatial infinity. For a soliton moving in a slowly varying external potential [1,9,20,36], or in the presence of rough yet small (nonlinear) perturbations [2,35], the long time dynamics of the center of mass of the soliton behaves like a *classical* particle in an effective potential that corresponds to the restriction of the potential or perturbation to the soliton manifold. On the other hand, there are situations such as the *"blind"* collision of two fast solitons in an external potential [3], or the scattering of solitons with high velocity by a delta impurity [32], where quantum effects dominate. In the latter reference, the authors show that the incoming soliton splits into two waves, a reflected one and a transmitted one, each being a single soliton, and the transmitted rate is well approximated by the quantum transmission rate of linear scattering from a single delta potential.

In [4], Abou Salem and Sulem showed that the phenomenon of *resonant tunneling*, referring to a well known situation in linear quantum mechanical scattering theory where incoming waves through potential barriers are fully transmitted at certain energies, can occur for nonlinear equations. More precisely, they considered the NLS equation in one dimension

$$\begin{cases} i\partial_t u = -\frac{1}{2}\partial_x^2 u + Vu + f(u) \\ u(x,0) = u_0(x) \end{cases} \tag{1.4.5}$$

where V is an external potential. The hypotheses on the nonlinearity are essentially those sufficient for existence of a global smooth solution and existence of (orbitally) stable solitary wave solutions, which include both Hartree and power nonlinearities. The assumptions on the potential V is that it has compact support around the origin, and is such that the Hamiltonian $H = -\frac{1}{2}\partial_x^2 + V$ has a positive continuous spectrum with no bound states. Furthermore, for $\lambda \in \mathbb{R}\backslash\{0\}$, the equation

$$(H - \lambda^2)u = 0$$

has unique solutions $e_\pm(x,\lambda)$ satisfying

$$e_\pm(x,\lambda) = \begin{cases} e^{\pm i\lambda x} + R(\lambda)e^{\mp i\lambda x}, & \pm x < -l, \\ T(\lambda)e^{\pm i\lambda x}, & \pm x > l, \end{cases} \tag{1.4.6}$$

for some $l > 0$. The transmission and reflection coefficients $T(\lambda)$ and $R(\lambda)$ respectively, satisfy the unitary condition

$$|T(\lambda)|^2 + |R(\lambda)|^2 = 1,$$

and are differentiable in $\lambda \in \mathbb{R}\backslash\{0\}$. The key hypothesis concerns *resonant tunneling*: there exists $\lambda_0 \in \mathbb{R}\backslash\{0\}$ that depends on V such that $R(\lambda_0) = 0$.

When the potential $V(x)$ is in the form of (1.4.3) or (1.4.4), the resonant tunneling condition is written explicitly in the form of a relation between λ and the parameters q and l entering in the definition of the potential. We give the detailed expressions in Section 4.1.

We recall below the precise result of [4] restricted for simplicity to the case of the 2-δ potential.

Theorem 1.4.1 ([4])**.** *Take as an initial condition a perturbed soliton in the form $u_0 = u_{\phi_0}(x,0) + w_0$, with initial velocity $v \gg 1$ and $\|w_0\|_{L^2} = O(v^{-1})$. Assume that $l = O(v^{-1})$ and $q^{-1} = O(v^{-1})$, such that the resonant condition is satisfied. Then for v sufficiently large, there exists positive constants C, C', σ, β and δ that are independent of v, such that*

$$\|u(t) - u_{\phi_0}(t)\|_{L^2} \leq Cv^{-\beta} + C'e^{-\delta(|a_0+vt-l|+|a_0+vt+l|)}, \tag{1.4.7}$$

uniformly in the time interval $t \in [0, \frac{|a_0|}{v} + \sigma \log v]$.

In other words, for special values of v, q, and l, the fast soliton tunnels through the potential barrier, up to an error term that decreases with increasing velocity v and with longer times. Notice that the size of the potential q is arbitrarily large, as long as the resonant condition is satisfied. The proof in [4] is based on decomposing the dynamics into three regimes: (i) the pre-collision phase, corresponding to $t \in [0, t_1 = \frac{|a_0|-v^\xi}{v}]$, (ii) the collision phase for $t \in [t_1, t_2 = \frac{|a_0|+v^\xi}{v}]$ and (iii) the post-collision phase $[t_2, t_3 = t_2 + \sigma \ln v]$, for some parameters $\xi \in (0,1)$ and $\sigma > 0$. In the pre- and post collision regime, the soliton is essentially not affected by the potential, and the dynamics approximately follows that of the NLS equation (without potential). This is shown by using the symplectic and group-theoretic structure of the soliton manifold and projecting the Hamiltonian flow

generated by the NLS equation onto the soliton manifold; see also [3, 20, 36]. In the intermediate regime, the dynamics is approximated by the linear flow due to the high velocity v of the moving soliton and consequently short time of interaction. This is shown by using Strichartz estimates and linear scattering theory, see also [3, 35].

In Chapter 4, we illustrate numerically this phenomenon and investigate the ranges of various parameters in the context of (1.4.2). In the following calculations, we choose that the initial condition $u_0 = u_{\phi_0}$ is centered at $a_0 \ll 0$ and moves from the left at velocity $v \gg 1$.

Our numerical results agree perfectly with the predictions of the analysis of [4]. To check the accuracy of our numerical scheme, we performed several tests. In particular, we check for the precise conservation of mass and energy under the Hamiltonian flow generated by the NLS equation. We also check the precision and the convergence properties of our scheme by comparing our numerical solution of the NLS equation (without potential) with exact explicit solutions (solitons) and calculated the rate of convergence in $O(h^2 + (dt)^2)$ in terms of the mesh size and time step. We reproduce the same results for different system sizes and a wide range of parameters (See Section 4.3 for details).

Chapter 2

Focusing Singularity in a Generalized Derivative Nonlinear Schrödinger Equation

In this chapter, we present a numerical study of a Derivative Nonlinear Schrödinger equation with a general power nonlinearity (1.1.1). In the L^2-supercritical regime, $\sigma > 1$, our simulations indicate that there is a finite time singularity. We obtain a precise description of the local structure of the solution in terms of blowup rate and asymptotic profile (1.3.3).

This chapter is organized as follows. In Section 2.1, we consider gDNLS with quintic nonlinearity ($\sigma = 2$). We first present a direct numerical simulation that suggests there is, indeed, a finite time singularity. We then refine our study by introducing the dynamic rescaling method. Section 2.2 shows our results for $\sigma \in (1, 2)$. In Section 2.3, we discuss the asymptotic profile of gDNLS. Details of our numerical methods are described in Sections 2.4 and 2.5. In Section 2.6, we discuss our results and mention open problems.

2.1 gDNLS with Quintic Nonlinearity

We first performed a direct numerical integration of gDNLS with quintic nonlinearity ($\sigma = 2$) and initial condition $\psi_0 = 3e^{-2x^2}$. We integrate the equation using a pseudo-spectral method with an exponential time-differencing fourth-order Runge-Kutta algorithm (ETDRK4), augmenting it with the numerical stabilization scheme presented in [37] to better resolve small wave numbers (See Section 2.4.1 for details). The computation was performed on the interval $[-8, 8)$, with 2^{12} grid points and a time step on the order

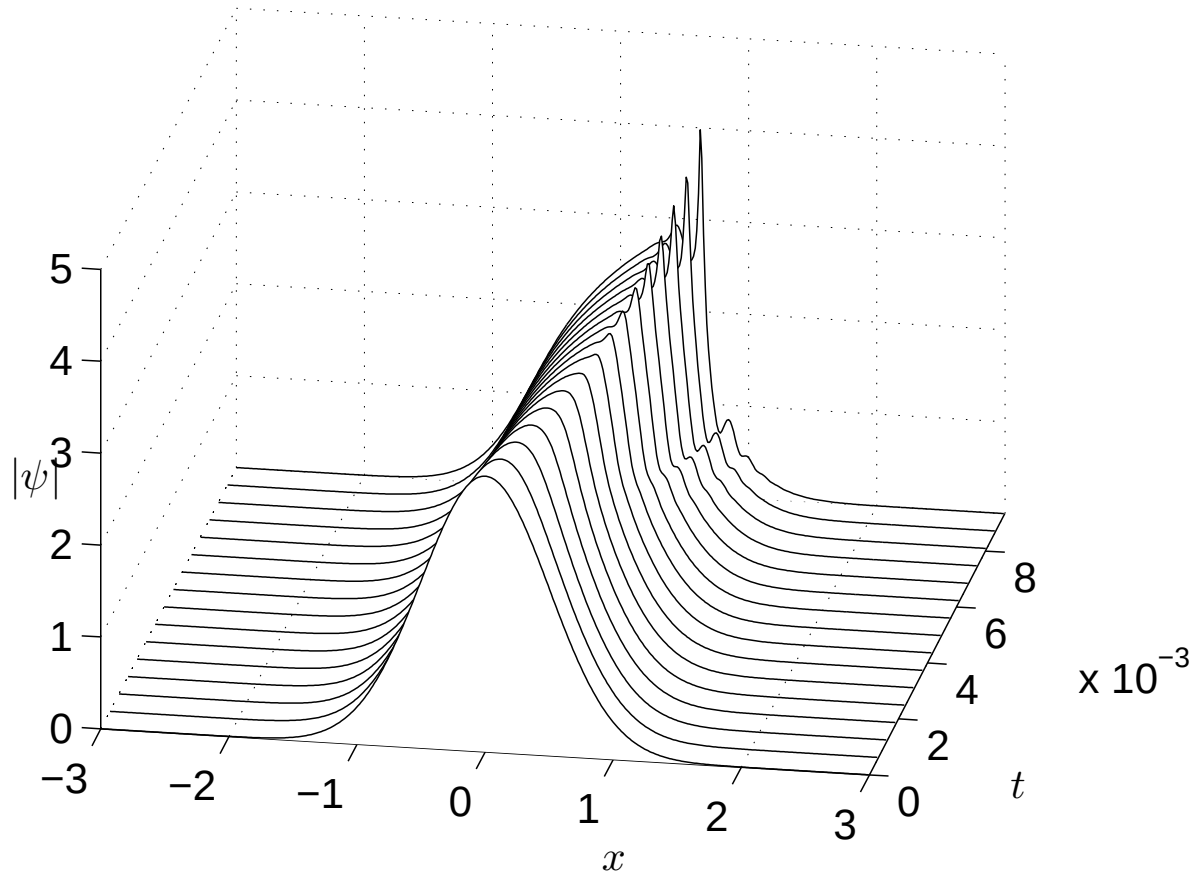

Figure 2.1: $|\psi(x,t)|$ versus x and t.

of 10^{-6}. Figure 2.1 shows that the wave first moves rightward and then begins to separate. Gradually, the leading edge of one wave sharpens and grows in time. The norms $\|\psi_x(\cdot,t)\|_{L^2}$ and $\|\psi_{xx}(\cdot,t)\|_{L^2}$ grow substantially during the lifetime of the simulation. The norm $\|\psi_x(\cdot,t)\|_{L^2}$ increases from 4 to about 18 while $\|\psi_{xx}(\cdot,t)\|_{L^2}$ increases from about 10 to 1720. This growth in norms is a first indication of collapse. In contrast, the L^∞ norm has only increased from 3 to 4.07. As a measure of the precision of the simulation, the energy remains equal to 7.976, with three digits of precision, up to time $t = 0.009$.

2.1.1 Dynamic Rescaling Formulation

To gain additional detail of the blowup, we employ the dynamic rescaling method. Based on the scaling invariance of the equation (1.2.2), we define the new variables:

$$\psi(x,t) = L^{-\frac{1}{2\sigma}}(t)u(\xi,\tau), \quad \xi = \frac{x - x_0(t)}{L(t)} \quad \text{and} \quad \tau = \int_0^t \frac{ds}{L^2(s)}, \tag{2.1.1}$$

where $L(t)$ is a length scale parameter chosen such that a certain norm of the solution remains bounded for all τ. The parameter x_0 will be chosen to follow the transport of the solution. Substituting the change of variables into (1.1.1) gives

$$\begin{aligned} &iu_\tau + u_{\xi\xi} + ia(\tau)(\tfrac{1}{2\sigma}u + \xi u_\xi) - ib(\tau)u_\xi + i|u|^{2\sigma}u_\xi = 0, \\ &u(\xi,0) = L_0^{-\frac{1}{2\sigma}}\psi(x/L_0,0), \end{aligned} \tag{2.1.2}$$

where

$$a(\tau) = -L(t)\dot{L}(t) = -\frac{d\ln L}{d\tau}, \tag{2.1.3a}$$

$$b(\tau) = L(t)\frac{dx_0}{dt}. \tag{2.1.3b}$$

There are several possibilities for the choice of $L(t)$. We define $L(t)$ such that $\|u_\xi(\cdot,\tau)\|_{L^2}$ remains constant. From (2.1.1),

$$\|\psi_x\|_{L^{2p}} = L^{-\frac{1}{q}}\|u_\xi\|_{L^{2p}}, \quad q = \left(1 + \frac{1}{2}\left(\frac{1}{\sigma} - \frac{1}{p}\right)\right)^{-1},$$

and

$$L(t) = \|u_\xi(\cdot,0)\|_{L^{2p}}^{q}\|\psi_x(\cdot,t)\|_{L^{2p}}^{-q},$$

leading to an integral expression for the function $a(\tau)$ defined in (2.1.3a):

$$a(\tau) = -q\|u_\xi(\cdot,0)\|_{L^{2p}}^{-2p}\int \Re\left\{(\bar{u}_\xi^p u_\xi^{p-1})_\xi(iu_{\xi\xi} - |u|^{2\sigma}u_\xi)\right\}d\xi, \tag{2.1.4}$$

Ideally, we would like to choose $x_0(t)$ to follow the highest maximum of the amplitude of the solution. After several attempts, we found that choosing

$$x_0 = \frac{\int x|\psi_{xx}|^{2p}dx}{\int |\psi_{xx}|^{2p}dx} \tag{2.1.5}$$

follows the maximum of the amplitude in a satisfactory way. The coefficient b takes the form

$$b(\tau) = 2p\frac{\int \Re\{(\xi|u_{\xi\xi}|^{2p-2}\bar{u}_{\xi\xi})_{\xi\xi}(iu_{\xi\xi} - |u|^{2\sigma}u_\xi)\}d\xi}{\int |u_{\xi\xi}|^{2p}d\xi}. \tag{2.1.6}$$

In summary, we now have a system of evolution equations for the rescaled solution u:

$$u_\tau = iu_{\xi\xi} - a(\tau)(\tfrac{1}{2\sigma}u + \xi u_\xi) + b(\tau)u_\xi - |u|^{2\sigma}u_\xi \tag{2.1.7a}$$

$$a(\tau) = -q\|u_\xi(0)\|_{L^{2p}}^{-2p} \int \Re\left\{(\bar{u}_\xi^p u_\xi^{p-1})_\xi (iu_{\xi\xi} - |u|^{2\sigma}u_\xi)\right\} d\xi, \tag{2.1.7b}$$

$$b(\tau) = 2p\frac{\int \Re\{(\xi|u_{\xi\xi}|^{2p-2}\bar{u}_{\xi\xi})_{\xi\xi}(iu_{\xi\xi} - |u|^{2\sigma}u_\xi)\}d\xi}{\int |u_{\xi\xi}|^{2p}d\xi}. \tag{2.1.7c}$$

where $p \in \mathbb{N}$ and $q = (1 + \frac{1}{2}(\frac{1}{\sigma} - \frac{1}{p}))^{-1}$. In practice, we integrate (2.1.7) with $p = 1$, and we choose $L_0 \in (0, 1]$ such that $\max_\tau(a)$ is not too large. The scaling factor $L(\tau)$ is computed by integration of (2.1.3a).

We expect $u(\xi, \tau)$ to be defined for all τ and that $L(\tau) \to 0$ fast enough so that $\tau \to \infty$ as $t \to t^*$. The behavior of $a(\tau)$ and $u(\xi, \tau)$ for large τ will give us information on the scaling factor $L(\tau)$ and the limiting profile. Under this rescaling, the invariants (3.1.20), (3.1.21) and (3.1.22) become

$$E(\psi(t)) = E(\psi(0)) = L(t)^{-\frac{1}{\sigma}-1}E(u(\tau)), \tag{2.1.8a}$$

$$M(\psi(t)) = M(\psi(0)) = L(t)^{-\frac{1}{\sigma}+1}M(u(\tau)), \tag{2.1.8b}$$

$$P(\psi(t)) = P(\psi(0)) = L(t)^{-\frac{1}{\sigma}}P(u(\tau)). \tag{2.1.8c}$$

These relations allow us to compute $L(t)$ in different ways and check the consistency of our calculations.

2.1.2 Singularity Formation

Integrating (2.1.7) using the ETDRK4 algorithm, we present our results for two families of initial conditions:

$$\psi_0(x) = A_0 e^{-2x^2} \quad (Gaussian) \tag{2.1.9}$$

and

$$\psi_0(x) = \frac{A_0}{1 + 9x^2} \quad (Lorentzian). \tag{2.1.10}$$

with various values of the amplitude coefficient A_0. We observed that for both families, the corresponding solutions present similar local structure near the blowup time.

In these simulations, there are typically 2^{18} points in the domain $[-l, l)$ with $l = 1024$. While the exponential time differencing removes the stiffness associated with the second

derivative term, the advective coefficient,

$$(a\xi - b + |u|^{2\sigma})u_\xi,$$

constrains our time step through a CFL condition. Near the origin, where u has initially an amplitude around 3, we have that the coefficient a can be close to 100 in the case of quintic nonlinearity. Far from the origin, $a\xi$ is the dominant term, and this coefficient can be ~ 1000. Consequently, the time step must be at least two to three orders of magnitude smaller than the grid spacing. For the indicated spatial resolution, $\Delta\xi \sim 10^{-2}$, we found it was necessary to take $\Delta\tau \sim 10^{-7}$ to ensure numerical stability.

Figure 2.2 shows the evolution of $|u(\xi,\tau)|$ with the Gaussian initial condition, $A_0 = 3$ and $L(0) = 0.2$. The rescaled wave $u(\xi,\tau)$ separates into three pieces. The middle one stays in the center of the domain while the other two waves move away from the origin on each side. Figure 2.3 shows that $\max_\xi |u(\xi,\tau)|$ slightly decreases with τ. Due to our choice of the rescaling factor, $\|u_\xi(\cdot,\tau)\|_{L^2}$ is constant. We also observe that $\|u_{\xi\xi}(\cdot,\tau)\|_{L^2}$ remains bounded. Returning to the primitive variables, the maximum integration time $\tau = 6$ corresponds to $t = 0.0098$, $\|\psi_x\|_{L^2} = 334.58$ and $\|\psi_{xx}\|_{L^2} = 1.56 \times 10^6$. For the Lorentzian initial condition (2.1.10) with $A_0 = 3$ and $L(0) = 1$, the maximum integration time $\tau = 0.16$ corresponds to $t = 0.008$, $\|\psi_x\|_{L^2} = 109.8$ and $\|\psi_{xx}\|_{L^2} = 1.17 \times 10^5$.

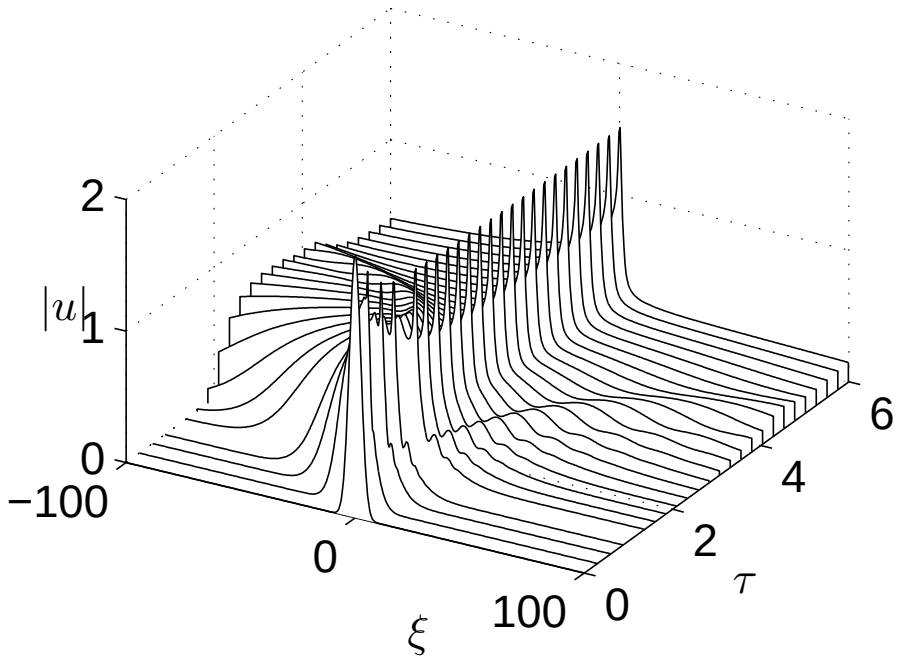

Figure 2.2: $|u|$ versus ξ and τ, for initial condition (2.1.9) with $A_0 = 3$, $L(0) = 0.2$, and nonlinearity $\sigma = 2$.

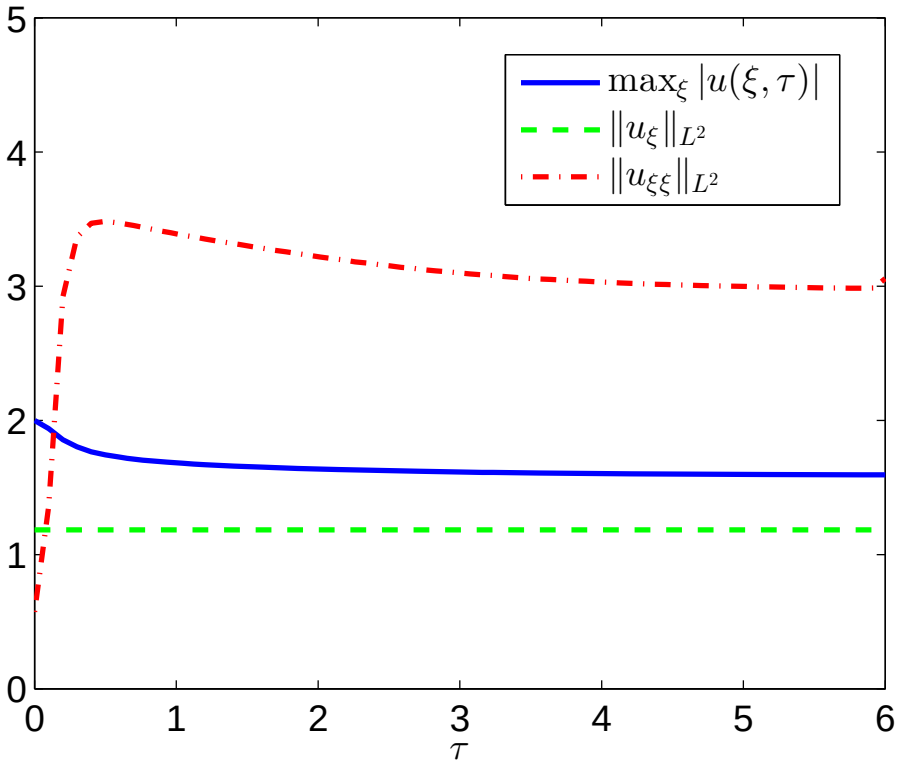

Figure 2.3: $\max_\xi |u(\xi,\tau)|$, $\|u_\xi(\cdot,\tau)\|_{L^2}$, and $\|u_{\xi\xi}(\cdot,\tau)\|_{L^2}$ versus τ, same initial conditions as in Fig. (2.2).

For a detailed description of singularity formation, we turn to the evolution of the parameters a and b as functions of τ. For both families of initial conditions (2.1.9) and (2.1.10) and amplitudes $A_0 = 2, 3, 4$, we observe that a and b tend to constants A and B as τ gets large. Figures 2.4 and 2.5 respectively display a and b versus τ for initial conditions (2.1.9) and (2.1.10) and $A_0 = 3$.

Turning to the limiting profile of the solution, we write u in terms of amplitude and phase in the form $u \equiv |u|e^{i\phi(\xi,\tau)}$, Figure 2.6 shows that $|u|$ tends to a fixed profile as τ increases. Moreover, as shown in Figure 2.7, the phase at the origin is linear for τ large enough, namely $\phi(0,\tau) \sim C\tau$. The constant C is obtained by fitting the phase at the origin using linear least squares over the interval $[\tau_{max}/2, \tau_{max}]$ After extracting this linear phase, the rescaled solution u tends to a time-independent function, (Figure 2.8):

$$u(\xi,\tau) \sim S(\xi)e^{i(\theta+C\tau)} \quad \text{as} \quad \tau \to \infty. \tag{2.1.11}$$

To check the accuracy of our computation, we compute the scaling factor $L(t)$ in

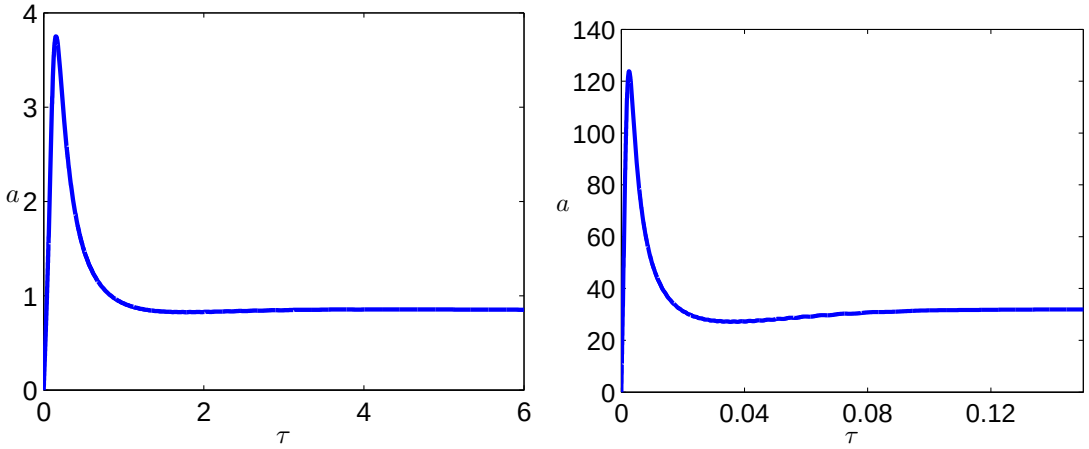

Figure 2.4: Time evolution of $a(\tau)$, with initial condition (2.1.9) (left) and (2.1.10) (right), $A_0 = 3$.

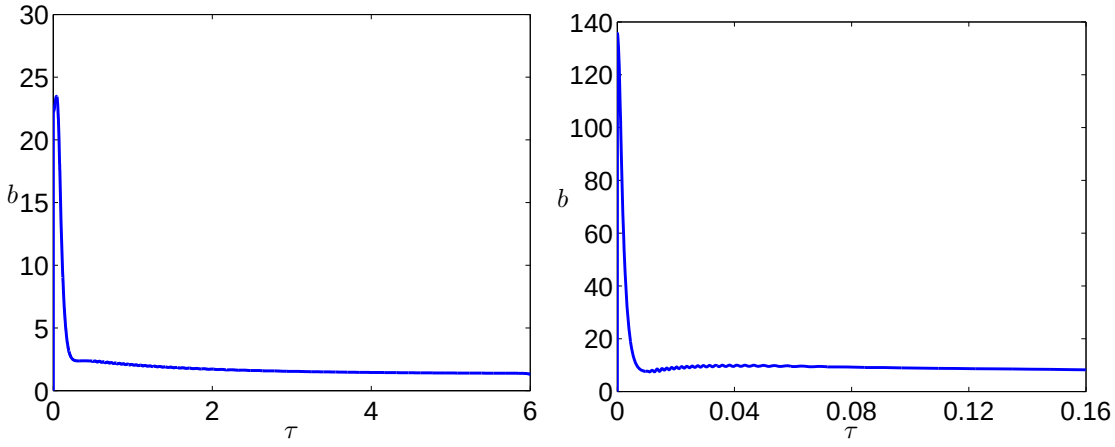

Figure 2.5: Time evolution of $b(\tau)$, with initial condition (2.1.9) (left) and (2.1.10) (right), $A_0 = 3$.

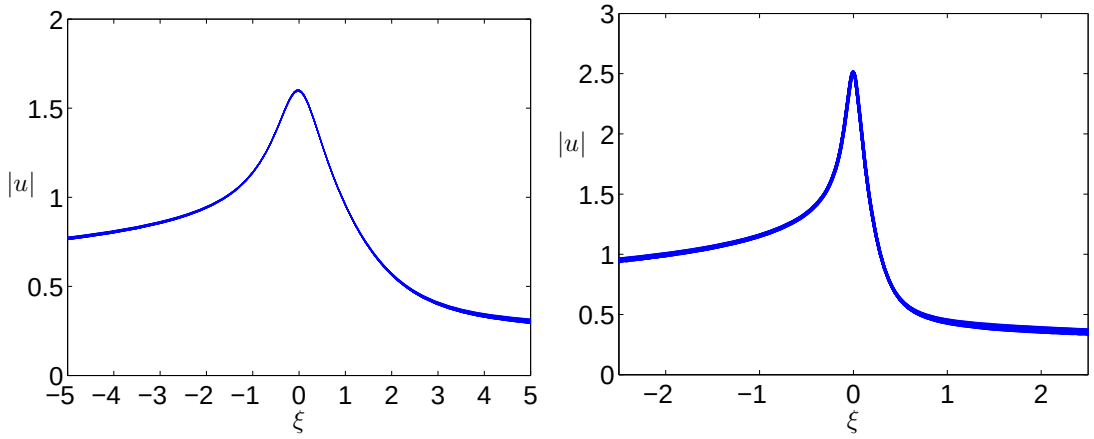

Figure 2.6: $|u(\xi,\tau)|$ versus ξ , with initial condition (2.1.9) for τ from 4.05 to 6 with an increment of 0.08. (left) and initial condition (2.1.10) for τ from 0.12 to 0.16 with an increment of 0.002. (right).

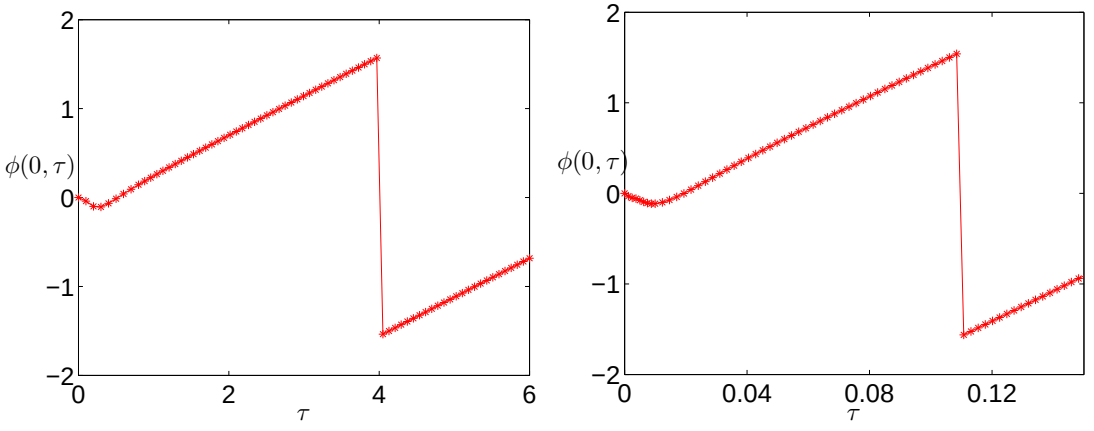

Figure 2.7: Time evolution of the phase at the origin $\phi(0,\tau)$, with initial conditions (2.1.9) (left) and (2.1.10) (right).

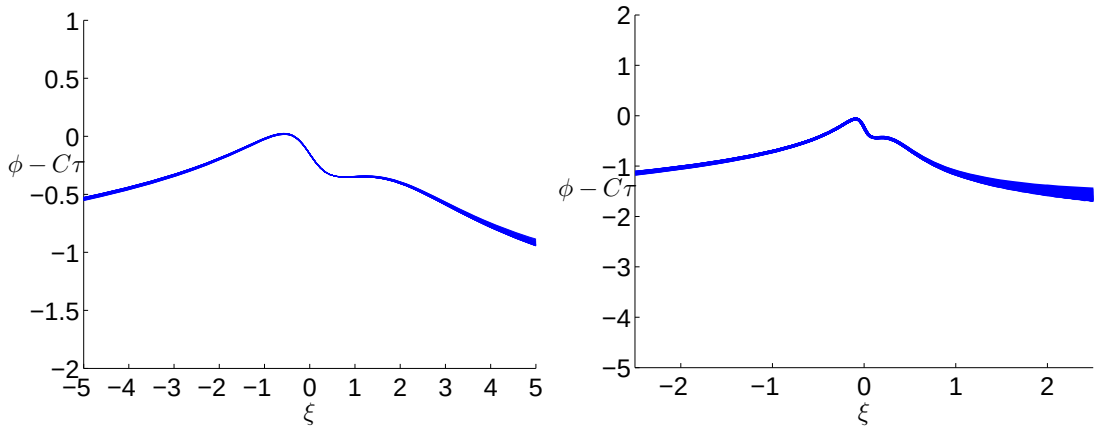

Figure 2.8: Time evolution of the modified phase $\phi(\xi,\tau)-\phi(0,\tau)$, with initial conditions (2.1.9) for τ from 4.05 to 6 with an increment of 0.08. (left) and (2.1.10) for τ from 0.12 to 0.16 with an increment of 0.002. (right).

different ways. Either from the invariant quantities (2.1.8)

$$L_e = \left(\frac{E(\psi)}{E(u)}\right)^{-\frac{\sigma}{1+\sigma}}, \quad L_m = \left(\frac{M(\psi)}{M(u)}\right)^{-\frac{\sigma}{1-\sigma}} \tag{2.1.12}$$

or from integration of (2.1.3a),

$$L_a = L_0 e^{-\int_0^\tau a(\tau)d\tau}. \tag{2.1.13}$$

Since we have real initial conditions, we cannot use the momentum. Table 2.1 shows the values of $L(t)$ obtained in the simulation corresponding to the initial condition $\psi_0(x) = 3e^{-2x^2}$ and $\sigma = 2$. The results are in good agreement.

Table 2.1: Estimates of $L(\tau)$, calculated using (2.1.12) and (2.1.13), with the initial condition (2.1.9), $A_0 = 3$.

τ	1	2	3	4	5	6
L_e	0.03545	0.015233	0.006588	0.002811	0.001196	0.000595
L_m	0.03545	0.015233	0.006588	0.002811	0.001196	0.000555
L_a	0.035449	0.015233	0.006588	0.002811	0.001196	0.000555

We also checked convergence of our algorithm with respect to the number of grid points. Table 2.2 shows that the L^∞-difference between simulations decreases rapidly as the resolution increases. For these comparisons, lower resolution simulations are spectrally interpolated onto the highest resolution grid.

Table 2.2: Convergence of our algorithm for initial condition (2.1.9) with $A_0 = 3$. u_{14}, u_{15}, u_{16}, and u_{17} are the solutions with $N = 2^{14}, 2^{15}, 2^{16}$ and 2^{17} grid points, respectively.

	$\tau = 0.8$	$\tau = 2.1$	$\tau = 3.4$	$\tau = 4.7$
$\|u_{14} - u_{17}\|_{L^\infty}$	2.3×10^{-1}	3.0×10^{-1}	2.4×10^{-1}	2.1×10^{-1}
$\|u_{15} - u_{17}\|_{L^\infty}$	3.0×10^{-3}	1.5×10^{-3}	8.1×10^{-4}	7.5×10^{-4}
$\|u_{16} - u_{17}\|_{L^\infty}$	3.4×10^{-8}	2.9×10^{-8}	2.7×10^{-8}	3.1×10^{-8}

Using (2.1.3) and the fact $a(\tau)$ and $b(\tau)$ tend to constants A and B (Figures 2.4 and 2.5), we conclude

$$L^2 \sim 2A(t^* - t), \tag{2.1.14}$$

and,

$$\frac{dx_0}{dt} = \frac{B}{\sqrt{2A(t^* - t)}},$$

where t^* is the blowup time. It follows that

$$x_0 \sim x^* - B\sqrt{2(t^* - t)/A}, \tag{2.1.15}$$

where x^* is the position of $\max_x |\psi(x, t^*)|$. Substituting into (2.1.7), we obtain

$$S_{\xi\xi} - CS + iA(\tfrac{1}{4}S + \xi S_\xi) - iBS_\xi + i|S|^4 S_\xi = 0. \tag{2.1.16}$$

Introducing the scaling

$$\widetilde{\xi} = \sqrt{C}\xi, \quad Q(\widetilde{\xi}) = C^{-\frac{1}{8}} S(\xi), \tag{2.1.17}$$

and dropping the tildes, we have

$$Q_{\xi\xi} - Q + i\alpha(\tfrac{1}{4}Q + \xi Q_\xi) - i\beta Q_\xi + i|Q|^4 Q_\xi = 0,$$

with the rescaled constants:

$$\alpha \equiv \frac{A}{C}, \quad \beta \equiv \frac{B}{\sqrt{C}}. \tag{2.1.18}$$

Like supercritical NLS, we find that the coefficients α and β and the function Q are independent of the initial conditions. Table 2.3 shows that the ratios α and β take the values $\alpha \sim 1.95$ and $\beta \sim 2.08$. In Figure 2.9 and 2.10, we see that the amplitude and phase of the function Q constructed from the different initial conditions coincide.

In conclusion, we have observed that for a large class of initial conditions, solutions to (1.1.1) with quintic nonlinearity ($\sigma = 2$) may blow up in a finite time. More precisely,

Table 2.3: Limiting values of the parameters for various initial conditions.

u_0	C	A	B	α	β
$2e^{-2x^2}$	1.615	3.159	2.639	1.96	2.08
$3e^{-2x^2}$	0.438	0.854	1.385	1.94	2.09
$4e^{-2x^2}$	2.44	4.759	3.29	1.95	2.10
$\frac{3}{(1+(3x)^2)}$	16.52	31.89	8.33	1.93	2.05

from the change of variable in (2.1.1) and (2.1.14), we have

$$\begin{aligned}\tau &= \int_0^t \frac{ds}{2A(t^*-t)} = -\frac{1}{2A}\ln(t^*-t)\Big|_0^t \\ &= \frac{1}{2A}\ln\left(\frac{t^*}{t^*-t}\right),\end{aligned} \tag{2.1.19}$$

and

$$\begin{aligned}\psi &= L^{-1/8}(t)u\left(\frac{x-x_0}{L},\tau\right) \\ &= (2A(t^*-t))^{-1/8}u\left(\frac{x-x_0}{L},\tau\right).\end{aligned} \tag{2.1.20}$$

Substituting (2.1.11) into the above equation,

$$\psi \sim (2A(t^*-t))^{-1/8}S\left(\frac{x-x_0}{L}\right)e^{i(\theta+C\tau)}.$$

Using (2.1.17), (2.1.15) and(2.1.19), we have

$$\begin{aligned}\psi &= (2A(t^*-t))^{-1/8}C^{1/8}Q\left(\sqrt{C}\frac{x-x_0}{L}\right)e^{i(\theta+C\tau)} \\ &= \left(\frac{C}{2A(t^*-t)}\right)^{1/8}Q\left(\frac{x-(x^*-B\sqrt{2(t^*-t)/A})}{\sqrt{2A(t^*-t)}}\right)e^{i(\theta+C\tau)} \\ &= \left(\frac{C}{2A(t^*-t)}\right)^{1/8}Q\left(\frac{x-x^*}{\sqrt{2A(t^*-t)/C}}+\frac{B\sqrt{C}}{A}\right)e^{i(\theta+\frac{C}{2A}\ln\left(\frac{t^*}{t^*-t}\right))}.\end{aligned} \tag{2.1.21}$$

Noting that $\alpha = A/C$ and $\beta = B/\sqrt{C}$, we have

$$\psi(x,t) \sim \left(\frac{1}{2\alpha(t^*-t)}\right)^{\frac{1}{8}}Q\left(\frac{x-x^*}{\sqrt{2\alpha(t^*-t)}}+\frac{\beta}{\alpha}\right)e^{i(\theta+\frac{1}{2\alpha}\ln\frac{t^*}{t^*-t})}, \tag{2.1.22}$$

which is the local description of the solution (1.3.3) near the singularity with $\sigma = 2$.

The inclusion of the translation parameter is a significant difference from NLS with power law nonlinearity. While later studies on singularity formation in NLS allowed for symmetry breaking [43], the preservation of radial symmetry under the flow strongly simplifies both the computations and the analysis. Due to the mixture of hyperbolic and dispersive terms in gDNLS, no such symmetry preservation is available, and we must be aware of the tendency for the solution to migrate rightwards.

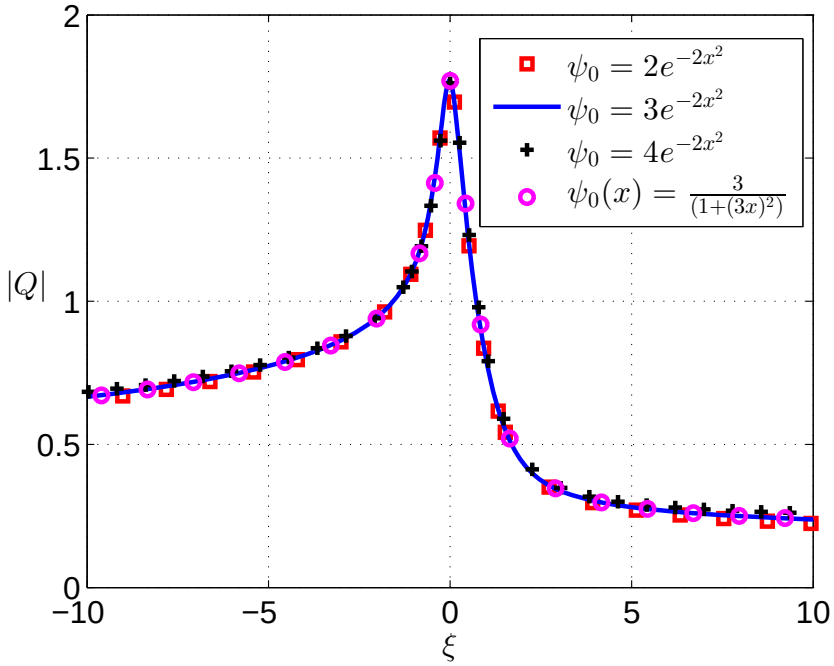

Figure 2.9: Asymptotic profile $|Q(\xi)|$ for different initial data.

2.2 gDNLS with Other Power Nonlinearities

The following calculations address the question of singularity for solutions of (1.1.1) when the power in the nonlinear term $|\psi|^{2\sigma}\psi_x$ is such that $1 < \sigma < 2$. We recall that $\sigma = 1$ corresponds to the usual DNLS equation which is L^2-critical. Our calculations cover the values of σ down to 1.1. Computational difficulties precluded us from reducing it much further. The initial condition is $\psi_0(x) = 3e^{-2x^2}$ when $\sigma = 1.7, 1.5$ and 1.3, while $\psi_0 = 4e^{-2x^2}$ for $\sigma = 1.1$. Our results are similar to that obtained with $\sigma = 2$. For convenience, we present the figures in the same order as Figures 2.4 to 2.8. Figures 2.11 and 2.12 show that a and b tend to constant values as τ gets large. As shown in Figure 2.13, $|u|$ tends to a fixed profile as τ increases. Figure 2.14 indicates that the phase at

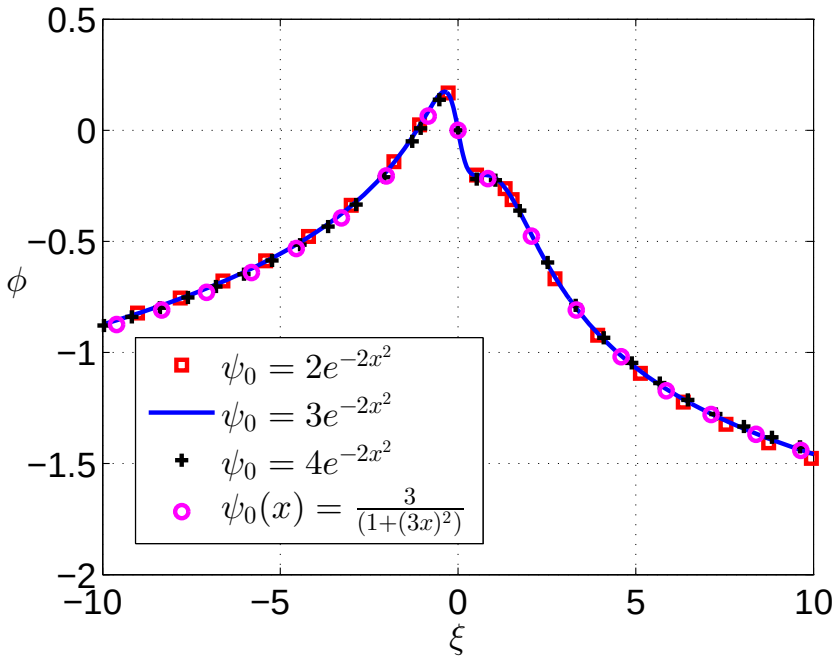

Figure 2.10: Asymptotic phase $\phi(\xi) \equiv \arg(Q(\xi))$ for different initial data.

the origin is linear for τ large enough. After extracting this linear phase, the phase of u tends to a time-independent function, Figure 2.15. We also notice that as σ increases, the transient period shortens. Table 2.4 shows that α decreases as σ varies from 2 to 1.1, while β first decreases and then increases.

The main conclusion of our study is that for this range of values of σ, solutions to (1.1.1) may blow up in a finite time. Their local structure is similar to that of the case $\sigma = 2$ discussed in the previous section and given by (1.3.3).

Table 2.4: Values of α and β as σ approaches to 1.

σ	2	1.7	1.5	1.3	1.1
α	1.95	1.31	0.85	0.38	0.04
β	2.08	1.82	1.65	1.61	1.82

2.3 Blowup Profile

This section is devoted to the study of the nonlinear elliptic equation (1.3.4) satisfied by the complex profile function Q. It is helpful to change variables, letting $\eta = \xi - \frac{\beta}{\alpha}$,

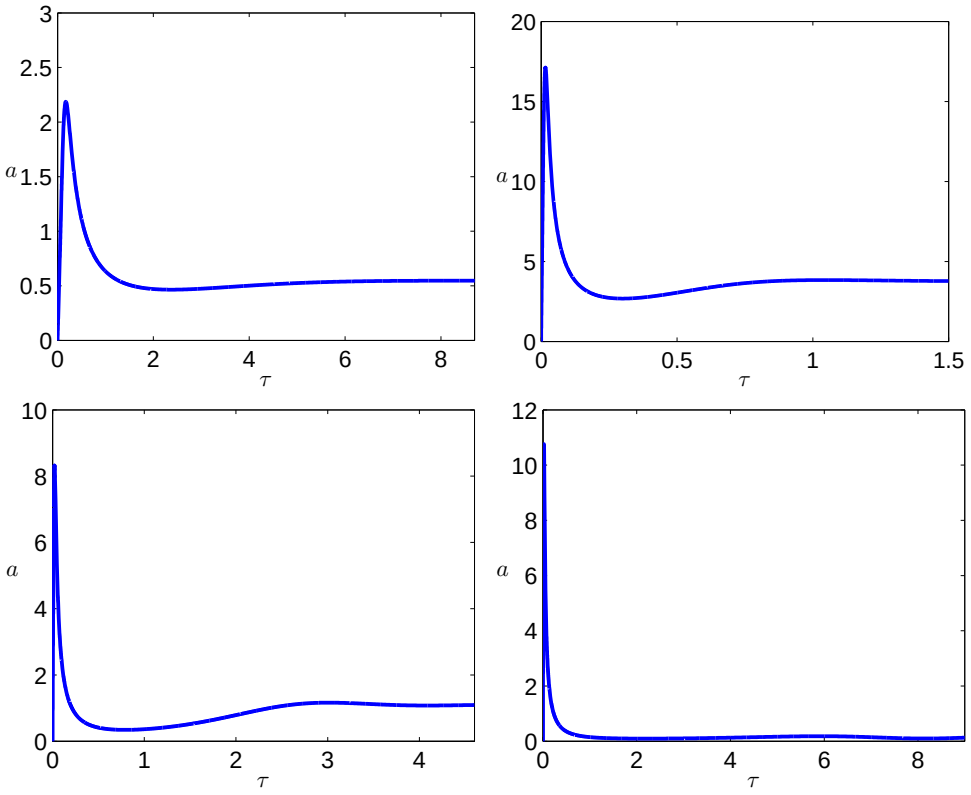

Figure 2.11: Time evolution of $a(\tau)$, for $\sigma = 1.7$ (upper left), $\sigma = 1.5$ (upper right), $\sigma = 1.3$ (lower left), and $\sigma = 1.1$ (lower right).

leading to

$$Q_{\eta\eta} - Q + i\alpha(\tfrac{1}{2\sigma}Q + \eta Q_\eta) + i|Q|^{2\sigma}Q_\eta = 0. \tag{2.3.1}$$

We seek profiles $|Q(\eta)|$ that decrease monotonically with $|\eta|$, satisfying the conditions

$$Q(\eta) \to 0 \quad \text{as} \quad \eta \to \pm\infty.$$

This can be viewed as a nonlinear eigenvalue problem, with eigenparameter α, and eigenfunction Q. As the equation is invariant under multiplication by a constant phase, we can assume, in addition, that $Q(0)$ is real (for example).

2.3.1 Properties of the Asymptotic Profile

Proposition 2.3.1. *Up to a constant phase, there are two kinds of large-distance behavior* ($|\eta| \to \infty$) *of the solutions* Q *of* (2.3.1)*:*

$$Q_1 \approx A_1|\eta|^{-\frac{i}{\alpha}-\frac{1}{2\sigma}} \tag{2.3.2}$$

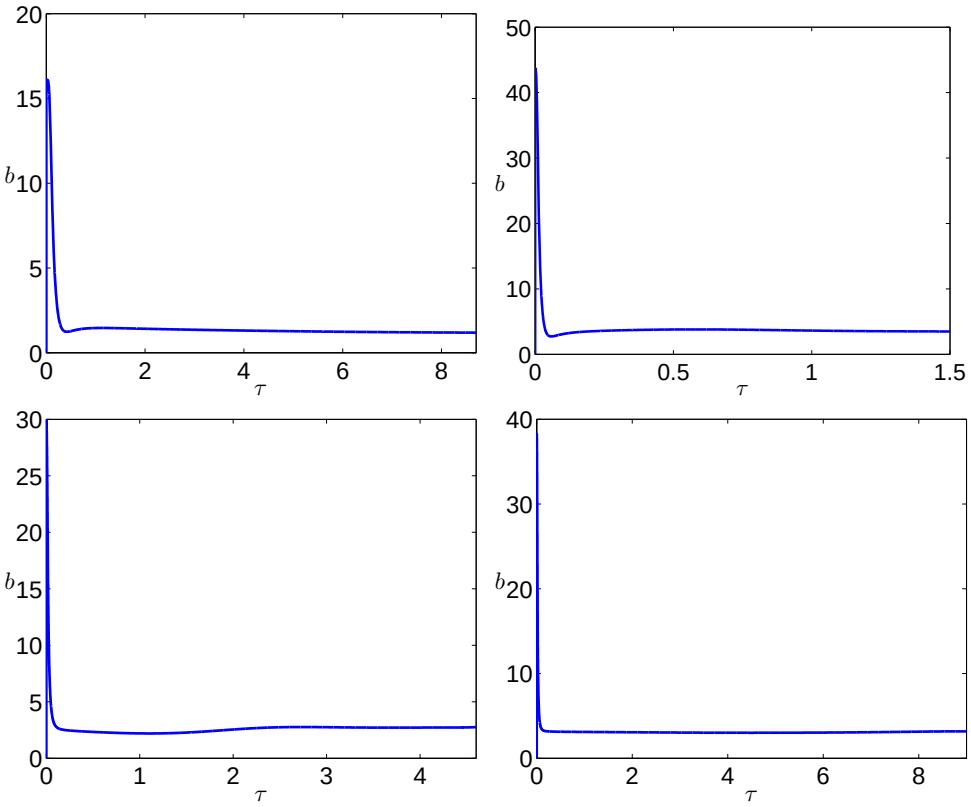

Figure 2.12: Time evolution of $b(\tau)$, for $\sigma = 1.7$ (upper left), $\sigma = 1.5$ (upper right), $\sigma = 1.3$ (lower left), and $\sigma = 1.1$ (lower right).

or

$$Q_2 \approx A_2 e^{-i\frac{\alpha}{2}\eta^2} |\eta|^{\frac{i}{\alpha}+\frac{1}{2\sigma}-1} \tag{2.3.3}$$

where A_1, A_2 are complex numbers.

Proof. We write $Q(\eta) = X(\eta)Z(\eta)$. It follows $Q_\eta = X_\eta Z + XZ_\eta$ and $Q_{\eta\eta} = X_{\eta\eta}Z + 2Z_\eta X_\eta + XZ_{\eta\eta}$. After substitution in (2.3.1), we have

$$\begin{aligned} &X_{\eta\eta}Z + 2Z_\eta X_\eta + XZ_{\eta\eta} - XZ + i\alpha(\frac{1}{2\sigma}XZ + \eta X_\eta Z + \eta XZ_\eta) \\ &\quad + i|X|^{2\sigma}|Z|^{2\sigma}(X_\eta Z + Z_\eta X) = 0. \end{aligned} \tag{2.3.4}$$

After simplification, it becomes

$$\begin{aligned} &XZ_{\eta\eta} + (2X_\eta + i\alpha\eta X + iX|X|^{2\sigma}|Z|^{2\sigma})Z_\eta \\ &\quad + (X_{\eta\eta} - X + i\frac{\alpha}{2\sigma}X + i\alpha\eta X_\eta + i|X|^{2\sigma}|Z|^{2\sigma}X_\eta)Z = 0. \end{aligned} \tag{2.3.5}$$

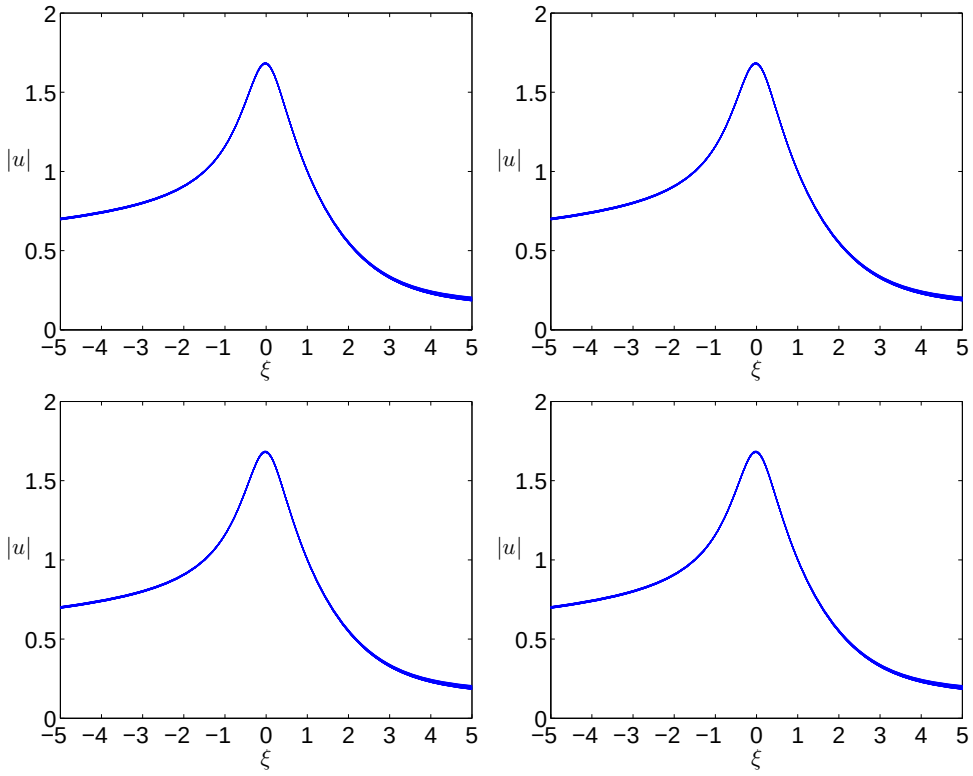

Figure 2.13: $|u(\xi,\tau)|$ versus ξ, for $\sigma = 1.7$ when τ changes from 6 to 8.7 with an increment of 0.09 (upper left), $\sigma = 1.5$ when τ changes from 1.2 to 1.5 with an increment of 0.04 (upper right), $\sigma = 1.3$ when τ changes from 3.1 to 4.6 with an increment of 0.16 (lower left), and $\sigma = 1.1$ when τ changes from 7.6 to 9 with an increment of 0.12 (lower right).

Choosing

$$X = e^{-i\frac{\alpha}{4}\eta^2 - i\frac{1}{2}\int_0^\eta |Z|^{2\sigma} d\eta} = e^{-i\frac{\alpha}{4}\eta^2 - i\frac{1}{2}\int_0^\eta |Q|^{2\sigma} d\eta} \tag{2.3.6}$$

we have

$$X_\eta = \frac{1}{2}(-i\alpha\eta - i|Z|^{2\sigma})X,$$

$$X_{\eta\eta} = \left(-\frac{i\alpha}{2} - \frac{i}{2}(|Z|^{2\sigma})_\eta + \frac{1}{4}(-i\alpha\eta - i|Z|^{2\sigma})^2\right) X.$$

and

$$Z_{\eta\eta} + \left(\frac{i\alpha(1-\sigma)}{2\sigma} - 1 + \frac{(\alpha\eta)^2}{4} + \frac{|Z|^{4\sigma}}{4} + \frac{\alpha}{2}\eta|Z|^{2\sigma} - \frac{i}{2}(|Z|^{2\sigma})_\eta\right) Z = 0 \tag{2.3.7}$$

Letting $Z = Ae^{i\phi}$ be an amplitude-phase decomposition, equation (2.3.7) is equivalent to

$$\frac{A''}{A} - (\phi')^2 - 1 + \frac{\alpha^2\eta^2}{4} + \frac{\alpha\eta}{2}A^{2\sigma} + \frac{1}{4}A^{4\sigma} = 0 \tag{2.3.8a}$$

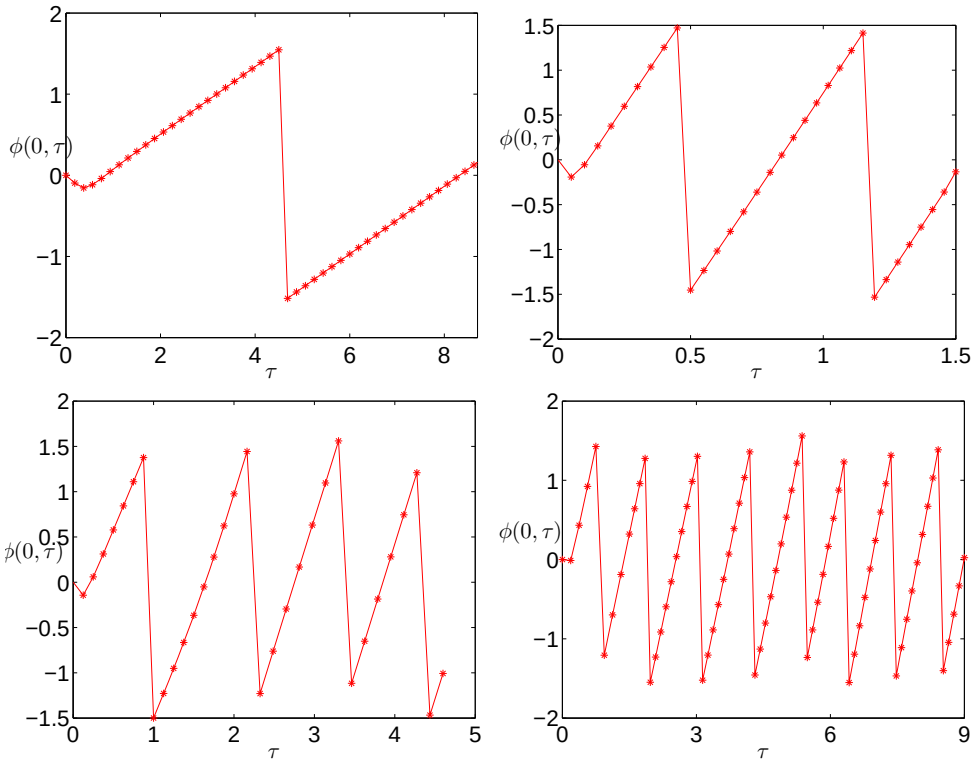

Figure 2.14: Time evolution of the phase at the origin $\phi(0,\tau)$, for $\sigma = 1.7$ (upper left), $\sigma = 1.5$ (upper right), $\sigma = 1.3$ (lower left), and $\sigma = 1.1$ (lower right).

$$\phi'' + 2\phi'\frac{A'}{A} + \frac{\alpha(1-\sigma)}{2\sigma} - \frac{1}{2}(A^{2\sigma})' = 0 \tag{2.3.8b}$$

Since $A \to 0$, as $\eta \to \pm\infty$, we assume that $A = A_0|\eta|^c + O(|\eta|^{c-1})$, where $A_0 \neq 0$ and $c < 0$. Denoting $\theta = \phi'$, equation (2.3.8a) becomes

$$-\theta^2 - 1 + \frac{\alpha^2\eta^2}{4} \pm \frac{\alpha}{2}A_0^{2\sigma}|\eta|^{2c\sigma+1} + \frac{1}{4}A_0^{4\sigma}|\eta|^{4c\sigma} = O(|\eta|^{-2}) + O(|\eta|^{2c\sigma}) \tag{2.3.9a}$$

$$\theta' + 2\theta c\eta^{-1} + \frac{\alpha(1-\sigma)}{2\sigma} \pm \sigma c|\eta|^{2\sigma c-1} = O(|\eta|^{2\sigma c-2}) + O(\theta|\eta|^{-2}). \tag{2.3.9b}$$

In (2.3.9a), since $c < 0$ and $\sigma > 1$, $4c\sigma < 2c\sigma + 1 < 1$. Thus, only the term $(\theta')^2$ can balance the $\frac{\alpha^2\eta^2}{4}$ in the above equation. It follows $\theta = \pm\frac{\alpha\eta}{2} + O(1)$.

Case 1: When $\theta = \frac{\alpha\eta}{2} + O(1)$, noticing that $|\eta|^{2\sigma c-2} < |\eta|^{-1} = O(\theta|\eta|^{-2})$, (2.3.9b) becomes

$$\frac{\alpha}{2} + \alpha c + \frac{1-\sigma}{2\sigma}\alpha \pm \sigma c|\eta|^{2\sigma c-1} = O(|\eta|^{-1}),$$

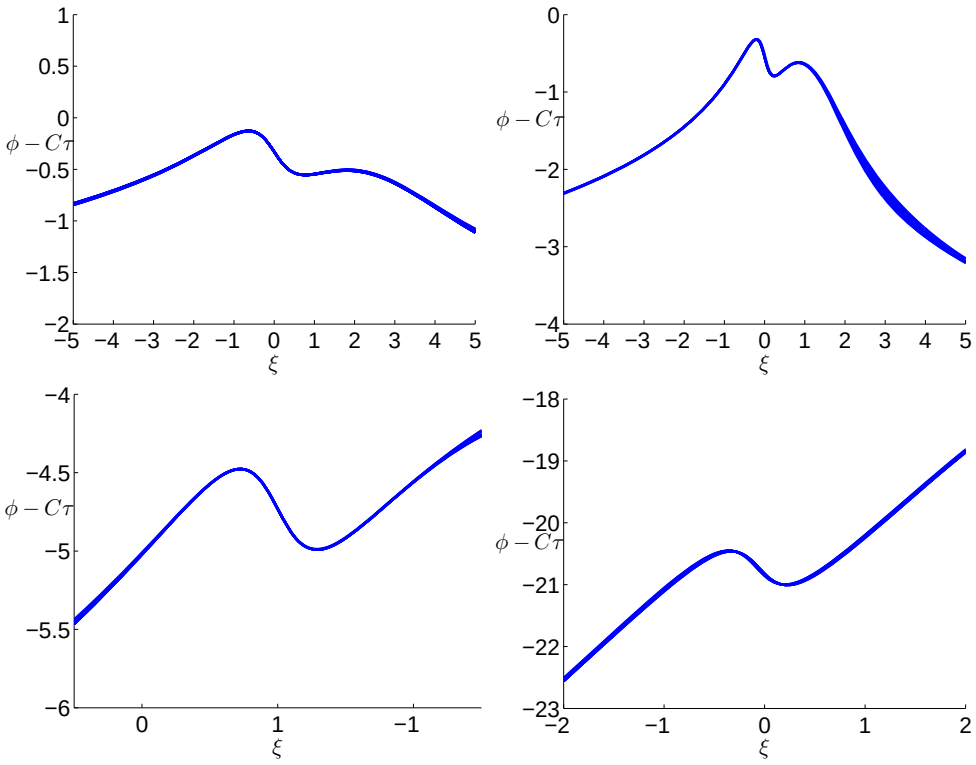

Figure 2.15: Time evolution of the modified phase $\phi(\xi,\tau) - \phi(0,\tau)$, for $\sigma = 1.7$ when τ changes from 6 to 8.7 with an increment of 0.09 (upper left), $\sigma = 1.5$ when τ changes from 1.2 to 1.5 with an increment of 0.04 (upper right), $\sigma = 1.3$ when τ changes from 3.1 to 4.6 with an increment of 0.16 (lower left), and $\sigma = 1.1$ when τ changes from 7.6 to 9 with an increment of 0.12 (lower right).

which implies $c = -\frac{1}{2\sigma}$. Hence, (2.3.9a) becomes

$$-\theta^2 - 1 + \frac{\alpha^2\eta^2}{4} \pm \frac{\alpha}{2}A_0^{2\sigma} = O(\eta^{-1}). \tag{2.3.10}$$

Let

$$\theta = \frac{\alpha}{2}\eta + c_0 + c_{-1}\eta^{-1} + O(\eta^{-2}),$$

equation (2.3.10) takes the form

$$\begin{aligned} -(\frac{\alpha^2}{4}\eta^2 + c_0^2 + c_{-1}^2\eta^{-2} + \alpha c_0\eta + \alpha c_{-1} + 2c_0c_{-1}\eta^{-1}) \\ + \frac{\alpha^2}{4}\eta^2 - 1 \pm \frac{\alpha}{2}A_0^{2\sigma} = O(\eta^{-1}), \end{aligned} \tag{2.3.11}$$

which simplifies to

$$-\alpha c_0\eta - c_0^2 - \alpha c_{-1} - 1 \pm \frac{\alpha}{2}A_0^{2\sigma} = O(\eta^{-1}). \tag{2.3.12}$$

Balancing the constant and first order terms in η gives us $c_0 = 0, c_{-1} = \pm\frac{1}{2}A_0^{2\sigma} - \frac{1}{\alpha}$. Thus,

$$\phi \approx \frac{\alpha}{4}\eta^2 + (\pm\frac{1}{2}A_0^{2\sigma} - \frac{1}{\alpha})\ln|\eta| + \phi_0.$$

Because (2.3.1) is invariant by adding a constant phase, we set $\phi_0 = 0$ and get

$$\phi \approx \frac{\alpha}{4}\eta^2 + (\pm\frac{1}{2}A_0^{2\sigma} - \frac{1}{\alpha})\ln|\eta|.$$

Therefore,

$$\begin{aligned} Z_1 &\approx A_0 e^{i\left(\frac{\alpha}{4}\eta^2 + (\pm\frac{1}{2}A_0^{2\sigma} - \frac{1}{\alpha})\ln|\eta|\right)}|\eta|^{-\frac{1}{2\sigma}} \\ &\approx A_0 e^{i\frac{\alpha}{4}\eta^2}|\eta|^{i(\pm\frac{1}{2}A_0^{2\sigma} - \frac{1}{\alpha}) - \frac{1}{2\sigma}}. \end{aligned} \tag{2.3.13}$$

Recalling

$$X = e^{-i\frac{\alpha}{4}\eta^2 - i\frac{1}{2}\int_0^\eta |Z|^{2\sigma}d\eta} \approx e^{-i\frac{\alpha}{4}\eta^2}|\eta|^{\mp\frac{i}{2}A_0^{2\sigma}}, \tag{2.3.14}$$

we have

$$Q_1 \approx XZ_1 = A_0|\eta|^{-\frac{i}{\alpha} - \frac{1}{2\sigma}}. \tag{2.3.15}$$

Case 2: When $\theta = -\frac{\alpha\eta}{2} + O(1)$, substituting it into (2.3.9b), we get

$$-\frac{\alpha}{2} - c\alpha + \frac{1-\sigma}{2\sigma}\alpha - \frac{1}{2}\sigma c\eta^{2\sigma c - 1} = O(|\eta|^{-1}),$$

which implies $c = \frac{1}{2\sigma} - 1$. (2.3.9a) then becomes

$$-\theta^2 - 1 + \frac{(\alpha\eta)^2}{4} \pm \frac{\alpha}{2}A_0^{2\sigma}|\eta|^{2-2\sigma} + \frac{1}{4}A_0^{4\sigma}|\eta|^{2-4\sigma} = O(|\eta|^{-2}) + O(|\eta|^{1-2\sigma}), \tag{2.3.16}$$

when $\sigma > 1$, $|\eta|^{2-4\sigma} \ll |\eta|^{1-2\sigma}$, so we have

$$-\theta^2 - 1 + \frac{(\alpha\eta)^2}{4} \pm \frac{\alpha}{2}A_0^{2\sigma}|\eta|^{2-2\sigma} = O(|\eta|^{-2}) + O(|\eta|^{1-2\sigma}). \tag{2.3.17}$$

Furthermore, since $|\eta|^{1-2\sigma} \ll 1, |\eta|^{-2} \ll 1$, and $|\eta|^{1-2\sigma} \ll 1$, equation (2.3.17) takes the form

$$-\theta^2 - 1 + \frac{(\alpha\eta)^2}{4} = o(1), \tag{2.3.18}$$

Let $\theta = -\frac{\alpha}{2}\eta + c_0 + c_{-1}\eta^{-1} + o(|\eta|^{-1})$, we get

$$\theta^2 = \frac{\alpha^2}{4}\eta^2 + c_0^2 - \alpha c_0 \eta - \alpha c_{-1} + o(1). \tag{2.3.19}$$

Substituting it into (2.3.18), we obtain

$$-c_0^2 + \alpha c_0 \eta + \alpha c_{-1} - 1 = o(1), \tag{2.3.20}$$

which implies $c_0 = 0$, and $c_{-1} = \frac{1}{\alpha}$. Hence,

$$\theta = -\frac{\alpha}{2}\eta + \frac{1}{\alpha}\eta^{-1} + o(|\eta|^{-1}),$$

and, up to a constant,

$$\phi = -\frac{\alpha}{4}\eta^2 + \frac{1}{\alpha}\ln|\eta| + o(1).$$

Therefore

$$\begin{aligned} Z_2 &\approx A_0 e^{i\left(-\frac{\alpha}{4}\eta^2 + \frac{1}{\alpha}\ln|\eta|\right)}|\eta|^{\frac{1}{2\sigma}-1} \\ &\approx A_0 e^{-i\frac{\alpha}{4}\eta^2}|\eta|^{\frac{i}{\alpha}+\frac{1}{2\sigma}-1} \end{aligned} \tag{2.3.21}$$

and

$$X = e^{-i\frac{\alpha}{4}\eta^2 - i\frac{1}{2}\int_0^\eta |Z|^{2\sigma}d\eta} \approx e^{-i\frac{\alpha}{4}\eta^2 \mp i\frac{1}{2(2-2\sigma)}|\eta|^{2-2\sigma}A_0^{2\sigma}}. \tag{2.3.22}$$

Since we only consider terms larger than $o(1)$ in the equation of phase (2.3.18), we can simplify the expression of X, using $|\eta|^{2-2\sigma} \ll O(1)$, and obtain

$$X \approx e^{-i\frac{\alpha}{4}\eta^2}.$$

Therefore,

$$Q_2 \approx A_0 e^{-i\frac{\alpha}{2}\eta^2}|\eta|^{\frac{i}{\alpha}+\frac{1}{2\sigma}-1}. \tag{2.3.23}$$

□

Remark 1. In Case 1, we balanced the phase equation (2.3.10) up to the order of $O(|\eta|^{-1})$, while in Case 2, we only considered the phase equation (2.3.18) with the reminder term in the order of $o(1)$. We can calculate the phase to the next correction in Case 2, and obtain different expressions of Q_2, depending on whether $1 < \sigma \leq 3/2$ or

$\sigma > 3/2$. More precisely, when $1 < \sigma \leq 3/2$, the expression is

$$Q_2 \approx A_2 e^{i(-\frac{\alpha}{2}\eta^2 \mp \frac{|A_2|^{2\sigma}}{(2-2\sigma)}|\eta|^{2-2\sigma})}|\eta|^{\frac{i}{\alpha}+\frac{1}{2\sigma}-1}, \tag{2.3.24}$$

and when $\sigma > 3/2$, the expression is the same as (2.3.3)

$$Q_2 \approx A_2 e^{-i\frac{\alpha}{2}\eta^2}|\eta|^{\frac{i}{\alpha}+\frac{1}{2\sigma}-1}, \tag{2.3.25}$$

where A_2 is a complex constant, and $'\mp'$ corresponds to $\eta \to \pm\infty$, respectively. Indeed, we simplify (2.3.17) into two cases:

Case 2.1 When $1 < \sigma \leq 3/2$, $|\eta|^{-2} \lesssim |\eta|^{1-2\sigma}$. It follows that equation (2.3.18) takes the form of

$$-\theta^2 - 1 + \frac{(\alpha\eta)^2}{4} \pm \frac{\alpha}{2}A_0^{2\sigma}|\eta|^{2-2\sigma} = O(|\eta|^{1-2\sigma}). \tag{2.3.26}$$

Let

$$\theta = -\frac{\alpha}{2}\eta + c_0 + c_{-1}\eta^{-1} + c_r|\eta|^r + O(\eta^{-2}), \tag{2.3.27}$$

where $-2 < r < -1$, we have

$$\begin{aligned}\theta^2 = &\frac{\alpha^2}{4}\eta^2 + c_0^2 + c_{-1}^2\eta^{-2} + c_r^2|\eta|^{2r} - \alpha c_0\eta - \alpha c_{-1} \mp \alpha c_r|\eta|^{1+r} \\ &+ 2c_0c_{-1}\eta^{-1} + 2c_0c_r|\eta|^r \pm 2c_{-1}c_r|\eta|^{-1+r} + O(\eta^{-1}) \\ = &\frac{\alpha^2}{4}\eta^2 - \alpha c_0\eta + c_0^2 - \alpha c_{-1} \mp \alpha c_r|\eta|^{1+r} + O(\eta^{-1}).\end{aligned} \tag{2.3.28}$$

Substituting into (2.3.26) gives

$$\alpha c_0\eta - c_0^2 + \alpha c_{-1} - 1 \pm \alpha c_r|\eta|^{1+r} \pm \frac{\alpha}{2}A_0^{2\sigma}|\eta|^{2-2\sigma} = O(\eta^{-1}). \tag{2.3.29}$$

This implies $c_0 = 0, c_{-1} = \frac{1}{\alpha}$, $c_r = -\frac{A_0^{2\sigma}}{2}$ and $r = 1 - 2\sigma$. Hence

$$\theta = -\frac{\alpha}{2}\eta + \frac{1}{\alpha}\eta^{-1} - \frac{A_0^{2\sigma}}{2}|\eta|^{1-2\sigma},$$

and, up to a constant,

$$\phi = -\frac{\alpha}{4}\eta^2 + \frac{1}{\alpha}\ln|\eta| \mp \frac{A_0^{2\sigma}}{2(2-2\sigma)}|\eta|^{2-2\sigma} + \phi_0.$$

Therefore,

$$\begin{aligned} Z_2 &= A_0 e^{i\left(-\frac{\alpha}{4}\eta^2+\frac{1}{\alpha}\ln|\eta|\mp\frac{A_0^{2\sigma}}{2(2-2\sigma)}|\eta|^{2-2\sigma}\right)}|\eta|^{\frac{1}{2\sigma}-1} \\ &= A_0 e^{i\left(-\frac{\alpha}{4}\eta^2\mp\frac{A_0^{2\sigma}}{2(2-2\sigma)}|\eta|^{2-2\sigma}\right)}|\eta|^{\frac{i}{\alpha}+\frac{1}{2\sigma}-1}. \end{aligned} \tag{2.3.30}$$

Using

$$X = e^{-i\frac{\alpha}{4}\eta^2-i\frac{1}{2}\int_0^\eta |Z|^{2\sigma}d\eta} \approx e^{-i\frac{\alpha}{4}\eta^2\mp\frac{A_0^{2\sigma}}{2(2-2\sigma)}|\eta|^{2-2\sigma}d\eta}, \tag{2.3.31}$$

we obtain

$$Q_2 = A_0 e^{-i\frac{\alpha}{2}\eta^2}|\eta|^{\frac{i}{\alpha}+\frac{1}{2\sigma}-1}e^{\mp i\frac{A_0^{2\sigma}}{(2-2\sigma)}|\eta|^{2-2\sigma}}. \tag{2.3.32}$$

Case 2.2 When $\sigma > 3/2$, $|\eta|^{1-2\sigma} \le |\eta|^{-2}$. Thus , (2.3.17) becomes

$$-\theta^2 - 1 + \frac{(\alpha\eta)^2}{4} \pm \frac{\alpha}{2}A_0^{2-2\sigma} = O(|\eta|^{-2}). \tag{2.3.33}$$

Defining θ as (2.3.27), and using $|\eta|^{2-2\sigma} < |\eta|^{-1}$, we have

$$\alpha c_0\eta - c_0^2 + \alpha c_{-1} - 1 \pm \alpha c_r|\eta|^{1+r} = O(|\eta|^{-1}). \tag{2.3.34}$$

It follows $c_0 = 0$, $c_{-1} = \frac{1}{\alpha}$ and $c_r = 0$. Hence

$$\theta \approx -\frac{\alpha}{2}\eta + \frac{1}{\alpha}\eta^{-1},$$

and, up to a constant,

$$\phi \approx -\frac{\alpha}{4}\eta^2 + \frac{1}{\alpha}\ln|\eta|.$$

Therefore

$$\begin{aligned} Z_2 &\approx A_0 e^{i\left(-\frac{\alpha}{4}\eta^2+\frac{1}{\alpha}\ln|\eta|\right)}|\eta|^{\frac{1}{2\sigma}-1} \\ &\approx A_0 e^{-i\frac{\alpha}{4}\eta^2}|\eta|^{\frac{i}{\alpha}+\frac{1}{2\sigma}-1} \end{aligned} \tag{2.3.35}$$

and

$$X = e^{-i\frac{\alpha}{4}\eta^2-i\frac{1}{2}\int_0^\eta |Z|^{2\sigma}d\eta} \approx e^{-i\frac{\alpha}{4}\eta^2\mp i\frac{1}{2(2-2\sigma)}|\eta|^{2-2\sigma}A_0^{2\sigma}}. \tag{2.3.36}$$

Since we only consider terms larger than $O(|\eta|^{-1})$ in the equation of phase (2.3.34), we

can simplify the expression of X, using $|\eta|^{2-2\sigma} \ll O(|\eta|^{-1})$, and obtain

$$X \approx e^{-i\frac{\alpha}{4}\eta^2}.$$

Therefore,

$$Q_2 \approx A_0 e^{-i\frac{\alpha}{2}\eta^2} |\eta|^{\frac{i}{\alpha}+\frac{1}{2\sigma}-1}. \tag{2.3.37}$$

The next property describes the energy of Q.

Proposition 2.3.2. *If Q is a solution of (2.3.1) with $Q_\eta \in L^2(\mathbb{R})$ and $Q \in L^{4\sigma+2}(\mathbb{R})$, its energy vanishes:*

$$\int_{-\infty}^{\infty} |Q_\eta|^2 d\eta + \frac{1}{(\sigma+1)} \Im \int_{-\infty}^{\infty} |Q|^{2\sigma} \bar{Q} Q_\eta d\eta = 0. \tag{2.3.38}$$

Proof. Multiplying (2.3.1) by $\bar{Q}_{\eta\eta}$, taking the imaginary parts, and integrating over the whole line gives

$$\alpha \Re \int \left(\frac{Q}{2\sigma} + \eta Q_\eta \right) \bar{Q}_{\eta\eta} d\eta + \Re \int |Q|^{2\sigma} Q_\eta \bar{Q}_{\eta\eta} d\eta = 0. \tag{2.3.39}$$

The first integral of (2.3.39) can be written

$$\alpha \Re \int \left(\frac{Q}{2\sigma} + \eta Q_\eta \right) \bar{Q}_{\eta\eta} d\eta = \left(-\frac{\sigma+1}{2\sigma} \right) \alpha \int |Q_\eta|^2 d\eta. \tag{2.3.40}$$

Using (2.3.1) to express $\bar{Q}_{\eta\eta}$, the second integral becomes

$$\begin{aligned} &\Re \int |Q|^{2\sigma} Q_\eta \left(\bar{Q} + i\alpha(\frac{1}{2\sigma}\bar{Q} + \eta \bar{Q}_\eta) + i|Q|^{2\sigma} \bar{Q}_\eta \right) d\eta \\ &= \Re \int |Q|^{2\sigma} Q_\eta \bar{Q} + \frac{i\alpha}{2\sigma} |Q|^{2\sigma} Q_\eta \bar{Q} d\eta \\ &= \frac{1}{2} \int (|Q|^{2\sigma} Q_\eta \bar{Q} + |Q|^{2\sigma} \bar{Q}_\eta Q) d\eta - \frac{\alpha}{2\sigma} \Im \int |Q|^{2\sigma} Q_\eta \bar{Q} d\eta \\ &= -\frac{\alpha}{2\sigma} \Im \int |Q|^{2\sigma} Q_\eta \bar{Q} d\eta. \end{aligned} \tag{2.3.41}$$

Combining (2.3.40) and (2.3.41), we obtain (2.3.38). □

The following property shows that solutions with finite energy have an infinite L^2-norm.

Proposition 2.3.3. *If Q is a solution of (2.3.1) with $\sigma > 1$ and $\alpha > 0$, and $Q \in H^1(\mathbb{R}) \bigcap L^{4\sigma+2}(\mathbb{R})$, then $Q \equiv 0$.*

Proof. Multiplying (2.3.1) by $\bar{Q}$, taking the imaginary part, and integrating over $\mathbb{R}$, we get

$$\frac{\alpha}{2}\left(\frac{1}{\sigma} - 1\right)\int |Q|^2 d\eta = 0, \tag{2.3.42}$$

thus Q has to be identically zero. □

Remark 2. When $\eta \to \infty$, By the Proposition 2.3.1, $Q_1 \approx |\eta|^{-\frac{i}{\alpha}-\frac{1}{2\sigma}} = e^{\frac{i}{\alpha}\ln|\eta|}|\eta|^{-\frac{1}{2\sigma}}$, so we have $|\partial_\eta Q_1| \approx |\eta|^{-\frac{1}{2\sigma}-1}$, this follows $|\partial_\eta Q_1|^2 \approx ||Q_1|^{2\sigma}\bar{Q}_1\partial_\eta Q_1| \approx |\eta|^{-\frac{1}{\sigma}-2}$. But $Q_2 \approx e^{-\frac{i\alpha\eta^2}{2}+\frac{i}{\alpha}\ln|\eta|}|\eta|^{\frac{1}{2\sigma}-1}$, hence we have $|\partial_\eta Q_2| \approx |\eta|^{\frac{1}{2\sigma}}$. Therefore $|\partial_\eta Q_2|^2 \approx |\eta|^{\frac{1}{\sigma}}$, while $||Q_2|^{2\sigma}\bar{Q}_2\partial_\eta Q_2| \approx |\eta|^{\frac{1}{\sigma}-2\sigma}$. This follows that Q_2 does not have a finite Hamiltonian. Hence, the "admissible solutions" should be in the form of $A_1 Q_1$.

2.3.2 Numerical Integration of the Boundary Value Problem

The purpose of this section is the numerical integration of the BVP (2.3.1) in order to better understand the asymptotic profile of the singular solutions of gDNLS. We look for solutions that behave like $A_1^{\pm}Q_1$ as $\eta \to \pm\infty$,where $A_1^{\pm}$ are complex constants, because Q_2 does not have finite energy. It is convenient to rewrite the large η behavior as a Robin boundary condition of the form

$$-Q + i\alpha\left(\frac{1}{2\sigma}Q + \eta Q_\eta\right) = 0, \quad |\eta| \to \infty. \tag{2.3.43}$$

Solutions of (2.3.1) depend on the coefficient α. Since the equation is invariant under phase translation, we need an additional condition; for example, setting the phase to zero at a particular point is satisfactory. This suggests that α needs to take particular values, like in the supercritical NLS problem, [62]. We are particularly interested in the character of the asymptotic profile and of the coefficient α as σ approaches the critical case $\sigma = 1$. Our approach is a continuation method in the parameter σ.

At first, we attempted to integrate (2.3.1) with boundary conditions (2.3.43) for values of σ starting from $\sigma = 2$ to about $\sigma = 1.2$. We observed that the peak of $|Q|$ rapidly moved to the left of the domain as σ decreased, limiting our calculations (Figure 2.16).

To reach values of σ closer to 1, we returned to (1.3.4) (which is equivalent to (2.3.1) after the translation $\xi = \eta + \beta/\alpha$). Now the parameter β is free and will be chosen so that the maximum of $|Q|$ is at $\xi = 0$. This adds a condition, namely $|Q|_\xi(0) = 0$ and an additional unknown, the coefficient β. Figure 2.17 shows that the solution of

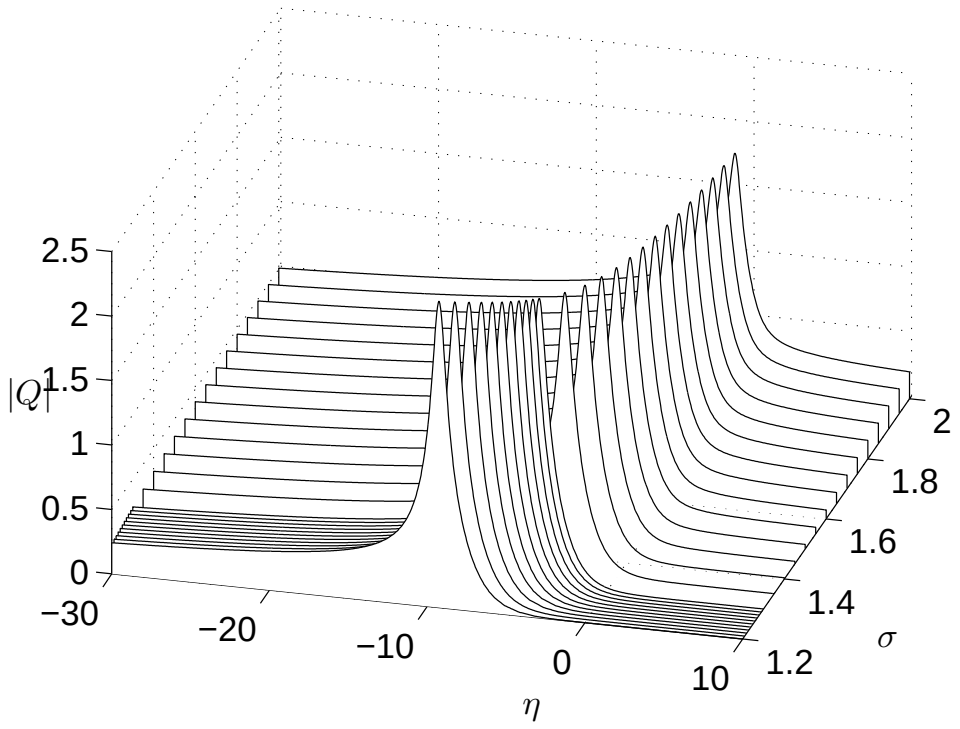

Figure 2.16: Asymptotic profile $|Q(\eta)|$ for various σ, where β has been translated to zero and the peak is permitted move.

(1.3.4) when σ varies from 2 to 1.08. As $\sigma \to 1$, we make several observations on Q. The amplitude increases, and the left shoulder becomes lower. Oscillations also appear in the real and imaginary components (Figure 2.18). We observe that the parameter α decreases as σ approaches 1, while β first decreases and then increases (Figure 2.19). A detailed analysis of the dependence of these parameters on σ is the subject of a future study.

In practice, we integrated (1.3.4) in two adjacent domains $(-\infty, 0]$ and $[0, \infty)$, using the multipoint feature of the MATLAB `bvp4c` solver, with Robin boundary conditions at $\pm\infty$ and continuity conditions on Q and its first derivative Q_ξ at $\xi = 0$. Additional details are given in Section 2.5.

2.4 Numerical Method for Integrating the Time Dependent Equation

Since the equation (1.1.3) is the same as the equation (2.1.7) with $a(\tau) = 0$ and $b(\tau) = 0$, we use the same code for the direct Fourier transform simulation and the dynamic rescaling simulation (Section 2.1). In order to overcome the difficulties introduced by

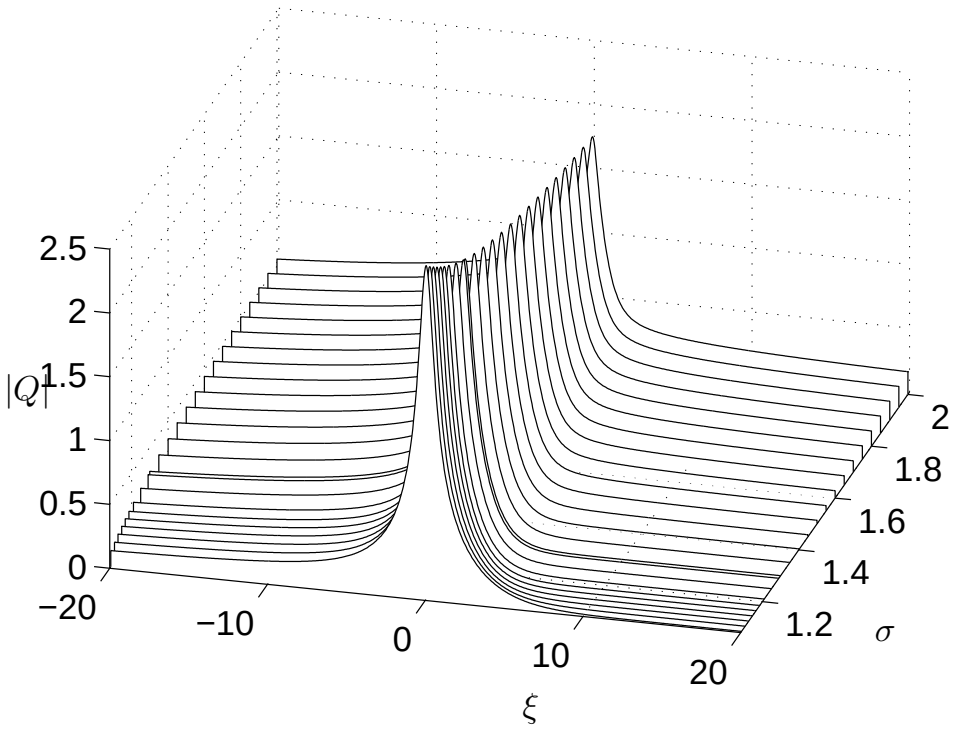

Figure 2.17: Asymptotic profile $|Q(\xi)|$ for various σ, where β is a free parameter and the peak is fixed at the origin.

the combination of nonlinearity and stiffness in (1.1.1), we use the modified fourth order exponential time-differencing Runge-Kutta scheme (ETDRK4). In this section, we first give a description about the ETDRK4 scheme, and then apply it to the gDNLS equation.

2.4.1 Exponential Time Differencing

The exponential time-differencing (ETD) schemes were firstly introduced by Cox and Matthews, and then improved by Kassam and Trefethen [16, 37]. It can handle certain problems associated with eigenvalues equal to or close to zero, especially when the matrix is not diagonal. More precisely, consider the PDE in the general form,

$$u_t = \mathcal{L}u + \mathcal{N}(u, t),$$

where $\mathcal{L}$ and $\mathcal{N}$ are linear and nonlinear operators, respectively. Discretizing the spatial part of this equation, we get a system of ODEs:

$$u_t = \mathbf{L}u + \mathbf{N}(u, t). \tag{2.4.1}$$

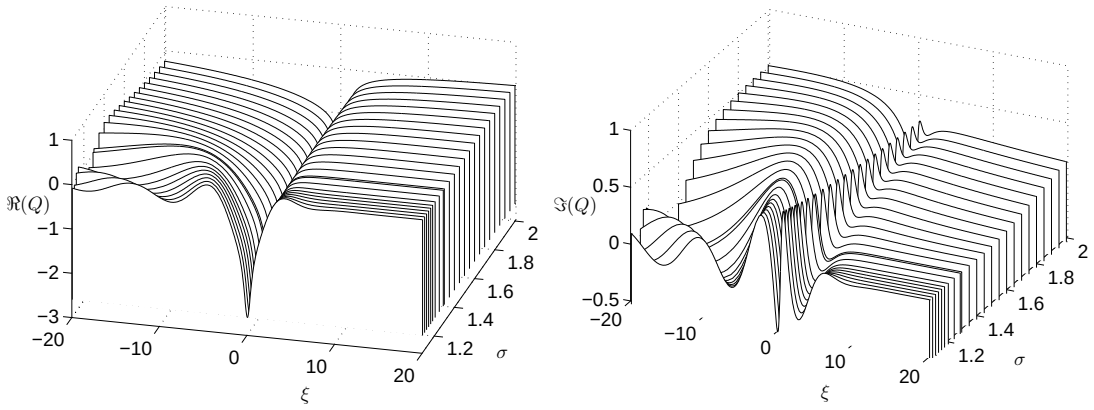

Figure 2.18: Asymptotic profile $\Re(Q)$ (left) and $\Im(Q)$ (right) for various σ.

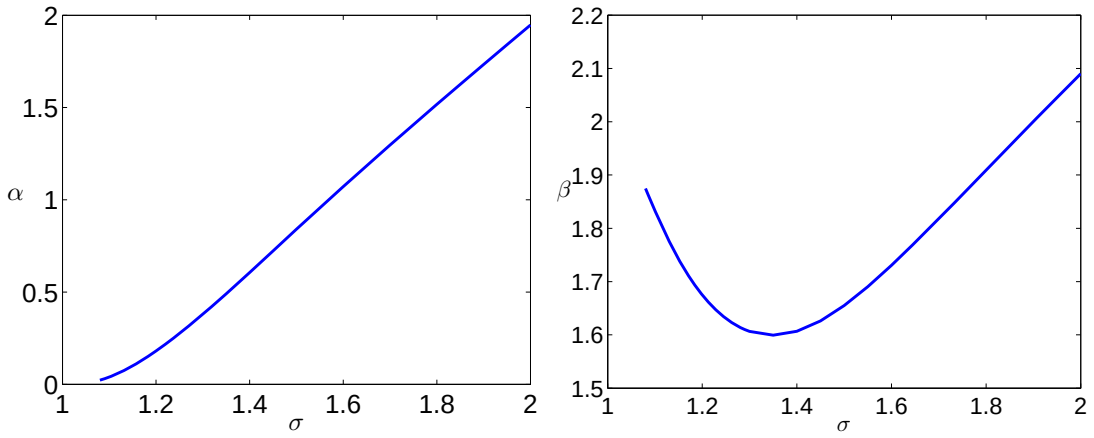

Figure 2.19: Coefficients α (left) and β (right) versus σ.

In order to solve the linear part exactly, we define

$$v = e^{-\mathbf{L}t}u, \tag{2.4.2}$$

where the term $e^{-\mathbf{L}t}$ is called the *integrating factor*, well known in the theory of ODEs. Differentiating (2.4.2) gives

$$v_t = -e^{-\mathbf{L}t}\mathbf{L}u + e^{-\mathbf{L}t}u_t. \tag{2.4.3}$$

Multiplying (2.4.1) by the integrating factor, we have

$$e^{-\mathbf{L}t}u = e^{-\mathbf{L}t}u + e^{-\mathbf{L}t}\mathbf{N}(u,t).$$

Substituting (2.4.3) into this equation gives

$$v_t = e^{-\mathbf{L}t}\mathbf{N}(e^{\mathbf{L}t}v, t). \tag{2.4.4}$$

The linear term in (2.4.1) involves high frequency that constrains the stability. Introducing the integrating factor allows in principle to use larger time steps. In classical methods, one directly applies a time-stepping method to (2.4.4). For example, at the n-th time step, defining $f(v_n, t_n) = e^{-\mathbf{L}t_n}\mathbf{N}(e^{\mathbf{L}t_n}v_n, t_n)$, the fourth order Runge-Kutta scheme is

$$\begin{aligned} a =& hf(v_n, t_n), \\ b =& hf(v_n + a/2, t_n + h/2), \\ c =& hf(v_n + b/2, t_n + h/2), \\ d =& hf(v_n + c, t_n + h), \\ v_{n+1} =& v_n + \frac{1}{6}(a + 2b + 2c + d), \end{aligned} \tag{2.4.5}$$

where h is the time step. However, in the ETD method, one integrates (2.4.4) over a single time step of length h,

$$u_{n+1} = e^{\mathbf{L}h}u_n + e^{\mathbf{L}h}\int_0^h e^{-\mathbf{L}h}\mathbf{N}(u(t_n + \tau), t_n + \tau)d\tau.$$

There are various methods to approximate the integral on the right hand side, Cox and Matthews present a sequence of recurrence formula that provide a high order accuracy approximation. The generating formula is

$$u_{n+1} = e^{\mathbf{L}h}u_n + h\sum_{n=0}^{s-1} g_m \sum_{k=0}^{m}(-1)^k \binom{m}{k}\mathbf{N}_{n-k},$$

where s is the order of the scheme. The coefficients g_m are computed by

$$\begin{aligned} \mathbf{L}hg_0 &= e^{\mathbf{L}h} - \mathbf{I}, \\ \mathbf{L}hg_{m+1} + \mathbf{I} &= g_m + \frac{1}{2}g_{m-1} + \frac{1}{3}g_{m-2} + \cdots + \frac{g_0}{m+1}, m \geq 0. \end{aligned}$$

Table 2.5: Computation of $g(z)$ by two different methods. All computations are done in double precision in Matlab.

z	Formula (2.4.7)	5-term Taylor	Exact
1	1.71828182845905	1.71666666666667	1.71828182845905
1e-1	1.05170918075648	1.05170916666667	1.05170918075648
1e-2	1.00501670841679	1.00501670841667	1.00501670841681
1e-3	1.00050016670838	1.00050016670834	1.00050016670834
1e-4	1.00005000166714	1.00005000166671	1.00005000166671
1e-5	1.00000500000696	1.00000500001667	1.00000500001667
1e-6	1.00000049996218	1.00000050000017	1.00000050000017
1e-7	1.00000004943368	1.00000005000000	1.00000005000000
1e-8	0.99999999392253	1.00000000500000	1.00000000500000
1e-9	1.00000008274037	1.00000000050000	1.00000000050000
1e-10	1.00000008274037	1.00000000005000	1.00000000005000
1e-11	1.00000008274037	1.00000000000500	1.00000000000500
1e-12	1.00008890058234	1.00000000000050	1.00000000000050
1e-13	0.99920072216264	1.00000000000005	1.00000000000005

Based on the fourth order Runge-Kutta time-stepping, Cox and Matthews give a fourth order exponential time differencing formula (ETDRK4),

$$\begin{aligned}
a_n =& e^{\mathbf{L}h/2}u_n + \mathbf{L}^{-1}(e^{\mathbf{L}h/2} - \mathbf{I})\mathbf{N}(u_n, t_n),\\
b_n =& e^{\mathbf{L}h/2}u_n + \mathbf{L}^{-1}(e^{\mathbf{L}h/2} - \mathbf{I})\mathbf{N}(a_n, t_n + h/2),\\
c_n =& e^{\mathbf{L}h/2}a_n + \mathbf{L}^{-1}(e^{\mathbf{L}h/2} - \mathbf{I})(2\mathbf{N}(b_n, t_n + h/2) - \mathbf{N}(u_n, t_n)),\\
u_{n+1} =& e^{\mathbf{L}h}u_n + h^{-2}\mathbf{L}^{-3}\{[-4 - \mathbf{L}h + e^{\mathbf{L}h}(4 - 3\mathbf{L}h + (\mathbf{L}h)^2)]\mathbf{N}(u_n, t_n)\\
&+ 2[2 + \mathbf{L}h + e^{\mathbf{L}h}(-2 + \mathbf{L}h)](\mathbf{N}(a_n, t_n + h/2) + \mathbf{N}(b_n, t_n + h/2))\\
&+ [-4 - 3\mathbf{L}h - (\mathbf{L}h)^2 + e^{\mathbf{L}h}(4 - \mathbf{L}h)]\mathbf{N}(c_n, t_n + h)\}.
\end{aligned} \tag{2.4.6}$$

However, this formula suffers form numerical instability. To understand this better, consider the function

$$g(z) = \frac{e^z - 1}{z}. \tag{2.4.7}$$

Computing this function accurately is a well known problem in numerical analysis (See [31]). Table 2.5 shows the value of $g(z)$ generated by direct computation of (2.4.7) and by five terms of a Taylor expansion. Both methods do not provide correct values for all z: for large z, the direct computation gives better results than the Taylor expansion method; on the other hand, for small z, the direct computation fails due to cancellation errors, but the Taylor expansion method give satisfactory results; especially, for $z = 10^{-2}$,

neither is accurate. In the ETDRK4 scheme, we need compute three coefficients,

$$\begin{aligned}\alpha =& h^{-2}\mathbf{L}^{-3}[-4-\mathbf{L}h+e^{\mathbf{L}h}(4-3\mathbf{L}h+(\mathbf{L}h)^2)],\\ \beta =& h^{-2}\mathbf{L}^{-3}[2+\mathbf{L}h+e^{\mathbf{L}h}(-2+\mathbf{L}h)],\\ \gamma =& h^{-2}\mathbf{L}^{-3}[-4-3\mathbf{L}h-(\mathbf{L}h)^2+e^{\mathbf{L}h}(4-\mathbf{L}h)].\end{aligned} \tag{2.4.8}$$

Those coefficients are analogues of (2.4.7), in the sense that they all suffer cancellation errors when $\mathbf{L}$ has eigenvalues close to zero. In order to compute these coefficients valued for all z, Kassam and Trefethen [37] use ideas of complex analysis . Consider a function $f(z)$, which is analytic except for a removable singularity at $z=0$, the goal is to find the exact value of $f(z)$ when z is near the singularity. This can be achieved by evaluating $f(z)$ via an integral over a contour Γ in the complex plane that contains z and is separated from zero:

$$f(z)=\frac{1}{2\pi i}\int_\Gamma \frac{f(t)}{t-z}dt.$$

When z is a matrix $\mathbf{L}$,

$$f(\mathbf{L})=\frac{1}{2\pi i}\int_\Gamma \frac{f(t)}{t\mathbf{I}-\mathbf{L}}dt,$$

where Γ is any contour containing the eigenvalues of $\mathbf{L}$. In practice, the contour integral is computed by the trapezoid rule. Thirty two equally spaced points are usually sufficient to obtain an accurate solution.

2.4.2 Integrating the Time Dependent Equation

To integrate (2.1.2) with ETDRK4, we need to convert the equation into the form of (2.4.4). This is achieved by the Fourier pseudospectral method. After Fourier transform and simplification, (2.1.2) becomes

$$\hat{u}_\tau + ik^2\hat{u} = -\frac{a(\tau)}{2\sigma}\hat{u} - a(\tau)\widehat{\xi u_\xi} - \widehat{|u|^{2\sigma}u_\xi}. \tag{2.4.9}$$

Multiplying both sides by the integration factor $e^{ik^2\tau}$, we get

$$(e^{ik^2\tau}\hat{u})_\tau = -\frac{a(\tau)}{2\sigma}e^{ik^2\tau}\hat{u} - a(\tau)e^{ik^2\tau}\widehat{\xi u_\xi} - e^{ik^2\tau}\widehat{|u|^{2\sigma}u_\xi}. \tag{2.4.10}$$

Let $v = e^{ik^2\tau}\hat{u}$, we have the main equation in our iteration:

$$\begin{aligned} v_\tau =& - e^{ik^2\tau}\left\{\frac{a(\tau)}{2\sigma}\hat{u} + a(\tau)\widehat{\xi u_\xi} + \widehat{|u|^{2\sigma}u_\xi}\right\} \\ =& - e^{ik^2\tau}\mathcal{F}\left(\frac{a(\tau)}{2\sigma}u + a(\tau)\xi u_\xi + |u|^{2\sigma}u_\xi\right), \end{aligned} \tag{2.4.11}$$

where $u = \mathcal{F}^{-1}(e^{-ik^2\tau}v)$. We then use the ETDRK4 scheme (2.4.6) for time discretization, and choose an integration domain large enough so that u is very small at the extremities.

2.5 Numerical Method of the Boundary Value Problem

2.5.1 `bvp4c` solver in MATLAB

"`bvp4c`" is a MATLAB solver for ordinary differential equations. It can integrate systems of ODEs of the form

$$\mathbf{y}' = \mathbf{f}(x, \mathbf{y}).$$

on an interval $[a, b]$ subject to two-point boundary value conditions

$$\mathbf{bc}(\mathbf{y}(a), \mathbf{y}(b)) = 0,$$

as presented in [41, 59]. It has the following features:

- It can integrate problems with unknown parameters, such as

  $$\mathbf{y}' = \mathbf{f}(x, \mathbf{y}, \mathbf{p}), \quad a \le x \le b$$

  subject to boundary conditions

  $$\mathbf{g}(\mathbf{y}(a), \mathbf{y}(b), \mathbf{p}) = 0.$$

  The solver provides approximations for the solution $\mathbf{y}(x)$ and the unknown parameter $\mathbf{p}$.

- It has fourth order accuracy, i.e. $\|\mathbf{y}(x) - \mathbf{S}(x)\| \le Ch^4$, where $\mathbf{S}(x)$ is the approximate solution, and h is the maximum value of the spatial mesh distance $h_n = x_{n+1} - x_n$.

- It is a method that provides automatically grid refinement.

- It can solve problems with conditions given not only at the boundary points, but also possibly inside the interval.

"bvp4c" is not a shooting method. The latter is based on solutions of initial value problems for ODEs, while "bvp4c" approximates the solution $\mathbf{y}(x)$ for all x at the same time. More specifically, for a spatial discretization $a = x_0 < x_1 < \cdots < x_n = b$, the approximate solution $\mathbf{S}(x)$ is generated as a cubic polynomial on each subinterval $[x_n, x_{n+1}]$ and is continuous on $[a, b]$. $\mathbf{S}(x)$ satisfies

$$\begin{aligned} \mathbf{S}'(x_n) &= f(x_n, \mathbf{S}(x_n)), \\ \mathbf{S}'((x_n + x_{n+1})/2) &= f((x_n + x_{n+1})/2, \mathbf{S}((x_n + x_{n+1})/2)), \\ \mathbf{S}'(x_{n+1}) &= f(x_{n+1}, \mathbf{S}(x_{n+1})). \end{aligned} \tag{2.5.1}$$

on both ends and the midpoint of each subinterval. It also meets the boundary conditions

$$\mathbf{bc}(\mathbf{S}(a), \mathbf{S}(b)) = 0.$$

The resulting system is composed of nonlinear algebraic equations for the coefficients of $\mathbf{S}(x)$, which are solved iteratively by linearization.

2.5.2 Integrating the Boundary Value Problem

To integrate the nonlinear elliptic equation (1.3.4) for Q, we rewrite it as a first order system with the four unknowns, $\Re(Q), \Im(Q), \Re(Q_\xi)$ and $\Im(Q_\xi)$. As discussed before, we solve the system in two adjacent domains $[-A_L, 0]$ and $[0, A_R]$. The solutions and their first order derivatives are matched by continuity at $\xi = 0$, while the boundary conditions at infinity are of Robin type. We denote

$$y_1^{\pm} = \Re(Q),\ y_2^{\pm} = \Im(Q),\ y_3^{\pm} = \Re(Q_\xi),\ y_4^{\pm} = \Im(Q_\xi),$$

where y^- and y^+ are the solutions in $[-A_L, 0]$ and $[0, A_R]$ respectively. The system takes the form:

$$\begin{aligned}
\frac{dy_1^\pm}{d\xi} &= y_3^\pm, \\
\frac{dy_2^\pm}{d\xi} &= y_4^\pm, \\
\frac{dy_3^\pm}{d\xi} &= y_1^\pm + \alpha(\frac{1}{2\sigma} y_2^\pm + \xi y_4^\pm) - \beta y_4^\pm + \left[(y_1^\pm)^2 + (y_2^\pm)^2\right]^\sigma y_4^\pm, \\
\frac{dy_4^\pm}{d\xi} &= y_2^\pm - \alpha(\frac{1}{2\sigma} y_1^\pm + \xi y_3^\pm) + \beta y_3^\pm - \left[(y_1^\pm)^2 + (y_2^\pm)^2\right]^\sigma y_3^\pm.
\end{aligned} \tag{2.5.2}$$

Solving four first order ODEs in two regions with two unknown parameters requires imposing ten boundary conditions. From Proposition 2.3.1,

$$Q_1 \approx A_1 |\eta|^{-\frac{i}{\alpha} - \frac{1}{2\sigma}} \approx A_1 |\xi|^{-\frac{i}{\alpha} - \frac{1}{2\sigma}},$$

we have the Robin condition

$$-Q + i\alpha \left(\frac{1}{2\sigma} Q + \xi Q_\xi \right) = 0, \quad |\xi| \to \infty.$$

It follows that four of boundary conditions relating to $\Re(Q), \Im(Q), \Re(Q_\xi)$ and $\Im(Q_\xi)$ at $\xi = -A_L$ and $\xi = A_R$, respectively are

$$\begin{aligned}
-y_1^- - \frac{\alpha}{2\sigma} y_2^- - \alpha \xi y_4^- &= 0 \text{ at } \xi = -A_L, \\
-y_2^- + \frac{\alpha}{2\sigma} y_1^- + \alpha \xi y_3^- &= 0 \text{ at } \xi = -A_L, \\
-y_1^+ - \frac{\alpha}{2\sigma} y_2^+ - \alpha \xi y_4^+ &= 0 \text{ at } \xi = A_R, \\
-y_2^+ + \frac{\alpha}{2\sigma} y_1^+ + \alpha \xi y_3^+ &= 0 \text{ at } \xi = A_R.
\end{aligned} \tag{2.5.3}$$

We impose the continuity of the solution at $\xi = 0$:

$$\begin{aligned}
y_1^+(0) &= y_1^-(0), \\
y_2^+(0) &= y_2^-(0), \\
y_3^+(0) &= y_3^-(0), \\
y_4^+(0) &= y_4^-(0).
\end{aligned} \tag{2.5.4}$$

The other two conditions are $|Q(0)|_\xi = 0$ (the maximum value of Q is attained at the origin) and $\Im(Q(0)) = 0$ (because the equation is invariant by phase translation) :

$$\begin{aligned} y_1^- y_3^- + y_2^- y_4^- &= 0 \text{ at } \xi = 0, \\ y_2^- &= 0 \text{ at } \xi = 0 \end{aligned} \tag{2.5.5}$$

We proceed using a continuation method with respect to σ, starting from $\sigma = 2$ down to $\sigma = 1.08$. The MATLAB nonlinear solver `bvp4c` is used to integrate the system for each σ. The two domains are automatically handled using the multipoint feature, which permits for matching conditions at 0. One needs to provide a well-chosen initial guess. We use the final profile from our time-dependent simulation with the initial condition (2.1.9), $A_0 = 3$ and $\sigma = 2$, in the domain $[-10, 10]$ to extract the maximum bulk of the solution, (see Figures 2.9 and 2.10). This solution is then extended to a larger domain $[-150, 50]$ with an increment of 10. As shown in Figure 2.18, more and more oscillations occur as σ approaches 1. The calculation becomes very delicate and we use smaller and smaller increments of σ, namely $0.05, 0.01$ and 0.005 for σ in the intervals $2 \geq \sigma \geq 1.3, 1.3 \geq \sigma \geq 1.2$ and $1.2 \geq \sigma \geq 1.08$, respectively. We set the maximum mesh points at 5×10^5 and the tolerance of the difference between two iterations at 10^{-6}.

2.6 Discussion

We have numerically solved a derivative NLS equation with a general power nonlinearity and found evidence of a finite time singularity. We have determined that there is a square root blowup rate for the scaling factor $L(t)$. This implies that Sobolev norms should grow as

$$\|\partial_x^s \psi(x,t)\|_{L^2} \sim (t^* - t)^{\frac{\sigma-1}{4\sigma} - \frac{s}{2}}.$$

As with supercritical NLS, this equation has a universal blowup profile of the form (1.3.3). Indeed, Q, α and β are solutions of a nonlinear eigenvalue problem, and they do not depend on the initial conditions. They depend on the power nonlinearity σ. Another similarity to supercritical NLS is that the blowup profile, Q, is not in L^2 and has zero energy. Note that there are other types of singular solutions to supercritical NLS that were found recently [19] [34].

To conclude, we present numerical simulations of the DNLS equation with $\sigma = 1$ and several Gaussian initial conditions ($A_0 = 3, 4, 5, 6$). In all our simulations, the solution separates into several waves and disperses. None of our simulations have shown any evidence of a finite time singularity, although the transient dynamics can be quite

violent. Figure 2.20 shows the evolution of $|\psi(x,t)|$ with the Gaussian initial condition: $\psi_0(x) = 6e^{-2x^2}$. The maximum value of $|\psi|$ increases slowly in time and then stabilizes. We also integrated DNLS using the dynamic rescaling method. We found that $a(\tau)$ rapidly tends to zero and that the scaling factor $L(t)$ has a lower bound away from zero, (Figure 2.21). This is different with the critical NLS, which has a blowup rate at $\{\ln\ln[(t^*-t)^{-1}]/(t^*-t)\}^{1/2}$, due to the slow decay rate of $a(\tau)$, [42].

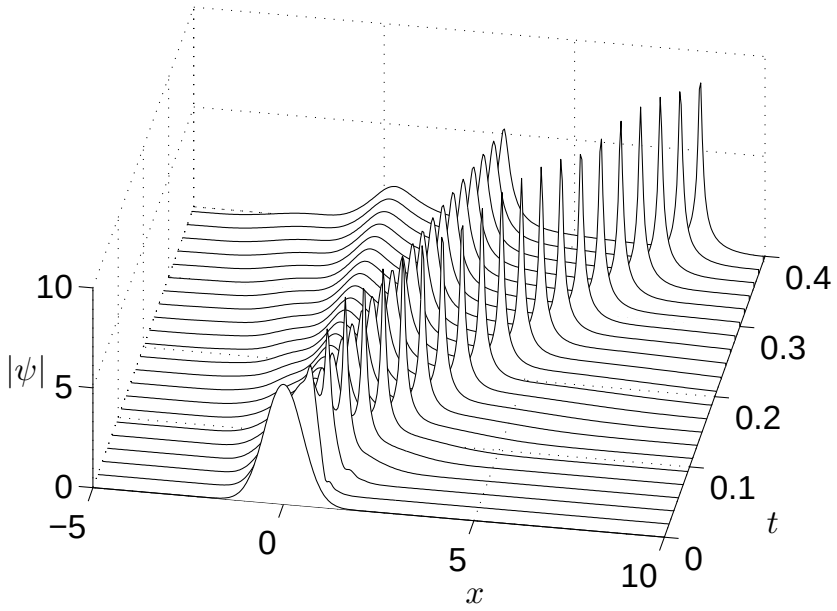

Figure 2.20: Time evolution of $|\psi(x,t)|$ for $\sigma = 1$.

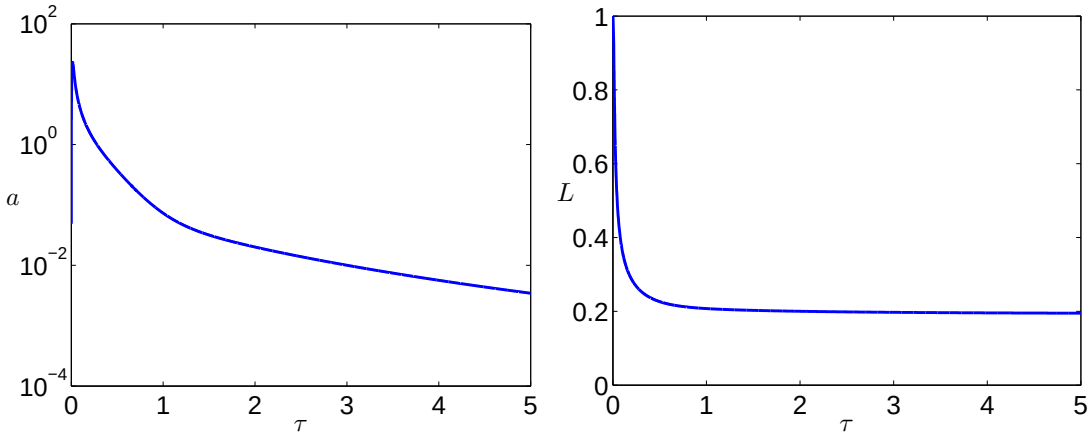

Figure 2.21: Time evolution of a (Left) and L (Right) for $\sigma = 1$.

Chapter 3

Stability of Solitary Waves for a Generalized Derivative Nonlinear Schrödinger Equation

In this chapter, we prove orbital stability/instability results for the solitary solution of gDNLS that depend on the strength of the nonlinearity and, in some instances, their velocity. In Section 3.2, we show that $n(H_\phi) = 1$, and in Section 3.3, we compute the number of positive eigenvalues of the Hessian, d''. We give the proofs of Theorems 1.3.3 to 1.3.5 in Section 3.4. Some basic spectral theorems used in Section 3.4 are presented in Section 3.5. In section 3.6, we illustrate our main theorem with numerical simulations of both stable and unstable solitons. In Section 3.7, we discuss our results.

Provided there is no ambiguity, we write ϕ, φ for $\phi_{\omega,c}, \varphi_{\omega,c}$ respectively. Furthermore, we only consider *admissible* values of (ω, c) satisfying the conditions $\omega > \frac{c^2}{4}, \quad c \in \mathbb{R}$.

3.1 Problem Setup

In this section, we calculate explicitly the soliton solution (1.2.5). We then define the linearized operator, the invariant quantities and the action functional for the soliton.

3.1.1 Explicit Form of Solitary Wave Solutions

We look for traveling solutions in the form

$$\psi(x,t) = \varphi(x-ct)\exp\left\{i\left(\omega t + \theta(x-ct)\right)\right\} = \varphi(x-ct)\Theta(x,t), \tag{3.1.1}$$

where φ and θ are unknown real valued functions and ω and c are undetermined constants. We assume that

$$|\varphi(y)| \to 0, \text{ as } |y| \to \infty. \tag{3.1.2}$$

It follows

$$\psi_x = (\varphi' + i\theta'\varphi)\Theta(x,t) \tag{3.1.3a}$$

$$\begin{aligned}\psi_{xx} &= (\varphi'' + i\theta''\varphi + i\theta'\varphi')\Theta(x,t) + i\theta'(\varphi' + i\theta'\varphi)\Theta(x,t) \\ &= \left(\varphi'' - (\theta')^2\varphi\right)\Theta(x,t) + i\left(\theta''\varphi + 2\theta'\varphi'\right)\Theta(x,t)\end{aligned} \tag{3.1.3b}$$

$$\psi_t = (-c\varphi' + i(\omega - c\theta')\varphi)\Theta(x,t). \tag{3.1.3c}$$

Substituting them into (1.1.1) and matching real and imaginary parts, we have

$$\varphi^{2\sigma}\varphi' - c\varphi' + 2\theta'\varphi' + \theta''\varphi = 0 \tag{3.1.4a}$$

$$\varphi^{2\sigma+1}\theta' + \omega\varphi - c\varphi\theta' + \varphi(\theta')^2 - \varphi'' = 0. \tag{3.1.4b}$$

Multiplying (3.1.4a) by φ, integrating it once and using (3.1.2), we obtain

$$\frac{1}{2\sigma+2}\varphi^{2\sigma} - \frac{c}{2} + \theta' = 0. \tag{3.1.5}$$

It follows, up to a constant,

$$\theta = \frac{c}{2}y - \frac{1}{2\sigma+2}\int_{-\infty}^{y}\varphi^{2\sigma}(s)ds. \tag{3.1.6}$$

Substituting it to (3.1.4b), we get

$$\frac{c}{2}\varphi^{2\sigma+1} - \frac{2\sigma+1}{(2\sigma+2)^2}\varphi^{4\sigma+1} + (\omega - \frac{c^2}{4})\varphi - \varphi'' = 0. \tag{3.1.7}$$

Multiplying this equation by φ' and integrating once,

$$\frac{c}{2\sigma+2}\varphi^{2\sigma+2} - \frac{1}{(2\sigma+2)^2}\varphi^{4\sigma+2} + (\omega - \frac{c^2}{4})\varphi^2 = (\varphi')^2. \tag{3.1.8}$$

Let

$$Q(\xi) = \alpha\varphi^{2\sigma}(\beta\xi), \tag{3.1.9}$$

where $\alpha > 0$ and $\beta > 0$. It follows

$$Q' = 2\sigma\alpha\beta\varphi^{2\sigma-1}\varphi',$$

and

$$\begin{aligned}(Q')^2 &= (2\sigma\alpha\beta)^2\varphi^{4\sigma-2}\left[\frac{c}{2\sigma+2}\varphi^{2\sigma+2} - \frac{1}{(2\sigma+2)^2}\varphi^{4\sigma+2} + (\omega - \frac{c^2}{4})\varphi^2\right] \\ &= (2\sigma\alpha\beta)^2\left[(\omega - \frac{c^2}{4})\varphi^{4\sigma} + \frac{c}{2\sigma+2}\varphi^{6\sigma} - \frac{1}{(2\sigma+2)^2}\varphi^{8\sigma}\right] \\ &= (2\sigma\alpha\beta)^2\left[(\omega - \frac{c^2}{4})\frac{1}{\alpha^2}Q^2 + \frac{c}{2\sigma+2}\frac{1}{\alpha^3}Q^3 - \frac{1}{(2\sigma+2)^2}\frac{1}{\alpha^4}Q^4\right].\end{aligned}$$

At this point assuming $c \neq 0$, $4\omega - c^2 > 0$ and setting

$$\beta = \frac{1}{\sigma\sqrt{4\omega - c^2}}, \tag{3.1.10a}$$

$$\alpha = \frac{2c\sigma^2\beta^2}{\sigma+1} = \frac{2|c|}{(\sigma+1)(4\omega - c^2)}, \tag{3.1.10b}$$

$$\gamma = \frac{\sigma^2\beta^2}{(\sigma+1)^2\alpha^2} = \frac{4\omega - c^2}{4c^2}, \tag{3.1.10c}$$

we obtain

$$(Q')^2 = Q^2 + \text{sign}(c)Q^3 - \gamma Q^4, \tag{3.1.11}$$

Substituting $F = \frac{1}{Q} + \frac{\text{sign}(c)}{2}$ into (3.1.11), we have

$$(F')^2 = F^2 - \left(\gamma + \frac{1}{4}\right),$$

which implies

$$F = \sqrt{\gamma + \frac{1}{4}}\cosh(\pm\xi + c_0), \quad c_0 \in \mathbb{R}.$$

Hence

$$Q(\xi;\gamma) = \left(\frac{\sqrt{1+4\gamma}}{2}\cosh(\xi) - \frac{\text{sign}(c)}{2}\right)^{-1}, \tag{3.1.12}$$

where we choose $c_0 = 0$ to obtain an even function. From (3.1.9), we obtain

$$\begin{aligned}\varphi(y) &= \left(\frac{1}{\alpha}Q(y/\beta)\right)^{1/(2\sigma)} \\ &= \left(\alpha Q(y/\beta)^{-1}\right)^{-1/(2\sigma)} \\ &= \left(\frac{2|c|}{(\sigma+1)(4\omega-c^2)}\left(\frac{\sqrt{\omega}}{|c|}\cosh(\sigma\sqrt{4\omega-c^2}y) - \frac{\operatorname{sign}(c)}{2}\right)\right)^{-1/(2\sigma)} \\ &= \left(\frac{2\sqrt{\omega}}{(\sigma+1)(4\omega-c^2)}\left(\cosh(\sigma\sqrt{4\omega-c^2}y) - \frac{c}{2\sqrt{\omega}}\right)\right)^{-1/(2\sigma)}.\end{aligned} \tag{3.1.13}$$

When $c = 0$, Q solves the equation

$$(Q')^2 = Q^2 - \gamma Q^4,$$

with $\beta = \frac{1}{2\sigma\sqrt{\omega}}$ and $\gamma = \frac{\sigma^2\beta^2}{(\sigma+1)^2\alpha^2} = \frac{1}{4\omega(\sigma+1)^2\alpha^2}$. Let $F = 1/Q$, we obtain

$$(F') = F^2 - \gamma,$$

which implies $F = \sqrt{\gamma}\cosh(\xi)$, and

$$Q = (\sqrt{\gamma}\cosh(\xi))^{-1}.$$

Thus

$$\varphi(y) = \left(\frac{1}{2\sqrt{\omega}(\sigma+1)}\cosh(2\sigma\sqrt{\omega}y)\right)^{-1/(2\sigma)}. \tag{3.1.14}$$

Combining (3.1.13) and (3.1.14) into a simple expression, we have, for all $c \in \mathbb{R}$,

$$\varphi(y) = \left(\frac{2\sqrt{\omega}}{(\sigma+1)(4\omega-c^2)}\left(\cosh(\sigma\sqrt{4\omega-c^2}y) - \frac{c}{2\sqrt{\omega}}\right)\right)^{-1/(2\sigma)}. \tag{3.1.15}$$

It follows, using (3.1.1) and (3.1.6), the solution of (1.1.1) takes the form of (1.2.5).

3.1.2 Linearized Hamiltonian

We study the problem in the space $X = H^1(\mathbb{R})$, with real inner product

$$(u, v) \equiv \Re \int_{\mathbb{R}} (u_x\bar{v}_x + u\bar{v})dx. \tag{3.1.16}$$

The dual of X is $X^* = H^{-1}(\mathbb{R})$. Let $I : X \to X^*$ be the natural isomorphism defined by

$$\langle Iu, v\rangle = (u, v), \tag{3.1.17}$$

where $\langle\cdot,\cdot\rangle$ is the pairing between X and X^*,

$$\langle f, u\rangle = \Re \int_{\mathbb{R}} f\bar{u}dx. \tag{3.1.18}$$

gDNLS can be formulated as the Hamiltonian system

$$\frac{d\psi}{dt} = JE'(\psi), \tag{3.1.19}$$

where the map $J : X^* \to X$ is $J = -i$, and E is the Hamiltonian:

$$E \equiv \frac{1}{2}\int_{-\infty}^{\infty} |\psi_x|^2 dx + \frac{1}{2(\sigma+1)}\Im \int_{-\infty}^{\infty} |\psi|^{2\sigma}\bar{\psi}\psi_x dx. \quad \text{(Energy)} \tag{3.1.20}$$

Two other conserved quantities are:

$$M \equiv \frac{1}{2}\int_{-\infty}^{\infty} |\psi|^2 dx, \quad \text{(Mass)} \tag{3.1.21}$$

$$P \equiv -\frac{1}{2}\Im \int_{-\infty}^{\infty} \bar{\psi}\psi_x dx. \quad \text{(Momentum)} \tag{3.1.22}$$

Let T_1 and T_2 be the one-parameter groups of unitary operator on X defined by

$$T_1(t)\Phi(x) \equiv e^{-it}\Phi(x), \quad \Phi(x) \in X, \quad t \in \mathbb{R} \tag{3.1.23a}$$

$$T_2(t)\Phi(x) \equiv \Phi(x+t). \tag{3.1.23b}$$

Then

$$\psi_{\omega,c} = T_1(-\omega t)T_2(-ct)\phi_{\omega,c}(x).$$

and

$$\partial_t T_1(\omega t)|_{t=0} = -i\omega, \;\; \partial_t T_2(ct)|_{t=0} = c\partial_x \; .$$

We define the linear operators

$$B_1 \equiv J^{-1}\partial_t T_1(\omega t)|_{t=0} = \omega, \tag{3.1.24a}$$

$$B_2 \equiv J^{-1}\partial_t T_2(ct)|_{t=0} = ic\partial_x. \tag{3.1.24b}$$

The mass and momentum invariants (3.1.21) and (3.1.22) are related to the symmetry groups via:

$$Q_1 \equiv \frac{1}{2}\langle B_1\phi, \phi\rangle = \frac{1}{2}\Re\int \omega\phi\bar{\phi}dx = \frac{\omega}{2}\int |\phi|^2 dx = \omega M, \tag{3.1.25a}$$

$$Q_2 \equiv \frac{1}{2}\langle B_2\phi, \phi\rangle = \frac{1}{2}\Re\int ic\partial_x\phi\bar{\phi}dx = -\frac{1}{2}c\Im\int \partial_x\phi\bar{\phi}dx = cP. \tag{3.1.25b}$$

Computing the first variations of (3.1.20), (3.1.21) and (3.1.22), we have

$$E'(\phi) = -\partial_x^2\phi - i|\phi|^{2\sigma}\partial_x\phi, \tag{3.1.26a}$$

$$M'(\phi) = \phi, \quad P'(\phi) = i\partial_x\phi. \tag{3.1.26b}$$

The second variations are:

$$\begin{aligned} E''(\phi)v = (&-\partial_x^2 - i\sigma|\phi|^{2\sigma-2}\bar{\phi}\partial_x\phi - i|\phi|^{2\sigma}\partial_x)v \\ &- i\sigma|\phi|^{2\sigma-2}\phi\partial_x\phi\bar{v}, \end{aligned} \tag{3.1.27a}$$

$$M''(\phi)v = v, \quad P''(\phi)v = i\partial_x v. \tag{3.1.27b}$$

The linearized Hamiltonian about the soliton ϕ is

$$\begin{aligned} H_\phi u &\equiv \left[E''(\phi) + M_1''(\phi) + M_2''(\phi)\right] u \\ &= \left[E''(\phi) + \omega M''(\phi) + cP''(\phi)\right] u \end{aligned} \tag{3.1.28}$$

for $u \in H^2(\mathbb{R})$. For later use, we give two equivalent expressions of H_ϕ. First, we decompose it into complex conjugates:

Lemma 3.1.1. *For any function u in the domain of H_ϕ,*

$$H_\phi u = L_1 u + L_2\bar{u},$$

where

$$L_1 \equiv -\partial_x^2 + \omega + ic\partial_x - i\sigma|\phi|^{2\sigma-2}\bar{\phi}\partial_x\phi - i|\phi|^{2\sigma}\partial_x, \tag{3.1.29a}$$

$$L_2 \equiv -i\sigma|\phi|^{2\sigma-2}\phi\partial_x\phi. \tag{3.1.29b}$$

Second, we give the expression of H_ϕ and the quadratic form it induces, after extraction of the soliton's phase:

Lemma 3.1.2. *Let $u \in H^1$ be decomposed as*

$$u = e^{i\theta}(u_1 + iu_2), \tag{3.1.30}$$

where θ is given by (1.2.9), and u_1 and u_2 are the real and imaginary parts of $ue^{-i\theta}$. Then

$$H_\phi u = e^{i\theta}\left[(L_{11}u_1 + L_{21}u_2) + i\left(L_{12}u_1 + L_{22}u_2\right)\right] \tag{3.1.31}$$

and

$$\begin{aligned}\langle H_\phi u, u\rangle = \langle L_{11}u_1, u_1\rangle + \langle L_{21}u_2, u_1\rangle \\ + \langle L_{12}u_1, u_2\rangle + \langle L_{22}u_2, u_2\rangle,\end{aligned} \tag{3.1.32}$$

where

$$L_{11} \equiv -\partial_{yy} + \omega - \frac{c^2}{4} + \frac{c(2\sigma+1)}{2}\varphi^{2\sigma} - \frac{4\sigma^2+6\sigma+1}{4(\sigma+1)^2}\varphi^{4\sigma}, \tag{3.1.33a}$$

$$L_{21} \equiv -\frac{\sigma}{\sigma+1}\varphi^{2\sigma-1}\varphi_y + \frac{\sigma}{\sigma+1}\varphi^{2\sigma}\partial_y, \tag{3.1.33b}$$

$$L_{12} \equiv -\frac{(2\sigma+1)\sigma}{\sigma+1}\varphi^{2\sigma-1}\varphi_y - \frac{\sigma}{\sigma+1}\varphi^{2\sigma}\partial_y, \tag{3.1.33c}$$

$$L_{22} \equiv -\partial_{yy} + \omega - \frac{c^2}{4} + \frac{c}{2}\varphi^{2\sigma} - \frac{2\sigma+1}{4(\sigma+1)^2}\varphi^{4\sigma}. \tag{3.1.33d}$$

Proof. Using (1.2.9),

$$\theta_y = \frac{c}{2} - \frac{1}{2\sigma+2}\varphi^{2\sigma}, \quad \theta_{yy} = -\frac{\sigma}{\sigma+1}\varphi^{2\sigma-1}\varphi_y. \tag{3.1.34}$$

We can then rewrite the operators L_1 and L_2 from Lemma 3.1.1 in terms of φ as

$$\begin{aligned}L_1 &= -\partial_y^2 + \omega + ic\partial_y - i\varphi^{2\sigma}\partial_y \\ &\quad + \frac{\sigma c}{2}\varphi^{2\sigma} - \frac{\sigma}{2\sigma+2}\varphi^{4\sigma} - i\sigma\varphi^{2\sigma-1}\varphi_y, \\ L_2 &= \left[\frac{c\sigma}{2}\varphi^{2\sigma} - \frac{\sigma}{2\sigma+2}\varphi^{4\sigma} - i\sigma\varphi^{2\sigma-1}\varphi_y\right]e^{2i\theta}.\end{aligned}$$

Letting $\chi = ue^{-i\theta}$, we have

$$\begin{aligned} H_\phi u =& e^{i\theta}\left[-\partial_{yy} + \omega - \frac{c^2}{4} + \frac{c(\sigma+1)}{2}\varphi^{2\sigma} - \frac{i\sigma^2}{\sigma+1}\varphi^{2\sigma-1}\varphi_y \right. \\ & \left. - \frac{i\sigma}{\sigma+1}\varphi^{2\sigma}\partial_y - \frac{2\sigma^2+4\sigma+1}{4(\sigma+1)^2}\varphi^{4\sigma}\right]\chi \\ & + e^{i\theta}\left[\frac{c\sigma}{2}\varphi^{2\sigma} - \frac{\sigma}{2\sigma+2}\varphi^{4\sigma} - i\sigma\varphi^{2\sigma-1}\varphi_y\right]\bar{\chi}. \end{aligned} \tag{3.1.35}$$

Since $\chi = u_1 + iu_2$, we get (3.1.31) and (3.1.32) by grouping terms appropriately. □

3.1.3 Action Functional

Using (1.2.11), we observe that when evaluated at the soliton ϕ,

$$E' + \omega M' + cP' = 0. \tag{3.1.36}$$

For any $\omega > c^2/4$, we define the scalar function

$$d(\omega, c) \equiv E(\phi_{\omega,c}) + Q_1(\phi_{\omega,c}) + Q_2(\phi_{\omega,c}), \tag{3.1.37}$$

which is the action functional evaluated at the soliton. It has the following properties:

Lemma 3.1.3.

$$d(\omega, c) = E(\phi) + \omega M(\phi) + cP(\phi), \tag{3.1.38}$$

$$\partial_\omega d(\omega, c) = M(\phi) > 0, \tag{3.1.39}$$

$$\partial_c d(\omega, c) = P(\phi). \tag{3.1.40}$$

The Hessian is

$$d''(\omega, c) = \begin{pmatrix} \partial_\omega M(\phi) & \partial_c M(\phi) \\ \partial_\omega P(\phi) & \partial_c P(\phi) \end{pmatrix}. \tag{3.1.41}$$

Proof. Using (3.1.25a), (3.1.25b) and (3.1.37), we have (3.1.38). Differentiating (3.1.38) with respect to ω and c respectively, and using (3.1.36), we obtain (3.1.39) and (3.1.40). The expression for the Hessian follows.

□

3.2 Spectral Decomposition of the Linearized Operator

This section provides a full description of the spectrum of the linearized operator H_ϕ. In particular, we prove:

Theorem 3.2.1. *For all values of $\sigma > 0$ and admissible (ω, c), the space $X = H^1$ can be decomposed as the direct sum*

$$X = N + Z + P, \tag{3.2.1}$$

where the three subspaces intersect trivially and:

(i) N is a one dimensional subspace such that for $u \in N$, $u \neq 0$,

$$\langle H_\phi u, u\rangle < 0. \tag{3.2.2}$$

(ii) Z is the two dimensional kernel of H_ϕ.

(iii) P is a subspace such that for $p \in P$,

$$\langle H_\phi p, p\rangle \geq \delta \|p\|_X^2 \tag{3.2.3}$$

where the constant $\delta > 0$ is independent of p.

Corollary 3.2.2. *For all values of $\sigma > 0$ and admissible (ω, c),*

$$n(H_\phi) = 1.$$

An important ingredient of the proof involves rewriting the quadratic form (3.1.32) induced by H_ϕ in a more favorable form. This rearrangement, inspired by [26], expresses it as a sum of a quadratic form involving an operator with exactly one negative eigenvalue and a nonnegative term.

Lemma 3.2.3. *Let*

$$u = e^{i\theta}(u_1 + iu_2),$$

where θ, u_1, u_2 are defined the same as Lemma 3.1.2, then

$$\langle H_\phi u, u\rangle = \langle \widetilde{L}_{11} u_1, u_1\rangle + \int_{-\infty}^{\infty} \left[\varphi \left(\varphi^{-1} u_2\right)_y + \frac{\sigma}{(\sigma+1)} \varphi^{2\sigma} u_1\right]^2 dy, \tag{3.2.4}$$

where

$$\widetilde{L}_{11} \equiv -\partial_{yy} + \omega - \frac{c^2}{4} + \frac{c(2\sigma+1)}{2}\varphi^{2\sigma} - \frac{8\sigma^2+6\sigma+1}{4(\sigma+1)^2}\varphi^{4\sigma}. \tag{3.2.5}$$

Proof. Recall the terms in the quadratic form (3.1.33). We first examine L_{11}. The relationship between L_{11} and $\widetilde{L}_{11}$ is

$$L_{11} = \widetilde{L}_{11} + \frac{\sigma^2}{(\sigma+1)^2}\varphi^{4\sigma}. \tag{3.2.6}$$

Next, consider L_{22}. From (1.2.7),

$$L_{22}\varphi = 0. \tag{3.2.7}$$

Letting $\tilde{u}_2 = \varphi^{-1}u_2$, we write

$$\begin{aligned}
\langle L_{22}u_2, u_2\rangle &= \langle -\partial_{yy}u_2, u_2\rangle + \left\langle (\omega - \frac{c^2}{4} + \frac{c}{2}\varphi^{2\sigma} - \frac{2\sigma+1}{4(\sigma+1)^2}\varphi^{4\sigma})u_2, u_2 \right\rangle \\
&= \langle -\varphi_{yy}\tilde{u}_2 - 2\varphi_y\tilde{u}_{2y} - \varphi\tilde{u}_{2yy}, \varphi\tilde{u}_2\rangle \\
&\qquad + \langle (\omega - \frac{c^2}{4} + \frac{c}{2}\varphi^{2\sigma} - \frac{2\sigma+1}{4(\sigma+1)^2}\varphi^{4\sigma})\varphi\tilde{u}_2, \varphi\tilde{u}_2\rangle \\
&= \langle \tilde{u}_2 L_{22}\varphi, \varphi\tilde{u}_2\rangle + \langle -2\varphi_y\tilde{u}_{2y} - \varphi\tilde{u}_{2yy}, \varphi\tilde{u}_2\rangle \\
&= \langle -(\varphi^2\tilde{u}_{2y})_y, \tilde{u}_2\rangle = \langle \varphi\tilde{u}_{2y}, \varphi\tilde{u}_{2y}\rangle,
\end{aligned} \tag{3.2.8}$$

where u_{2y} and u_{2yy} denote $\partial_y u_2$ and $\partial_{yy}u_2$, respectively. Lastly, we simplify the off diagonal entries, L_{21} and L_{12}. Integrating by parts, we have

$$\begin{aligned}
\langle L_{12}u_1, u_2\rangle =& \left\langle \left(-\frac{(2\sigma+1)\sigma}{\sigma+1}\varphi^{2\sigma-1}\varphi_y - \frac{\sigma}{\sigma+1}\varphi^{2\sigma}\partial_y \right) u_1, u_2 \right\rangle \\
=& -\frac{2\sigma+1}{2(\sigma+1)}\left\langle (\varphi^{2\sigma})_y, u_1u_2\right\rangle - \frac{\sigma}{\sigma+1}\left\langle \varphi^{2\sigma}u_{1y}, u_2\right\rangle \\
=& \frac{2\sigma+1}{2(\sigma+1)}\left\langle \varphi^{2\sigma}u_{2y}, u_1\right\rangle + \frac{2\sigma+1}{2(\sigma+1)}\left\langle \varphi^{2\sigma}u_{1y}, u_2\right\rangle - \frac{\sigma}{\sigma+1}\left\langle \varphi^{2\sigma}u_{1y}, u_2\right\rangle \\
=& \frac{2\sigma+1}{2(\sigma+1)}\left\langle \varphi^{2\sigma}u_{2y}, u_1\right\rangle + \frac{1}{2(\sigma+1)}\left\langle \varphi^{2\sigma}u_{1y}, u_2\right\rangle.
\end{aligned}$$

Similarly,

$$\begin{aligned}\langle L_{21}u_2, u_1\rangle =& \left\langle \left(-\frac{\sigma}{\sigma+1}\varphi^{2\sigma-1}\varphi_y + \frac{\sigma}{\sigma+1}\varphi^{2\sigma}\partial_y\right) u_2, u_1 \right\rangle \\ =& -\frac{1}{2(\sigma+1)}\left\langle (\varphi^{2\sigma})_y, u_1u_2\right\rangle + \frac{\sigma}{\sigma+1}\left\langle \varphi^{2\sigma}u_{2y}, u_1\right\rangle \\ =& \frac{1}{2(\sigma+1)}\left\langle \varphi^{2\sigma}u_{2y}, u_1\right\rangle + \frac{1}{2(\sigma+1)}\left\langle \varphi^{2\sigma}u_{1y}, u_2\right\rangle + \frac{\sigma}{\sigma+1}\left\langle \varphi^{2\sigma}u_{2y}, u_1\right\rangle \\ =& \frac{2\sigma+1}{2(\sigma+1)}\left\langle \varphi^{2\sigma}u_{2y}, u_1\right\rangle + \frac{1}{2(\sigma+1)}\left\langle \varphi^{2\sigma}u_{1y}, u_2\right\rangle.\end{aligned}$$

The off diagonal terms then sum to

$$\langle L_{12}u_1, u_2\rangle + \langle L_{21}u_2, u_1\rangle = \frac{2\sigma+1}{\sigma+1}\left\langle \varphi^{2\sigma}u_{2y}, u_1\right\rangle + \frac{1}{\sigma+1}\left\langle \varphi^{2\sigma}u_{1y}, u_2\right\rangle.$$

Introducing $\tilde{u}_2 = \varphi^{-1}u_2$ into the above expression, and integrating by parts,

$$\langle L_{12}u_1, u_2\rangle + \langle L_{21}u_2, u_1\rangle = \frac{2\sigma}{\sigma+1}\left\langle \varphi^{2\sigma+1}\tilde{u}_{2y}, u_1\right\rangle. \tag{3.2.9}$$

Combining (3.2.6), (3.2.8) and (3.2.9),

$$\begin{aligned}\langle H_\phi u, u\rangle =& \langle \widetilde{L}_{11}u_1, u_1\rangle + \langle \varphi\tilde{u}_{2y}, \varphi\tilde{u}_{2y}\rangle \\ &+ \left\langle \frac{\sigma}{\sigma+1}\varphi^{2\sigma}u_1, \frac{\sigma}{\sigma+1}\varphi^{2\sigma}u_1\right\rangle + \left\langle \frac{2\sigma}{\sigma+1}\varphi^{2\sigma}u_1, \varphi\tilde{u}_{2y}\right\rangle \\ =& \langle \widetilde{L}_{11}u_1, u_1\rangle + \int_{-\infty}^{\infty}\left[\varphi\tilde{u}_{2y} + \frac{\sigma}{\sigma+1}\varphi^{2\sigma}u_1\right]^2 dy.\end{aligned}$$

□

3.2.1 The Negative Subspace

Next, we characterize the negative subspace, N. For that, we need the following lemma on $\widetilde{L}_{11}$.

Lemma 3.2.4. *The spectrum of $\widetilde{L}_{11}$ can be characterized as follows:*

- *$\widetilde{L}_{11}$ has exactly one negative eigenvalue, denoted $-\lambda_{11}^2$, with multiplicity one, and eigenfunction χ_{11},*
- *$0 \in \sigma(\widetilde{L}_{11})$, and the kernel is spanned by φ_y,*

- *There exists* $\mu_{11} > 0$ *such that*

$$\sigma(\widetilde{L}_{11}) \setminus \left\{-\lambda_{11}^2, 0\right\} \subset [\mu_{11}, \infty).$$

Proof. First, we observe that since φ is exponentially localized, $\widetilde{L}_{11}$ is a relatively compact perturbation of $-\partial_y^2 + \omega - \frac{c^2}{4}$. By Weyl's theorem, the essential spectrum is then

$$\sigma_{\text{ess}}(\widetilde{L}_{11}) = \sigma_{\text{ess}}(-\partial_y^2 + \omega - \tfrac{c^2}{4}) = \left[\omega - \tfrac{c^2}{4}, \infty\right).$$

Consequently, all eigenvalues below the lower bound of the essential spectrum correspond to isolated eigenvalues of finite multiplicity. By differentiating (1.2.7) with respect to y, we see that

$$\widetilde{L}_{11}\varphi_y = 0. \tag{3.2.10}$$

Hence, $\widetilde{L}_{11}$ has a kernel. Viewed as a linear second order ordinary differential equation, $\widetilde{L}_{11}f = 0$ has two linearly independent solutions. As $y \to -\infty$, one solution decays exponentially while the other grows exponentially. Thus, up to a multiplicative constant, there can be at most one spatially localized solution to $\widetilde{L}_{11}f = 0$. Therefore, the kernel is spanned by φ_y.

From Sturm-Liouville theory, this implies that zero is the second eigenvalue of $\widetilde{L}_{11}$, and $\widetilde{L}_{11}$ has exactly one strictly negative eigenvalue, $-\lambda_{11}^2$, with a L^2 normalized eigenfunction χ_{11}:

$$\widetilde{L}_{11}\chi_{11} = -\lambda_{11}^2\chi_{11}. \tag{3.2.11}$$

If we now let

$$\mu_{11} \equiv \inf_{f\neq 0, f\perp\varphi_y, f\perp\chi_{11}} \frac{\left\langle \widetilde{L}_{11}f, f\right\rangle}{\langle f, f\rangle}, \tag{3.2.12}$$

we see that $\mu_{11} > 0$, since if it were not, it would correspond to another discrete eigenvalue less than or equal to zero. It is either a discrete eigenvalue in the gap $(0, \omega - \frac{c^2}{4})$ or the base of the essential spectrum. Regardless, $\sigma(\widetilde{L}_{11}) \setminus \{-\lambda_{11}^2, 0\}$ is bounded away from zero.

□

Using χ_{11}, we construct the negative subspace N.

Proposition 3.2.5. *Let*

$$N \equiv \text{span}\left\{\chi_-\right\}, \tag{3.2.13}$$

where

$$\chi_- \equiv (\chi_{11} + i\chi_{12})e^{i\theta}, \tag{3.2.14a}$$

$$\chi_{12} \equiv \varphi\left[-\frac{\sigma}{\sigma+1}\int_{-\infty}^{y}\varphi^{2\sigma-1}(s)\chi_{11}(s)ds + k_{12}\right], \tag{3.2.14b}$$

and $k_{12} \in \mathbb{R}$ *is chosen such that*

$$\langle \chi_{12}, \varphi\rangle = 0. \tag{3.2.15}$$

For $u \in N \setminus \{0\}$,

$$\langle H_\phi u, u\rangle < 0.$$

Proof. The function χ_{12} is in L^2. Indeed, the integral in (3.2.14b) is well defined since, as $|y| \to \infty$,

$$|\varphi(y)| \lesssim \exp\left\{-\sqrt{\omega - c^2/4}\,|y|\right\},$$
$$|\chi_{11}(y)| \lesssim \exp\left\{-\sqrt{\omega - c^2/4 + \lambda_{11}^2}\,|y|\right\}.$$

Thus the integrand is bounded. From (3.2.4) and (3.2.11),

$$\langle H_\phi \chi_-, \chi_-\rangle = \langle \widetilde{L}_{11}\chi_{11}, \chi_{11}\rangle = -\lambda_{11}^2 < 0.$$

□

3.2.2 The Kernel

We give an explicit characterization of the kernel of H_ϕ.

Proposition 3.2.6. *Let*

$$Z = \operatorname{span}\{\chi_1, \chi_2\}, \tag{3.2.16}$$

where

$$\chi_1 = \left(\varphi_y + i(k_2 - \frac{1}{2\sigma+2}\varphi^{2\sigma})\varphi\right)e^{i\theta}, \tag{3.2.17a}$$

$$\chi_2 = i\varphi e^{i\theta} \tag{3.2.17b}$$

with k_2 *is a real constant such that*

$$\left\langle \left(k_2 - \frac{1}{2\sigma+2}\varphi^{2\sigma}\right)\varphi, \varphi\right\rangle = 0. \tag{3.2.18}$$

Then $Z = \ker H_\phi$.

Proof. We first prove that χ_1 and χ_2 are linearly independent elements of the kernel, and then show that the kernel is at most two dimensional. Applying H_ϕ (in the form (3.1.31)) to χ_2 and using that $L_{21}\varphi = 0$ and (3.2.7), we get $H_\phi\chi_2 = 0$. For χ_1, we compute

$$\begin{aligned} &L_{11}\varphi_y + L_{21}(k_2 - \frac{1}{2\sigma+2}\varphi^{2\sigma})\varphi \\ &\quad = \widetilde{L}_{11}\varphi_y + \frac{\sigma^2}{(\sigma+1)^2}\varphi^{4\sigma}\varphi_y + k_2 L_{21}\varphi - \frac{1}{2\sigma+2}L_{21}\varphi^{2\sigma+1} \\ &\quad = \frac{\sigma^2}{(\sigma+1)^2}\varphi^{4\sigma}\varphi_y - \frac{1}{2\sigma+2}\frac{2\sigma^2}{\sigma+1}\varphi^{4\sigma}\varphi_y = 0 \end{aligned}$$

and

$$\begin{aligned} &L_{12}\varphi_y + L_{22}(k_2 - \frac{1}{2\sigma+2}\varphi^{2\sigma})\varphi \\ &\quad = -\frac{2\sigma^2+\sigma}{\sigma+1}\varphi^{2\sigma-1}\varphi_y^2 - \frac{\sigma}{\sigma+1}\varphi^{2\sigma}\varphi_{yy} \\ &\qquad - \frac{1}{2\sigma+2}\left[-2\sigma(2\sigma+1)\varphi^{2\sigma-1}\varphi_y^2 - 2\sigma\varphi^{2\sigma}\varphi_{yy} + \varphi^{2\sigma}L_{22}\varphi\right] = 0. \end{aligned}$$

Thus, $Z \subset \ker H_\phi$, and the kernel is at least two dimensional.

We now show that it is exactly two dimensional. If we consider the problem

$$H_\phi f = 0,$$

as a second order system of two real valued functions, we know there are four linearly independent solutions. As $y \to -\infty$, two of these solutions decay exponentially, while two grow exponentially. However, only the two exponentially decay solutions are in H^1. Thus, there are at most two linearly independent solutions which are spatially localized, and $Z = \ker H_\phi$.

□

3.2.3 The Positive Subspace and the Spectral Decomposition

We define the subspace P and prove Theorem 3.2.1. For that, we need the following lemmas about $\widetilde{L}_{11}$ and L_{22}.

Lemma 3.2.7. *For any real function* $f \in H^1(\mathbb{R})$ *satisfying the orthogonality conditions*

$$\langle f, \varphi_y\rangle = \langle f, \chi_{11}\rangle = 0, \tag{3.2.19}$$

there exists $\delta_{11} > 0$, such that

$$\langle \widetilde{L}_{11} f, f\rangle \geq \delta_{11} \|f\|_{H^1}^2. \tag{3.2.20}$$

Proof. From Lemma 3.2.4, (3.2.12) holds on the subspace orthogonal to φ_y and χ_{11}, so

$$\langle \widetilde{L}_{11} f, f\rangle \geq \mu_{11} \|f\|_{L_2}^2.$$

To get the H^1 lower bound, let

$$V_1(y) = \omega - \frac{c^2}{4} + \frac{c(2\sigma+1)}{2}\varphi^{2\sigma} - \frac{8\sigma^2+6\sigma+1}{4(\sigma+1)^2}\varphi^{4\sigma},$$

so that $\widetilde{L}_{11} = -\partial_{yy} + V_1$, with $\|V_1\|_{L^\infty} < \infty$. Thus,

$$\begin{aligned}
\langle \widetilde{L}_{11} f, f\rangle &= \langle -\partial_{yy} f, f\rangle + \langle V_1 f, f\rangle \\
&\geq \langle -\partial_{yy} f, f\rangle - \|V_1\|_{L^\infty}\|f\|_{L^2}^2 \\
&= \|\partial_y f\|_{L^2}^2 - \frac{1}{\mu_{11}}\|V_1\|_{L^\infty}\langle \widetilde{L}_{11} f, f\rangle.
\end{aligned}$$

It follows that

$$\langle \widetilde{L}_{11} f, f\rangle \geq \frac{1}{1+\mu_{11}^{-1}\|V_1\|_{L^\infty}}\|\partial_y f\|_{L^2}^2.$$

Taking δ_{11} sufficiently small, we have

$$\langle \widetilde{L}_{11} f, f\rangle \geq \delta_{11} \|f\|_{H^1}^2.$$

□

Lemma 3.2.8. *For any real function $f \in H^1(\mathbb{R})$ satisfying*

$$\langle f, \varphi\rangle = 0, \tag{3.2.21}$$

there exists $\delta_{22} > 0$, such that

$$\langle L_{22} f, f\rangle \geq \delta_{22} \|f\|_{H^1}^2. \tag{3.2.22}$$

Proof. As was the case for $\widetilde{L}_{11}$, L_{22} is a relatively compact perturbation of $-\partial_y^2 + \omega - c^2/4$, so it also has

$$\sigma_{\text{ess}}(L_{22}) = \left[\omega - \tfrac{c^2}{4}, \infty\right).$$

Thus, all points in the spectrum below $\omega - c^2/4$ correspond to discrete eigenvalues. From (3.2.7) and φ is strictly positive, Sturm-Liouville theory implies that zero is the lowest eigenvalue. Let

$$\mu_{22} \equiv \inf_{f\neq 0, f\perp\varphi} \frac{\langle L_{22}f, f\rangle}{\langle f, f\rangle}. \tag{3.2.23}$$

We know that $\mu_{22} > 0$, otherwise this would contradict with 0 being the lowest eigenvalue. Therefore

$$\langle L_{22}f, f\rangle \geq \mu_{22} \|f\|_{L^2}.$$

Using the same argument as in Lemma 3.2.7, we obtain (3.2.22). □

We now prove Theorem 3.2.1.

Proof. Recall N, Z as defined define by (3.2.13) and (3.2.16). We define P as

$$P = \{p \in X \mid \langle \Re(e^{-i\theta}p), \chi_{11}\rangle = \langle \Re(e^{-i\theta}p), \varphi_y\rangle = \langle \Im(e^{-i\theta}p), \varphi\rangle = 0\}. \tag{3.2.24}$$

We express $u \in X$ as

$$u = a_1\chi_- + (b_1\chi_1 + b_2\chi_2) + p,$$

where

$$a_1 = \langle u_1, \chi_{11}\rangle, \quad b_1 = \frac{\langle u_1, \varphi_y\rangle}{\|\varphi_y\|_{L^2}^2}, \quad b_2 = \frac{\langle u_2, \varphi\rangle}{\|\varphi\|_{L^2}^2},$$

with u_1 and u_2 are real and imaginary part of $e^{-i\theta}u$. Clearly, $a_1\chi_- \in N$ and $b_1\chi_1 + b_2\chi_2 \in Z$. It suffices to show $p \in P$. We write $p = (p_1 + ip_2)e^{i\theta}$ with p_1 and p_2 real. Since φ_y is odd and χ_{11} is even, $\langle \varphi_y, \chi_{11}\rangle = 0$, and we readily check that $\langle p_1, \chi_{11}\rangle = \langle p_1, \varphi_y\rangle = 0$. Furthermore, by (3.2.15) and (3.2.18), we also have $\langle p_2, \varphi\rangle = 0$. Thus, $p \in P$, and u is indeed decomposed into elements of N, Z and P.

Finally, we show that H_ϕ is positive on P. Let $\tilde{p}_2 = \varphi^{-1}p_2$. By (3.2.4),

$$\langle H_\phi p, p\rangle = \langle \widetilde{L}_{11}p_1, p_1\rangle + \int_{-\infty}^{\infty} (\varphi\partial_y\tilde{p}_2 + \frac{\sigma}{\sigma+1}\varphi^{2\sigma}p_1)^2 dy. \tag{3.2.25}$$

Lemma 3.2.7 gives the desired lower bound on the first term. For the second term, we break it into two cases, depending on how $\|\varphi\partial_y\tilde{p}_2\|_{L^2}$ and $\|p_1\|_{L^2}$ compare. Let

$$C_\sigma \equiv \frac{2\sigma}{\sigma+1}\|\varphi\|_{L^\infty}^{2\sigma}. \tag{3.2.26}$$

(a) If $\|\varphi\partial_y\tilde{p}_2\|_{L^2} \geq C_\sigma\|p_1\|_{L^2}$, we estimate the second term in (3.2.25) as follows,

$$\begin{aligned}\left\|\varphi\partial_y\tilde{p}_2 + \frac{\sigma}{\sigma+1}\varphi^{2\sigma}p_1\right\|_{L^2} &\geq \|\varphi\partial_y\tilde{p}_2\|_{L^2} - \frac{\sigma}{\sigma+1}\|\varphi\|_{L^\infty}^{2\sigma}\|p_1\|_{L^2} \\ &= \|\varphi\partial_y\tilde{p}_2\|_{L^2} - \frac{1}{2}C_\sigma\|p_1\|_{L^2} \geq \frac{1}{2}\|\varphi\partial_y\tilde{p}_2\|_{L^2}.\end{aligned}$$

From (3.2.8), we have

$$\left\|\varphi\partial_y\tilde{p}_2 + \frac{\sigma}{\sigma+1}\varphi^{2\sigma}p_1\right\|_{L^2}^2 \geq \frac{1}{4}\langle L_{22}p_2, p_2\rangle.$$

From Lemmas 3.2.7 and 3.2.8, we get

$$\langle H_\phi p, p\rangle \geq \left\langle \widetilde{L}_{11}p_1, p_1\right\rangle + \frac{1}{4}\langle L_{22}p_2, p_2\rangle \geq \delta_a\|p\|_{H^1}^2,$$

for some small enough δ_a.

(b) Conversely, if $\|\varphi\partial_y\tilde{p}_2\|_{L^2} < C_\sigma\|p_1\|_{L^2}$, then,

$$\begin{aligned}\langle H_\phi p, p\rangle \geq \left\langle \widetilde{L}_{11}p_1, p_1\right\rangle &\geq \frac{\delta_{11}}{2}\|p_1\|_{H^1}^2 + \frac{\delta_{11}}{2}\|p_1\|_{L^2}^2 \\ &\geq \frac{\delta_{11}}{2}\|p_1\|_{H^1}^2 + \frac{\delta_{11}}{2C_\sigma^2}\|\varphi\partial_y\tilde{p}_2\|_{L^2}^2 \\ &= \frac{\delta_{11}}{2}\|p_1\|_{H^1}^2 + \frac{\delta_{11}}{2C_\sigma^2}\langle L_{22}p_2, p_2\rangle \geq \delta_b\|p\|_{H^1}^2.\end{aligned} \tag{3.2.27}$$

Taking the smaller value of δ_a and δ_b as δ, we have

$$\langle H_\phi p, p\rangle \geq \delta\|p\|_{H^1}^2. \tag{3.2.28}$$

It follows that N, Z and P have trivial intersections among one another. Hence $X = N + Z + P$. □

3.3 Analysis of the Hessian Matrix

In this section, we compute the number of the positive eigenvalues $p(d''(\omega, c))$ of the Hessian matrix (3.1.41) of the action functional $d(\omega, c)$ defined in (3.1.37). Since the number of negative eigenvalues of $H_{\phi_{\omega,c}}$ is in all cases equal to one, $p(d''(\omega, c))$ will determine whether or not the soliton is stable.

To make this assessment, we examine the determinant and the trace of $d''(\omega, c)$. In the following, we denote $\kappa = \sqrt{4\omega - c^2} > 0$ and rewrite the solitary solution (1.2.6) as $\varphi(x)^{2\sigma} = f(\omega, c)h(\omega, c; x)^{-1}$, with

$$f(\omega, c) = \frac{(\sigma+1)\kappa^2}{2\sqrt{\omega}}\ , \quad h(x; \sigma; \omega, c) = \cosh(\sigma\kappa x) - \frac{c}{2\sqrt{\omega}}.$$

We also rewrite the functionals M, P defined in (3.1.21)-(3.1.22) and their derivatives in terms of h and f:

$$M = \frac{1}{2}\int_0^\infty |\varphi|^2 dx = f^{\frac{1}{\sigma}} \int_0^\infty h^{-\frac{1}{\sigma}} dx, \tag{3.3.1}$$

$$\begin{aligned} P &= -\frac{c}{2}\int_0^\infty \varphi^2 dx + \frac{1}{2\sigma+2}\int_0^\infty \varphi^{2\sigma+2} dx \\ &= -\frac{c}{2} f^{\frac{1}{\sigma}} \int_0^\infty h^{-\frac{1}{\sigma}} dx + \frac{1}{2\sigma+2} f^{\frac{\sigma+1}{\sigma}} \int_0^\infty h^{-\frac{\sigma+1}{\sigma}} dx. \end{aligned} \tag{3.3.2}$$

$$\partial_c M = \frac{1}{\sigma} f^{\frac{1-\sigma}{\sigma}} f_c \int_0^\infty h^{-\frac{1}{\sigma}} dx - \frac{1}{\sigma} f^{\frac{1}{\sigma}} \int_0^\infty h^{-\frac{\sigma+1}{\sigma}} h_c dx, \tag{3.3.3}$$

$$\partial_\omega M = \frac{1}{\sigma} f^{\frac{1-\sigma}{\sigma}} f_\omega \int_0^\infty h^{-\frac{1}{\sigma}} dx - \frac{1}{\sigma} f^{\frac{1}{\sigma}} \int_0^\infty h^{-\frac{\sigma+1}{\sigma}} h_\omega dx, \tag{3.3.4}$$

$$\begin{aligned} \partial_c P = &-\frac{1}{2} f^{\frac{1}{\sigma}} \int_0^\infty h^{-\frac{1}{\sigma}} dx - \frac{c}{2\sigma} f^{\frac{1-\sigma}{\sigma}} f_c \int_0^\infty h^{-\frac{1}{\sigma}} dx \\ &+ \frac{c}{2\sigma} f^{\frac{1}{\sigma}} \int_0^\infty h^{-\frac{\sigma+1}{\sigma}} h_c dx + \frac{1}{2\sigma} f^{\frac{1}{\sigma}} f_c \int_0^\infty h^{-\frac{1+\sigma}{\sigma}} dx \\ &- \frac{1}{2\sigma} f^{\frac{1+\sigma}{\sigma}} \int_0^\infty h^{-\frac{1+2\sigma}{\sigma}} h_c dx, \end{aligned} \tag{3.3.5}$$

$$\begin{aligned} \partial_\omega P = &-\frac{c}{2\sigma} f^{\frac{1-\sigma}{\sigma}} f_\omega \int_0^\infty h^{-\frac{1}{\sigma}} dx + \frac{c}{2\sigma} f^{\frac{1}{\sigma}} \int_0^\infty h^{-\frac{\sigma+1}{\sigma}} h_\omega dx \\ &+ \frac{1}{2\sigma} f^{\frac{1}{\sigma}} f_\omega \int_0^\infty h^{-\frac{1+\sigma}{\sigma}} dx - \frac{1}{2\sigma} f^{\frac{1+\sigma}{\sigma}} \int_0^\infty h^{-\frac{1+2\sigma}{\sigma}} h_\omega dx, \end{aligned} \tag{3.3.6}$$

where

$$\begin{aligned} f_c &= -\frac{c(1+\sigma)}{\sqrt{\omega}}, \quad f_\omega = \frac{(1+\sigma)(4\omega + c^2)}{4\omega^{3/2}}, \\ h_c &= -\frac{\sigma c}{\kappa} x \sinh(\sigma\kappa x) - \frac{1}{2}\omega^{-1/2},\ h_\omega = \frac{2\sigma}{\kappa} x \sinh(\sigma\kappa x) + \frac{c}{4}\omega^{-\frac{3}{2}}. \end{aligned}$$

The expressions in (3.3.3)-(3.3.6) involve various integrals. The next lemmas show that

all of them can be expressed simply in terms of

$$\alpha_n = \int_0^\infty h^{-\frac{1}{\sigma}-n} dx.$$

First, we have

Lemma 3.3.1.

$$\alpha_2 = \frac{4\omega}{(\sigma+1)\kappa^2}\alpha_0 + \frac{2c\sqrt{\omega}(2+\sigma)}{(\sigma+1)\kappa^2}\alpha_1 \tag{3.3.7}$$

Proof. We first rewrite α_0, and then integrate by parts:

$$\begin{aligned}\alpha_0 = \int_0^\infty h^{-\frac{1}{\sigma}-1} h dx &= \frac{1}{\sigma\kappa}\int_0^\infty h^{-\frac{1}{\sigma}-1}(\sinh(\sigma\kappa x))' dx - \alpha_1 \frac{c}{2\sqrt{\omega}} \\ &= \frac{(\sigma+1)}{\sigma^2}\int_0^\infty h^{-\frac{1}{\sigma}-2}(\sinh^2(\sigma\kappa x)) dx - \alpha_1 \frac{c}{2\sqrt{\omega}} \\ &= \frac{(\sigma+1)}{\sigma^2}\int_0^\infty h^{-\frac{1}{\sigma}-2}((h+\frac{c}{2\sqrt{\omega}})^2 - 1) dx - \alpha_1 \frac{c}{2\sqrt{\omega}}.\end{aligned}$$

Regrouping the terms in this last expression, we obtain (3.3.7). □

Lemma 3.3.2. *We have the following relations:*

$$\int_0^\infty h^{-\frac{1}{\sigma}-2} h_c dx = -\frac{1}{2\sqrt{\omega}}\alpha_2 - \frac{c\sigma}{(\sigma+1)\kappa^2}\alpha_1, \tag{3.3.8}$$

$$\int_0^\infty h^{-\frac{1}{\sigma}-1} h_c dx = -\frac{1}{2\sqrt{\omega}}\alpha_1 - \frac{c\sigma}{\kappa^2}\alpha_0, \tag{3.3.9}$$

$$\int_0^\infty h^{-\frac{1}{\sigma}-2} h_\omega dx = \frac{c}{4\omega^{3/2}}\alpha_2 + \frac{2\sigma}{(\sigma+1)\kappa^2}\alpha_1, \tag{3.3.10}$$

$$\int_0^\infty h^{-\frac{1}{\sigma}-1} h_\omega dx = \frac{c}{4\omega^{3/2}}\alpha_1 + \frac{2\sigma}{\kappa^2}\alpha_0. \tag{3.3.11}$$

Proof. By integration by parts, and n integer,

$$\int_0^\infty h^{-\frac{1}{\sigma}-n} h_c dx = \frac{c}{\kappa^2(-\frac{1}{\sigma}-n+1)}\int_0^\infty h^{-\frac{1}{\sigma}-n+1} dx - \frac{1}{2\sqrt{\omega}}\int_0^\infty h^{-\frac{1}{\sigma}-n} dx,$$

Choosing $n = 2, 1$, we get (3.3.8) and (3.3.9). The relations (3.3.10) and (3.3.11) are obtained from (3.3.8), (3.3.9) and $h_\omega = -\frac{2}{c}h_c - \frac{\kappa^2}{4\omega^{3/2}c}$. □

Using Lemmas 3.3.1 and 3.3.2, we have:

Lemma 3.3.3. *Denoting* $\tilde{\kappa} = 2^{-\frac{1}{\sigma}-2}\sigma^{-1}(1+\sigma)^{\frac{1}{\sigma}}\kappa^{2(\frac{1}{\sigma}-1)}\omega^{-\frac{1}{2\sigma}-\frac{1}{2}}$, *we have*

$$\begin{aligned}
\partial_c M &= 2\tilde{\kappa}\left[2c(\sigma-2)\omega^{1/2}\alpha_0 + \kappa^2\alpha_1\right],\\
\partial_\omega M &= \tilde{\kappa}\omega^{-1}\left[\left(2c^2 - 8(\sigma-1)\omega\right)\omega^{1/2}\alpha_0 - \kappa^2 c\alpha_1\right],\\
\partial_c P &= \tilde{\kappa}\left[\left(2c^2 - 8(\sigma-1)\omega\right)\omega^{1/2}\alpha_0 - \kappa^2 c\alpha_1\right],\\
\partial_\omega P &= 2\tilde{\kappa}\left[2c(\sigma-2)\omega^{1/2}\alpha_0 + \kappa^2\alpha_1\right].
\end{aligned}$$

From Lemmas 3.1.3 and 3.3.3, the determinant can be expressed as

$$\begin{aligned}
\det[d''(\omega,c)] &= \partial_\omega M\partial_c P - \partial_c M\partial_\omega P\\
&= 2^{-\frac{2}{\sigma}-4}\sigma^{-2}(1+\sigma)^{\frac{2}{\sigma}}(4\omega-c^2)^{\frac{2}{\sigma}-1}\omega^{-\frac{1}{\sigma}-2}\\
&\quad\times\left[4(\sigma-1)\omega\alpha_0 - 2\sqrt{\omega}c\alpha_0 + (4\omega-c^2)\alpha_1\right]\\
&\quad\times\left[4(\sigma-1)\omega\alpha_0 + 2\sqrt{\omega}c\alpha_0 - (4\omega-c^2)\alpha_1\right],
\end{aligned} \tag{3.3.12}$$

where

$$\begin{aligned}
\alpha_n(\omega,c;\sigma) &\equiv \int_0^\infty h^{-\frac{1}{\sigma}-n}dx > 0,\\
h(x;\sigma;\omega,c) &\equiv \cosh(\sigma\sqrt{4\omega-c^2}x) - \tfrac{c}{2\sqrt{\omega}}.
\end{aligned}$$

Meanwhile, the trace is

$$\begin{aligned}
\mathrm{tr}[d''(\omega,c)] &= \partial_\omega M + \partial_c P\\
&= 2^{-\frac{1}{\sigma}-2}\sigma^{-1}(1+\sigma)^{\frac{1}{\sigma}}(4\omega-c^2)^{\frac{1}{\sigma}-1}(1+\omega)\omega^{-\frac{1}{2\sigma}-\frac{3}{2}}\\
&\quad\times\left(c(c^2-4\omega)\alpha_1 + 2\sqrt{\omega}(c^2-4(\sigma-1)\omega)\alpha_0\right).
\end{aligned} \tag{3.3.13}$$

Theorem 3.3.4. *If* $\sigma \geq 2$, *and* $4\omega > c^2$, $p(d''(\omega,c)) = 0$.

Proof. We examine the terms appearing in (3.3.12). The first term is clearly positive. The second term is also positive,

$$\begin{aligned}
&4(\sigma-1)\omega\alpha_0 - 2\sqrt{\omega}c\alpha_0 + (4\omega-c^2)\alpha_1\\
=&4\omega\left[(\sigma-1-\frac{c}{2\sqrt{\omega}})\alpha_0 + (1-\frac{c^2}{4\omega})\alpha_1\right] > 0.
\end{aligned}$$

For the third term,

$$\begin{aligned}
&4(\sigma-1)\omega\alpha_0+2\sqrt{\omega}c\alpha_0-(4\omega-c^2)\alpha_1\\
\geq&(4\omega+2\sqrt{\omega}c)\alpha_0-(4\omega-c^2)\alpha_1\\
=&4\omega(1+\frac{c}{2\sqrt{\omega}})\int_0^\infty h^{-\frac{1}{\sigma}-1}(\cosh(\sigma\sqrt{4\omega-c^2}x)-1)dx>0.
\end{aligned}$$

Thus $\det[d''(\omega,c)]>0$, implying the eigenvalues of $d''(\omega,c)$ have the same sign. Turning to the trace, $c^2-4(\sigma-1)\omega\leq c^2-4\omega<0$ for $\sigma\geq 2$. By (3.3.13), $\mathrm{tr}[d''(\omega,c)]<0$. Hence, the two eigenvalues of $d''(\omega,c)$ are negative. □

In order to obtain the positive eigenvalue $p(d''(\omega,c))$ for $\sigma\in(0,2)$, we need the following lemma,

Lemma 3.3.5. *For $\sigma\in(0,2)$ and admissible (ω,c), $\det[d''(\omega,c)]$ has the same sign as $F(\frac{c}{2\sqrt{\omega}};\sigma)$, where*

$$\begin{aligned}
F(z;\sigma)\equiv&(\sigma-1)^2\left[\int_0^\infty(\cosh y-z)^{-\frac{1}{\sigma}}dy\right]^2\\
&-\left[\int_0^\infty(\cosh y-z)^{-\frac{1}{\sigma}-1}(z\cosh y-1)dy\right]^2.
\end{aligned}\tag{3.3.14}$$

Proof. We rewrite (3.3.12) as,

$$\begin{aligned}
&\frac{\det[d''(\omega,c)]}{2^{-\frac{2}{\sigma}-4}\sigma^{-2}(1+\sigma)^{\frac{2}{\sigma}}(4\omega-c^2)^{\frac{2}{\sigma}-1}\omega^{-\frac{1}{\sigma}-2}}\\
=&16(\sigma-1)^2\omega^2\alpha_0^2-\left[\alpha_1(c^2-4\omega)+2\sqrt{\omega}c\alpha_0\right]^2\\
=&16\omega^2\left\{(\sigma-1)^2\alpha_0^2-\left[\int_0^\infty h^{-\frac{1}{\sigma}-1}\left(\tfrac{c}{2\sqrt{\omega}}\cosh(\sigma\sqrt{4\omega-c^2}x)-1\right)dx\right]^2\right\}.
\end{aligned}$$

Letting $y=\sigma\sqrt{4\omega-c^2}x$,

$$\frac{\det[d''(\omega,c)]}{2^{-\frac{2}{\sigma}-4}\sigma^{-2}(1+\sigma)^{\frac{2}{\sigma}}(4\omega-c^2)^{\frac{2}{\sigma}-1}\omega^{-\frac{1}{\sigma}-2}}=\frac{16\omega^2}{\sigma^2(4\omega-c^2)}F\left(\frac{c}{2\sqrt{\omega}};\sigma\right).\tag{3.3.15}$$

□

When $\sigma=1$ and $z\in(-1,1)$, we have $F(z;\sigma)=-1$ and $\det[d''(\omega,c)]=-1/\omega$. For $\sigma\in(0,1)\cup(1,2)$, we can evaluate the function $F(z;\sigma)$ numerically, as shown in Figures 3.1 and 3.2. For any fixed $\sigma\in(1,2)$, $F(z;\sigma)$ is monotonically increasing in z and has exactly one root z_0 in the interval $(-1,1)$. For fixed $\sigma\in(0,1)$, $F(z;\sigma)$ is monotonically

decreasing in z and strictly negative. It is this numerical computation of F which is used to complete the proofs of Theorems 1.3.4 and 1.3.5. In contrast, for $\sigma \geq 2$, we can prove that $F(z;\sigma)$ is strictly positive without resorting to computation.

We thus have the following theorem about $p(d''(\omega,c))$:

Theorem 3.3.6. *For admissible (ω,c),*

(i) when $\sigma \in (1,2)$ and $c = 2z_0\sqrt{\omega}$, $\det[d''(\omega,c)] = 0$.

(ii) when $\sigma \in (1,2)$ and $c < 2z_0\sqrt{\omega}$, $\det[d''(\omega,c)] < 0$; $p(d''(\omega,c)) = 1$.

(iii) when $\sigma \in (1,2)$ and $c > 2z_0\sqrt{\omega}$, $\det[d''(\omega,c)] > 0$; $p(d''(\omega,c)) = 0$ or $p(d''(\omega,c)) = 2$.

(iv) when $\sigma \in (0,1)$,$\det[d''(\omega,c)] < 0$; $p(d''(\omega,c)) = 1$.

(v) when $\sigma = 1$, $\det[d''(\omega,c)] = -1/\omega < 0$; $p(d''(\omega,c)) = 1$.

3.4 Orbital Stability and Orbital Instability

In this section, we complete the proof of orbital stability/instability.

Proof of Theorem 1.3.3. From Theorem 3.2.1 and Theorem 3.3.4, $n(H) = 1$ for any $\sigma > 0$, and $p(d'') = 0$ for $\sigma \geq 2$. Thus $n(H) - p(d'') = 1$, is odd, and by Theorem 1.3.6, all solitary waves are orbitally unstable. □

Proof of Theorem 1.3.4. By Theorem 3.3.6, $\det[d''(\omega,c)] < 0$ for admissible (ω,c) satisfying $c < 2z_0\sqrt{\omega}$. It follows that $d''(\omega,c)$ has one positive eigenvalue and one negative eigenvalue. Therefore, $p(d'') = 1$. Furthermore, from Theorem 3.2.1, $n(H) = 1$. Hence

$$n(H) - p(d'') = 0,$$

and solitary waves are orbital stable.

When $c > 2z_0\sqrt{\omega}$, also by Theorem 3.3.6, $\det[d''(\omega,c)] > 0$. So the signs of the two eigenvalues of $d''(\omega,c)$ are the same. If both of eigenvalues were positive, then $2 = p(d'') > n(H_\phi) = 1$. This would contradict (1.3.10). Hence both eigenvalues are negative and $p(d'') = 0$. It follows that

$$n(H) - p(d'') = 1,$$

and solitary waves are orbitally unstable. □

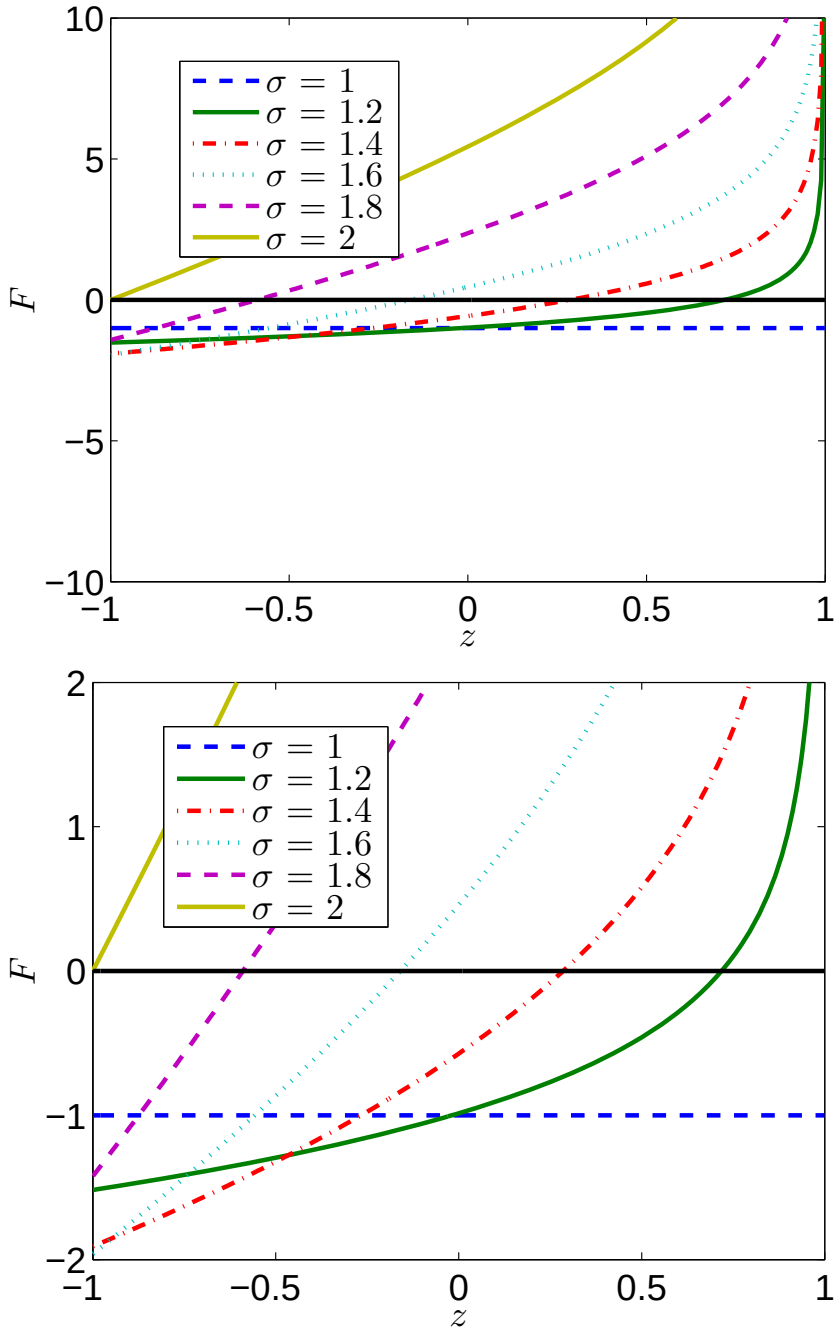

Figure 3.1: (a) Function $F(z;\sigma)$, (3.3.14), for several values of $\sigma \in [1,2]$. (b) is a magnified plot near the z-axis.

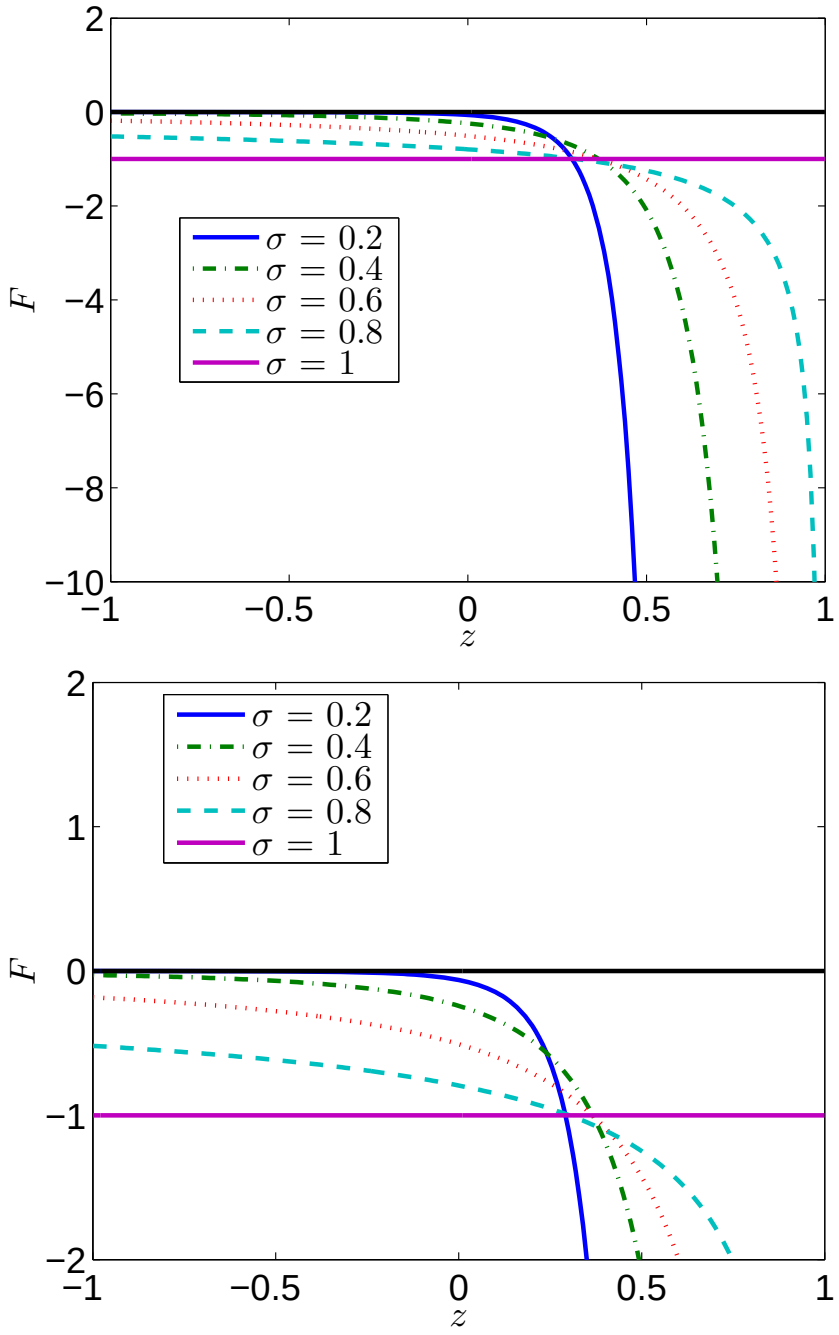

Figure 3.2: (a) Function $F(z;\sigma)$, (3.3.14), for several values of $\sigma \in (0,1]$. (b) is a magnified plot near the z-axis.

We prove Theorem 1.3.5 following the same argument, .

Proof of Theorem 1.3.5. When $\sigma \in (0,1]$, from Theorem 3.3.6, $\det[d''(\omega,c)] < 0$ for admissible (ω,c). Consequently, $d''(\omega,c)$ has one positive eigenvalue and one negative eigenvalue; $p(d'')=1$. By Theorem 3.2.1, $n(H)=1$. Hence

$$n(H)-p(d'')=0,$$

and solitary waves are orbitally stable. □

3.5 Basic Spectral Theorems

In this section we establish some basic theorems using in the previous sections. We present some results of spectral theorem in Section 3.5.1, and we discuss the Sturm-Liouville theory in Section 3.5.2.

3.5.1 Weyl's Essential Spectral Theorem

In this part, we will prove the Weyl's essential spectral theorem we use in Chapter 3:

Theorem 3.5.1. *If operator $L=-\partial_{xx}+V(x)+c$ on $L^2(\mathbb{R})$ with $V(x)\to 0$ as $|x|\to\infty$, then*

$$\sigma_{ess}(L)=[c,\infty). \tag{3.5.1}$$

We use the following theorems in Chapter 5 of the book by Gustafson and Sigal [27] to proof this theorem. First we need recall the definition of *Weyl sequence* for operator A and λ on a Hilbert space $\mathcal{H}$.

Definition 3.5.2. We say $\{\psi_n\}\subset\mathcal{H}$ is a *Weyl sequence* for operator A and λ on a Hilbert space $\mathcal{H}$ if

(a) $\|\psi_n\|=1$ for all n.

(b) $\|(A-\lambda)\psi_n\|\to 0$ as $n\to\infty$.

(c) $\psi_n\to 0$ weakly as $n\to\infty$.

We also define the *Weyl spectrum*:

Definition 3.5.3. The *Weyl spectrum* of an operator A is

$$\sigma_w(A)=\{\lambda|\text{there is a Weyl sequence for } A \text{ and } \lambda\}. \tag{3.5.2}$$

Moreover, we need two theorems

Theorem 3.5.4 (**Weyl**). *If $A = A^*$, where A^* is the adjoint operator of A. then*

$$\sigma_{ess}(A) = \sigma_w(A).$$

Theorem 3.5.5 (Theorem 5.20 in [27]). *Let $V : \mathbb{R} \to \mathbb{R}$ be continuous, with $V(x) \to 0$ as $|x| \to \infty$. Then*

1. *$H = -\partial_{xx} + V$ is self-adjoint on $L^2(\mathbb{R})$.*

2. *$\sigma_{ess}(H) = [0, \infty)$.*

Now we can prove the Theorem 3.5.1.

Proof of the Theorem 3.5.1. If $\lambda \in \sigma_{ess}(L)$, then by the theorem 3.5.4 and the Definition 3.5.2 and 3.5.3, we know there is a Weyl sequence $\{\psi_n\}$ for L and λ. It follows

$$\|(L - \lambda)\psi_n\| \to 0 \text{ as } n \to \infty. \tag{3.5.3}$$

Hence

$$\|(-\partial_{xx} + V + c - \lambda)\psi_n\| \to 0 \text{ as } n \to \infty. \tag{3.5.4}$$

and

$$\|(H - \tilde{\lambda})\psi_n\| \to 0 \text{ as } n \to \infty, \tag{3.5.5}$$

where $H = -\partial_{xx} + V$ and $\tilde{\lambda} = \lambda - c$. Therefore, $\{\psi_n\}$ is also the Weyl sequence for H and $\tilde{\lambda}$. By the theorem 3.5.4 and 3.5.5,

$$\tilde{\lambda} \in \sigma_{ess}(H) = [0, \infty).$$

Thus

$$\lambda = \tilde{\lambda} + c \in [c, \infty).$$

Conversely, If $\lambda \in [c, \infty)$, then $\tilde{\lambda} \in \sigma_{ess}(H)$. Thus, there exists a Weyl sequence $\{\psi_n\}$ for H and $\tilde{\lambda}$. Similar argument as above will give us $\{\psi_n\}$ is also a Weyl sequence for L and λ. Therefore

$$\lambda \in \sigma_{ess}(L).$$

□

3.5.2 Sturm-Liouville Theory

We recall here some basic theories on the Sturm-Liouville problem,

$$-\frac{d}{dx}\left(p(x)\frac{dy}{dx}\right)+q(x)y=\lambda w(x)y, \tag{3.5.6}$$

where $p(x)>0$, $w(x)>0$ and λ is an eigenvalue. If the domain is a bounded interval $[a,b]$, and the boundary conditions are separated, namely

$$\begin{aligned}\alpha_1 y(a)+\alpha_2 y'(a)&=0 \qquad (\alpha_1^2+\alpha_2^2>0),\\ \beta_1 y(b)+\beta_2 y'(b)&=0 \qquad (\beta_1^2+\beta_2^2>0),\end{aligned} \tag{3.5.7}$$

we have the existence of eigenvalues and properties of the eigenfunctions,

Theorem 3.5.6 ([72]). *Consider the equation* (3.5.6) *with the boundary conditions* (3.5.7). *If* $p(x), w(x)>0$, *and* $p(x), p'(x), q(x)$, *and* $w(x)$ *are continuous functions over the finite interval* $[a,b]$, *then*

- *The eigenvalues* $\lambda_1, \lambda_2, \lambda_3, \cdots$ *are real and isolated, i.e.*

$$\lambda_1<\lambda_2<\lambda_3<\cdots<\lambda_n<\cdots\to\infty;$$

- *Corresponding to each eigenvalue* λ_n, *there is a unique (up to a normalization constant) eigenfunction* $y_n(x)$ *which has exactly* $n-1$ *zeros in* (a,b).

In the proof of Lemma 3.2.4 and Lemma 3.2.8, we consider boundary value problems on the real line. The following theorem gives properties of the first two eigenvalues.

Theorem 3.5.7 ([8]). *Suppose that* $\phi\in L^2(\mathbb{R})$ *satisfies the differential equation*

$$-\phi''+c\phi-f(\phi)=0,$$

where $c>0$, *and* $f(x):\mathbb{R}\to\mathbb{R}$ *is a smooth function satisfying* $f(0)=f'(0)=0$. *If* ϕ' *has exactly one unique zero, then*

- *the differential operator*

$$\mathcal{L}_0\psi\equiv-\psi''+[c-f'(\phi)]\psi$$

defined in $L^2(\mathbb{R})$ *has exactly one simple negative eigenvalue* λ_0;

- *the eigenvalue zero is simple with associated eigenfunction* ϕ'*;*
- *there exists* $\delta > 0$ *such that every* $\lambda \in \sigma(\mathcal{L}_0) - \{\lambda_0, 0\}$ *satisfies* $\lambda > \delta$*, where* $\sigma(\mathcal{L}_0)$ *is the continuous spectrum of* $\mathcal{L}_0$*.*

3.6 Numerical Illustrations

In this section, we present some numerical study of the spectrum of the linearized operator H_ϕ and the time evolution of the perturbed solution.

3.6.1 Numerical Integration of the Spectrum of the Linearized Operator

Using Lemma 3.1.1, the self-adjoint operator

$$L \equiv \begin{pmatrix} L_1 & L_2 \\ \bar{L}_2 & \bar{L}_1 \end{pmatrix} \tag{3.6.1}$$

acts on $(u, \bar{u})^T$ as

$$L \begin{pmatrix} u \\ \bar{u} \end{pmatrix} = \begin{pmatrix} L_1 & L_2 \\ \bar{L}_2 & \bar{L}_1 \end{pmatrix} \begin{pmatrix} u \\ \bar{u} \end{pmatrix} = \begin{pmatrix} H_\phi u \\ \overline{H_\phi u} \end{pmatrix}. \tag{3.6.2}$$

It follows the spectrum of L is the same as H_ϕ. We compute the spectrum of L using the sinc-collocation spectral method. The sinc-collocation method was introduced by Stenger [60], and it has been used in a wide variety of problems involving differential equations [48, 49, 61]. The sinc function is define as

$$sinc(z) \equiv \begin{cases} \frac{sin(\pi z)}{\pi z}, & \text{if } z \neq 0; \\ 1, & \text{if } z = 0. \end{cases} \tag{3.6.3}$$

In the sinc-collocation method, a function $f : \mathbb{R} \to \mathbb{R}$ is approximated using a superposition of shifted and scaled sinc function,

$$G_M(f, h)(x) \equiv \sum_{k=-M}^{M} f(x_k) S_{k,h}(x), \tag{3.6.4}$$

where

$$S_{k,h}(x) = sinc\left(\frac{x - x_k}{h}\right), \quad h > 0,$$

and $x_k = kh$ for $k = -M, \cdots, M$. There are two useful features in this spectral method:

- The decay of f to 0 as $x \to \pm\infty$ is naturally incorporated in the definition of sinc function.
- The shifted and scaled sinc function $S_{k,h}$ acts like discrete delta functions,

$$S_{k,h}(x_j) = \begin{cases} 1, & j = k; \\ 0, & j \neq k. \end{cases}$$

  where $j = -M, \cdots, M$. It follows

$$G_M(f,h)(x_k) = f(x_k).$$

For sufficiently smooth functions, the following theory shows that the approximate function G_M quickly converges to f as M goes to infinity,

Theorem 3.6.1 (Theorem 2.16 of [48]). *Assume that f is an analytic function on a strip*

$$D_\nu = \{z \in \mathbb{C} \big| |\Im(z)| < \nu\}.$$

If f satisfies

$$\|f(t + i\cdot)\|_{L^1(-\nu,\nu)} = O(|t|^a), \text{ as } t \to \pm\infty, \text{ with } a \in [0,1],$$
$$\lim_{y\to\nu^-} \|f(\cdot + iy)\|_{L^p} + \lim_{y\to\nu^-} \|f(\cdot - iy)\|_{L^p} < \infty.$$

and the decay estimate

$$|f(x)| \leq C \exp(-\alpha|x|),$$

then

$$\|\partial_x^n f - \partial_x^n G_M(f,h)\|_{L^\infty} \leq C M^{(n+1)/2} \exp\left(-\sqrt{\pi\nu\alpha M}\right),$$

where h is selected such that

$$h = \sqrt{\pi\nu/(\alpha M)} \leq \min\{\pi\nu, \pi/\sqrt{2}\}. \tag{3.6.5}$$

In practice, it is non-trivial to check a function satisfies all these hypotheses, so we choose the parameters based on the soliton solution $\psi_{\omega,c}$ (1.2.5) of gDNLS. To make $\psi_{\omega,c}$ analytic on the strip D_ν,

$$\cosh(\sigma\sqrt{4\omega - c^2}x) \neq \frac{c}{2\sqrt{\omega}}.$$

It follows when $x = i\nu$,

$$\cosh(\sigma\sqrt{4\omega - c^2}x) = \cos(\sigma\sqrt{4\omega - c^2}\nu) \neq \frac{c}{2\sqrt{\omega}}.$$

Hence the largest possibility of ν is

$$\nu = \frac{\arccos\left(c/(2\sqrt{\omega})\right)}{\sigma\sqrt{4\omega - c^2}}. \tag{3.6.6}$$

On the other hand, from (1.2.5),

$$\psi_{\omega,c} \sim \cosh(\sigma\sqrt{4\omega - c^2}x)^{-1/(2\sigma)} \sim \exp\left(-\frac{1}{2}\sqrt{4\omega - c^2}\right), \text{ as } |x| \to \infty.$$

Thus, the decay rate of f is $\frac{1}{2}\sqrt{4\omega - c^2}$. It follows, from (3.6.6) and (3.6.5), the mesh distance is

$$h = \sqrt{\frac{2\pi \arccos\left(c/(2\sqrt{\omega})\right)}{\sigma(4\omega - c^2)M}}.$$

Table 3.1 shows the values of the first four eigenvalues of the operator L, when $\omega = 1, \sigma = 2, c = -1, 0, 1$ and $M = 1024$. In all three cases, there are two zero eigenvalues and one negative eigenvalue, which confirms Theorem 3.2.1. Figure 3.3 shows a typical spectrum of L using $\omega = 1, \sigma = 2, c = 1$ and $M = 1024$, with one negative eigenvalue, two superposition zero eigenvalues in the graph, and all other eigenvalues bounded away from zero.

Table 3.1: The first four eigenvalues of the operator L, when $\omega = 1, \sigma = 2, c = -1, 0, 1$ and $M = 1024$.

	e_1	e_2	e_3	e_4
$c = -1$	-8.26209	1.63648e-12	2.72519e-12	0.754352
$c = 0$	-17.0998	-1.33112e-11	2.49993e-13	1.00774
$c = 1$	-26.5972	-9.21356e-13	1.54734e-12	0.758772

3.6.2 Numerical Simulation with an Initial Condition in the Form of Perturbed Soliton

From Theorem 1.3.4, there are both orbitally stable and unstable branches for every $\sigma \in (1, 2)$, and they are separated by a turning curve $c = 2z_0(\sigma)\sqrt{\omega}$. We take an initial

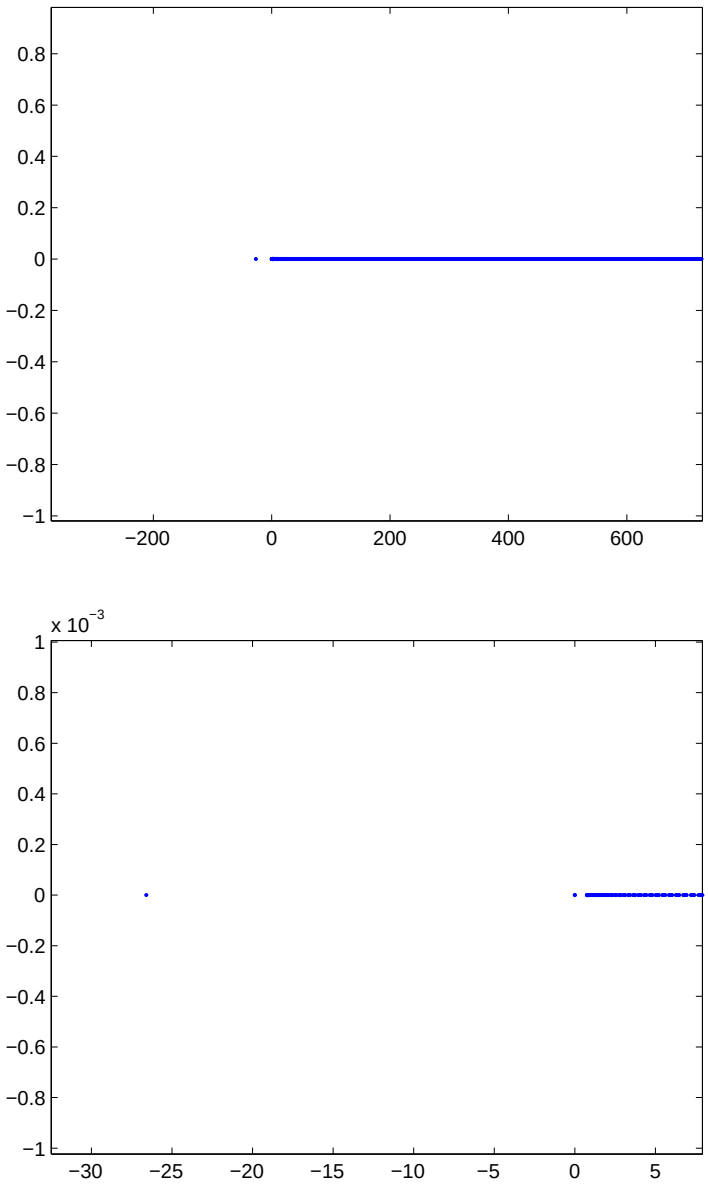

Figure 3.3: The spectrum of L when $\omega = 1, c = 1, \sigma = 2$ and $M = 1024$. The lower figure is a zoom in of the upper figure.

condition

$$\psi_0(x,0) = \psi_{\omega,c}(x,0) + 0.0001e^{-2x^2} \tag{3.6.7}$$

with c and ω close to the turning curve $c = 2z_0\sqrt{\omega}$, and integrate (1.1.1) with $\sigma = 1.5$ using the fourth order exponential time difference scheme [37]. Though the nonlinearity is not polynomial in its arguments, ψ, $\bar{\psi}$ and ψ_x,

$$|\psi|^3 \psi_x = \psi\bar{\psi}\,|\psi|\,\psi_x,$$

we found that using dealiasing associated to the quintic problem proved robust.

Our results are as follows:

1. When $\omega = 1$ and $c = 0 < 2z = 0.1236606$, Figure 3.4 shows that the solitary wave retains its shape for a long time ($t = 100$).

2. When $\omega = 1$ and $c = 0.2 > 2z = 0.1236606$, Figure 3.5 shows that the amplitude of the solitary wave increases rapidly near $t = 10$ and it is not stable.

Our simulation of the unstable soliton suggests that, rather than dispersing or converging to a stable soliton, gDNLS may result in a finite time singularity. The potential for singularity formation is studied in Chapter 2.

3.7 Discussion

We have explored the stability and instability of solitons for a generalized derivative nonlinear Schrödinger equation. We have found that for $\sigma \geq 2$, all solitons are orbital unstable. Using a numerical calculation of the function $F(z;\sigma)$ defined in (3.3.14). we have also shown that for $0 < \sigma \leq 1$, all solitons are orbital stable. For $1 < \sigma < 2$, our computation of $F(z;\sigma)$ indicates there exist both stable and unstable solitons, depending on the values of ω and c. In particular, for fixed ω and $\sigma > 1$, there are always both stable and unstable solitons for properly selected c. For σ near 1, the unstable solitons are always rightward moving, but, as Figure 3.1 shows, the root, z_0, becomes negative as σ approaches 2. Once $z_0 < 0$, unstable solitons can be both rightward and leftward moving.

Other dispersive PDEs possessing both stable and unstable solitons, such as NLS and KdV with saturating nonlinearities, [14, 15, 49, 56, 62], achieve this when introducing a nonlinearity that breaks scaling. In contrast, gDNLS always has a scaling symmetry, and throughout the regime $1 < \sigma < 2$, the scaling is L^2 supercritical. This also implies the

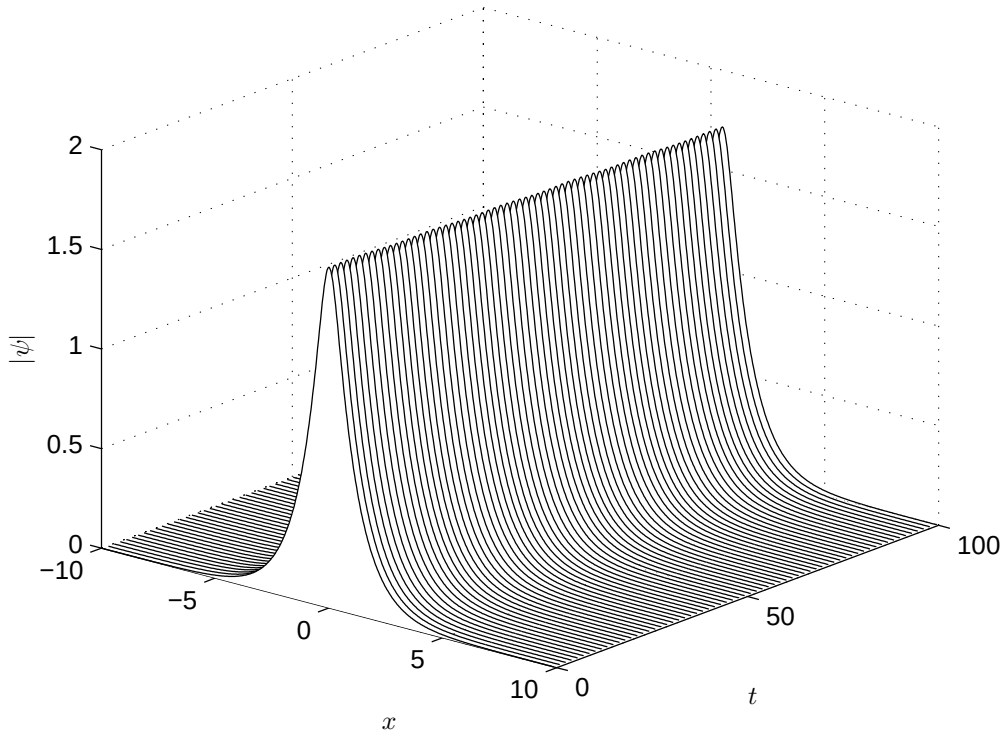

Figure 3.4: Evolution of a perturbed orbitally stable soliton, $\omega = 1$ and $c = 0$, with initial condition (3.6.7).

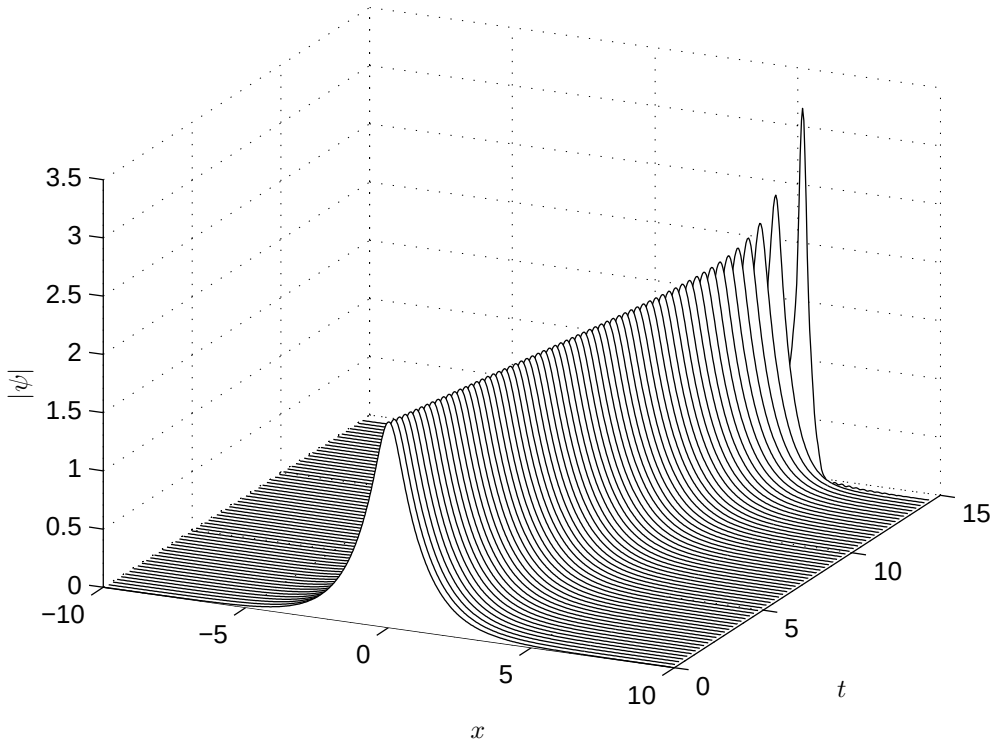

Figure 3.5: Evolution of a perturbed orbitally unstable soliton, $\omega = 1$ and $c = .2$, with initial condition (3.6.7).

existence of an entire manifold of *critical* solitons, precisely when $c = 2z_0\sqrt{\omega}$. Along this curve, the standard stability results of [24, 25, 69, 70], break down, and a more detailed analysis is required. In this degenerate case, the stability can be obtained provided $d(\omega, c)$ remains convex [25]. Given that within any neighborhood of a critical soliton there exist unstable solitons, we conjecture that it is unstable. While there has been recent work on critical one-parameter solitons for NLS type equations, [14, 15, 49, 56], to the best our knowledge, there has not been an analogous work on two-parameter solitons.

We observe that, in contrast to NLS solitons, not all gDNLS solitons can be obtained from scaling. Indeed, for (1.3.1), all solitons $e^{i\lambda t}R(\mathbf{x};\lambda)$, solving

$$-\Delta R + \lambda R - R^{2\sigma+1} = 0$$

can be obtained from the $\lambda = 1$ soliton via the transformation

$$e^{i\lambda t}R(\mathbf{x};\lambda) = e^{i\lambda t}\lambda^{\frac{1}{2\sigma}}R(\lambda^{\frac{1}{2}}\mathbf{x};1).$$

In contrast, while the gDNLS solitons inherit the scaling symmetry of gDNLS, not all admissible (ω, c) can be scaled to a particular soliton. Instead,

$$\psi_{\omega,c}(x,t) = e^{i\omega t}\phi_{\omega,c}(x-ct) = e^{i\omega t}\phi_{1,c/\sqrt{\omega}}(\sqrt{\omega}(x-ct)). \tag{3.7.1}$$

Only solitons for which

$$\frac{c_1}{\sqrt{\omega_1}} = \frac{c_2}{\sqrt{\omega_2}}$$

can be scaled into one another.

Our results are based on the assumption that a weak solution exists in H^1 . While we do not have an H^1 theory in general, our results can, in part, be made rigorous as follows. For $\sigma \geq 2$, one should be able to apply the technique of [64] to obtain a local solution in H^s, with $s > 1$. Alternatively, for $\sigma \geq 2$ and integer valued, [39, 40] can be invoked. Again, this yields a local solution in H^s, $s > 1$. For s sufficiently large, the solution will also conserve the invariants.

This is sufficient to fully justify the instability of the unstable solitons, since there is sufficient regularity such that if the solution leaves a neighborhood of the soliton in H^1, it also leaves in H^s, $s > 1$. However, this is insufficient to prove stability, because even if the solution stays close in the H^1 norm, the norm of the solution could grow in a higher Sobolev norm.

There is also the question of the monotonicity of F, for which we relied on numerical

computation for $\sigma < 2$. Looking at Figures 3.1 and 3.2, it would appear that the $F(z;\sigma = 2)$ is an upper bound on $F(z;\sigma)$ for $1 < \sigma < 2$. In addition, there appears to be a singularity at $z = 1$. Likewise, the line $F = 0$ appears to be an upper bound in the range $\sigma \leq 1$. A more subtle analysis may permit a rigorous justification of our work in this regime.

Finally, the solitary solution $\phi_{\omega,c}$ (1.2.5) is only defined when $c^2 < 4\omega$. What happens when $c^2 \to 4\omega$? Computing the integral in the phase of the solitary solution (1.2.5), we get

$$\begin{aligned}\int_{-\infty}^{y} \varphi^{2\sigma} dy =& \int_{-\infty}^{y} \left(\frac{2\sqrt{\omega}}{(\sigma+1)(4\omega - c^2)} \left(\cosh(\sigma\sqrt{4\omega - c^2}y) - \frac{c}{2\sqrt{\omega}} \right) \right)^{-1} dy \\ =& 2(1+\frac{1}{\sigma}) \left(\arctan(\frac{c+2\sqrt{\omega}}{\sqrt{4\omega - c^2}}) + \arctan\left(\tanh(\frac{\sigma y\sqrt{4\omega - c^2}}{2}) \frac{c+2\sqrt{\omega}}{\sqrt{4\omega - c^2}} \right) \right).\end{aligned} \tag{3.7.2}$$

when $c \to 2\sqrt{\omega}$,

$$\arctan(\frac{c+2\sqrt{\omega}}{\sqrt{4\omega - c^2}}) \to \frac{\pi}{2} \tag{3.7.3}$$

and

$$\tanh(\frac{\sigma y\sqrt{4\omega - c^2}}{2}) \frac{1}{\sqrt{4\omega - c^2}} \to \frac{\sigma y}{2}. \tag{3.7.4}$$

Thus

$$\int_{-\infty}^{y} \varphi^{2\sigma} dy \to 2(1+\frac{1}{\sigma}) \left(\frac{\pi}{2} + \arctan(2\sqrt{\omega}\sigma y) \right). \tag{3.7.5}$$

It follows that

$$\theta \to \sqrt{\omega}y - \frac{1}{\sigma} \left(\frac{\pi}{2} + \arctan(2\sqrt{\omega}\sigma y) \right). \tag{3.7.6}$$

Furthermore,

$$\varphi(y)^{2\sigma} \sim \frac{(1+\sigma)(4\omega - c^2)}{2\sqrt{\omega}\left(1 + \frac{1}{2}\sigma^2 y^2(4\omega - c^2) - \frac{c}{2\sqrt{\omega}}\right)} = \frac{(1+\sigma)(2\sqrt{\omega} + c)}{1 + \sqrt{\omega}\sigma^2 y^2(2\sqrt{\omega} + c)} \to \frac{4\sqrt{\omega}(1+\sigma)}{1 + 4\omega\sigma^2 y^2}.$$

Therefore, the limiting soliton (lump soliton) is

$$\begin{aligned}\psi(y) &= \left(\frac{4\sqrt{\omega}(1+\sigma)}{1 + 4\omega\sigma^2 y^2} \right)^{\frac{1}{2\sigma}} e^{i(\omega t + \sqrt{\omega}y - \frac{1}{\sigma}\left(\frac{\pi}{2} + \arctan(2\sqrt{\omega}\sigma y)\right))} \\ &= \left(\frac{2c(1+\sigma)}{1 + c^2\sigma^2 y^2} \right)^{\frac{1}{2\sigma}} e^{i(\frac{c^2}{4}t + \frac{c}{2}y - \frac{1}{\sigma}\left(\frac{\pi}{2} + \arctan(c\sigma y)\right))},\end{aligned} \tag{3.7.7}$$

and has an algebraic decay as $y \to \pm\infty$.

On the other hand, when $c \to -2\sqrt{\omega}$,

$$\varphi(y)^{2\sigma} \sim \frac{(1+\sigma)(4\omega - c^2)}{2\sqrt{\omega}\left(1 + \frac{1}{2}\sigma^2 y^2(4\omega - c^2) - \frac{c}{2\sqrt{\omega}}\right)} = \frac{(1+\sigma)(2\sqrt{\omega}+c)}{1 + \sqrt{\omega}\sigma^2 y^2(2\sqrt{\omega}+c)} \to 0.$$

Hence,

$$\psi(y) \to 0,$$

and there are no nontrivial solutions when $c = -2\sqrt{\omega}$.

A natural question is whether the lump soliton (3.7.7) is orbitally stable. A preliminary study shows that, when $4\omega = c^2$, the operator $\tilde{L}_{11}$ in (3.2.4) takes the form

$$\tilde{L}_{11} = -\partial_{yy} + \frac{c(2\sigma+1)}{2}\varphi^{2\sigma} - \frac{8\sigma^2 + 6\sigma + 1}{4(\sigma+1)^2}\varphi^{4\sigma}.$$

The continuous spectrum of $\tilde{L}_{11}$ is equal to $[0, \infty)$, which is not bounded away from 0. We plan to further study this problem in the future.

Chapter 4

Numerical Simulation of Resonant Tunneling of Fast Solitons for the Nonlinear Schrödinger Equation

In this chapter, we illustrate numerically that the phenomenon of resonant tunneling, described in Section (1.4), occurs in a nonlinear setting, namely, for the one dimensional cubic NLS equation (1.4.2) with two classes of potentials, the 'box' potential (1.4.4) and a repulsive 2-delta potential (1.4.3).

We consider an initial condition in the form of a slightly perturbed, fast moving NLS soliton. Under a certain resonant condition, we show that the incoming soliton almost fully passes trough the potential barrier. We calculate the transmitted mass of the soliton, and show that it converges to the total mass of the solution as the velocity of the soliton increases.

This chapter is organized as follows. In Section 4.1 we recall some basic facts about linear scattering theory and apply it to the two examples of potential under consideration. In Section 4.2, we give a detailed description of our numerical results. Lastly, we describe the numerical method and some tests to validate the computations in Section 4.3.

4.1 Linear Quantum Mechanical Scattering

In this section, we derive the resonant tunneling condition using the linear scattering theory. Considering the linear Schrödinger equation with external potential $V(x)$,

$$iu_t + \frac{1}{2}u_{xx} - qV(x)u = 0, \tag{4.1.1}$$

where the potential $V(x)$ is the repulsive 2-δ potential (1.4.3) and the 'box' potential (1.4.4). We will refer to the 2-δ potential (1.4.3) as potential (P1), and to the box potential (1.4.4) as potential (P2).

2-δ Potential (P1)

We consider the "eigenvalue" problem related to (4.1.1)

$$\beta u + \frac{1}{2}u_{xx} - qVu = 0, \tag{4.1.2}$$

where $\beta \in \mathbb{R}$. On the intervals $(-\infty, -l), (-l, l)$ and (l, ∞), this equation has the general solution $u = e^{\pm i\lambda x}$, where $\lambda = \sqrt{2\beta}$. Thus the solution of (4.1.2) has the form

$$\begin{cases} u = e^{i\lambda x} + Re^{-\lambda x}, & x < -l; \\ u = Be^{i\lambda x} + Ae^{-i\lambda x}, & -l < x < l; \\ u = Te^{i\lambda x}, & x > l. \end{cases} \tag{4.1.3}$$

where R, A, B, T are coefficients to be determined. Imposing that $u(x)$ is continuous at $x = \pm l$, we have

$$\begin{aligned} Be^{il\lambda} + Ae^{-il\lambda} &= Te^{il\lambda}, \\ e^{-il\lambda} + Re^{il\lambda} &= Be^{-il\lambda} + Ae^{il\lambda}. \end{aligned} \tag{4.1.4}$$

In order to solve the four unknown coefficients, we get another two equations by integrating the equation (4.1.2) across the point $x = \pm l$, respectively,

$$\begin{aligned} &\lim_{\epsilon\to 0}\int_{\pm l-\epsilon}^{\pm l+\epsilon} -\frac{1}{2}u_{xx} + q(\delta(x+l) + \delta(x-l))u dx \\ =&\beta \lim_{\epsilon\to 0}\int_{\pm l-\epsilon}^{\pm l+\epsilon} u dx = 0. \end{aligned} \tag{4.1.5}$$

It follows

$$\begin{aligned} -\frac{1}{2}\lim_{\epsilon\to 0}[u_x(l+\epsilon) - u_x(l-\epsilon)] + qu(l) = 0, \\ -\frac{1}{2}\lim_{\epsilon\to 0}[u_x(-l+\epsilon) - u_x(-l-\epsilon)] + qu(-l) = 0. \end{aligned} \tag{4.1.6}$$

Using

$$\begin{cases} u_x = i\lambda e^{i\lambda x} - i\lambda R e^{-\lambda x}, & x < -l; \\ u_x = i\lambda B e^{i\lambda x} - ik_2 A e^{-i\lambda x}, & -l < x < l; \\ u_x = i\lambda T e^{i\lambda x}, & x > l, \end{cases} \tag{4.1.7}$$

equation (4.1.6) becomes

$$\begin{aligned} \frac{1}{2}[i\lambda T e^{i\lambda l} - i\lambda B e^{i\lambda l} + i\lambda A e^{-i\lambda l}] &= qBe^{i\lambda l} + qAe^{-i\lambda l} \\ \frac{1}{2}[-i\lambda e^{-i\lambda l} + i\lambda R e^{i\lambda l} + i\lambda B e^{-i\lambda l} - i\lambda A e^{i\lambda l}] &= qBe^{-i\lambda l} + qAe^{i\lambda l}. \end{aligned} \tag{4.1.8}$$

Solving (4.1.4) and (4.1.8)),we get

$$\begin{aligned} R =& q\frac{-ie^{-il\lambda}(\lambda(1+e^{4il\lambda}) + iq(1-e^{4il\lambda}))}{\lambda^2 + 2i\lambda q - q^2 + e^{4il\lambda}q^2} \\ T =& \frac{\lambda^2}{\lambda^2 + 2i\lambda q - q^2 + e^{4il\lambda}q^2}. \end{aligned} \tag{4.1.9}$$

The numerator of $R(\lambda)$ identifies to $-2iq(\lambda\cos(2l\lambda) + q\sin(2l\lambda))$. Thus, if λ_0 is such that $\tan(2l\lambda_0) = -\lambda_0/q$, $R(\lambda_0) = 0$, and resonant tunneling occurs. In the NLS equation, the role of the wave number λ is played by the velocity, which is assumed to be large. Therefore, we will choose our parameters so that the velocity v of the initial solitary wave satisfies $\frac{v}{q} = -\tan(2lv)$.

Box Potential (P2)

Consider the related "eigenvalue" problem

$$\beta u + \frac{1}{2}u_{xx} - qVu = 0, \tag{4.1.10}$$

where β is a constant. When $x \in (-\infty, -l) \cup (l, \infty)$, (4.1.10) has the form

$$\beta u + \frac{1}{2}u_{xx} = 0, \tag{4.1.11}$$

and $u = e^{\pm i\lambda x}$, where $\lambda = \sqrt{2\beta}$. When $-l < x < l$, (4.1.10) becomes

$$\beta u + \frac{1}{2}u_{xx} - qu = 0,$$

which implies $u = e^{\pm ikx}$ with $k = \sqrt{2\beta - 2q}$. Thus, we have the solution of (4.1.10) on the real line,

$$\begin{cases} u = e^{i\lambda x} + Re^{-\lambda x}, & x < -l; \\ u = Be^{ikx} + Ae^{-ikx}, & -l < x < l; \\ u = Te^{i\lambda x}, & x > l, \end{cases} \tag{4.1.12}$$

where R, A, B, T are constants to be determined by the continuity of u and u_x. Imposing that $u(x)$ is continuous at the point $x = -l$ and $x = l$, we have

$$\begin{aligned} e^{-i\lambda l} + Re^{i\lambda l} &= Be^{-ilk} + Ae^{ilk}, \\ Be^{ilk} + Ae^{-ilk} &= Te^{il\lambda}. \end{aligned} \tag{4.1.13}$$

Using

$$\begin{cases} u_x = i\lambda e^{i\lambda x} - i\lambda Re^{-\lambda x}, & x < -l; \\ u_x = ikBe^{ikx} - ikAe^{-ikx}, & -l < x < l; \\ u_x = i\lambda Te^{i\lambda x}, & x > l. \end{cases} \tag{4.1.14}$$

and the continuity of u_x at $x = \pm l$, we obtain

$$\begin{aligned} i\lambda e^{-il\lambda} - i\lambda Re^{il\lambda} &= ikBe^{-ilk} - ikAe^{ikl}, \\ ikBe^{ilk} - ikAe^{-ilk} &= i\lambda Te^{i\lambda l}. \end{aligned} \tag{4.1.15}$$

Solving (4.1.13) and (4.1.15), we get

$$\begin{aligned} R &= \frac{e^{-2il\lambda}(1 - e^{4ilk})(\lambda^2 - k^2)}{e^{4ilk}(\lambda - k)^2 - (\lambda + k)^2}, \\ T &= \frac{4e^{-2il(\lambda - k)}\lambda k}{e^{4ilk}(\lambda - k)^2 - (\lambda + k)^2}. \end{aligned} \tag{4.1.16}$$

It follows

$$R = q\frac{ie^{-2il\lambda}\sin(2l\sqrt{\lambda^2 - 2q})}{\cos(2l\sqrt{\lambda^2 - 2q})\lambda\sqrt{\lambda^2 - 2q} - i\sin(2l\sqrt{\lambda^2 - 2q})(\lambda^2 - q)} \tag{4.1.17}$$

and

$$T = -\frac{e^{-2il\lambda}\lambda\sqrt{\lambda^2 - 2q}}{\cos(2l\sqrt{\lambda^2 - 2q})\lambda\sqrt{\lambda^2 - 2q} - i\sin(2l\sqrt{\lambda^2 - 2q})(\lambda^2 - q)}, \tag{4.1.18}$$

by $k = \sqrt{\lambda^2 - 2q}$. We will choose the initial solitary wave with velocity v satisfying $\sin(2l\sqrt{v^2 - 2q}) = 0$, which corresponds to the resonant tunneling condition.

4.2 Numerical Results

4.2.1 Numerical Evidence of Resonant Tunneling

We now present the results of the numerical simulation of the NLS equation with potential (P1) and (P2), using the method presented in Section 4.3.

Figure 4.1 shows the evolution of the initial condition (4.3.1) in the case of the potential (P1). The velocity v is chosen to satisfy the equation $\frac{v}{q} = -\tan(2lv)$, and we choose $v = q = 12.5\pi$, $l = 0.03$ and $dt = 1.7 \times 10^{-4}$. The first panel (a) represents the initial solitary wave. The second and third (b, c) shows the interaction of the solitary wave with the barriers, at time $t = 0.19975, 0.29975$. Finally, the last panel (d) at time $t = 0.5$ is the transmitted wave in the post-collision phase. We see that for this choice of parameters, most of the wave is transmitted, and a small fraction of it is reflected. To describe this dynamics more precisely, define the transmission rate

$$T_q^s(v) = \frac{\int_l^\infty |u(x,t)|^2 dx}{\int_{\mathbb{R}} |u(x,t)|^2 dx} \tag{4.2.1}$$

and the reflection rate,

$$R_q^s(v) = \frac{\int_{-\infty}^{-l} |u(x,t)|^2 dx}{\int_{\mathbb{R}} |u(x,t)|^2 dx} \tag{4.2.2}$$

where the total mass is $\int_{\mathbb{R}} |u(x,t)|^2 dx = 2$. Although the numerical integration is over a domain with finite size, the latter is large enough since the contribution away from the center of mass is exponentially small. This is supported by the fact that we get the same numerical results for different, yet large, domain sizes. We find that at time $t = 0.5$ (corresponding to the last panel of Figure 4.1), $T_q^s(v) = 0.9866$.

Table 4.1 shows that R_q^s and T_q^s for $l = 0.05, q = v$ and different values $v = \frac{(n-1/4)\pi}{2l}, n \in \mathbb{Z}$ for $n = 1, 2, 3, 4, 5$. As v increases, T_q^s tends to 1 and R_q^s tends to 0.

In contrast, when v, q do not satisfy the relation $\frac{v}{q} = -\tan(2lv)$, resonant tunneling does not occur. Figure 4.2 shows the time evolution of the solitary wave when $v = 8.75\pi$, $q = 40$, $l = 0.1$ and $dt \approx 2 \times 10^{-4}$. The wave clearly splits into 2 waves and the transmission rate is $T_p^s(v) = 0.5851$.

We repeat this numerical calculation with potential (P2). Choosing v, q such that $2l\sqrt{v^2 - 2q} = \pi$, namely, $q = 10v, v \approx 42.97$, $l = 0.05$ and $dt \approx 10^{-5}$, resonant tunneling occurs. Figure 4.3 represents the three regimes of the dynamics, at $t = 0$, $t = 0.1976$,

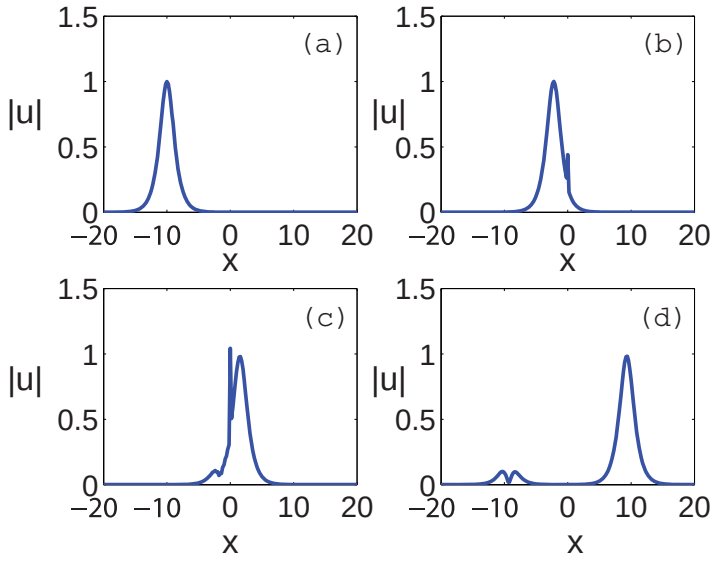

Figure 4.1: Resonant tunneling ($2-\delta$ potential (P1))

Table 4.1: Transmission and reflection rate, T_q^s and R_q^s, for potential (P1) with parameters $l = 0.05$ and $v = q$.

n	v	T_q^s	R_q^s
1	23.5619	0.96557	0.03443
2	54.9778	0.97167	0.02833
3	86.3938	0.97322	0.02678
4	117.809	0.97393	0.02607
5	149.225	0.97435	0.02565

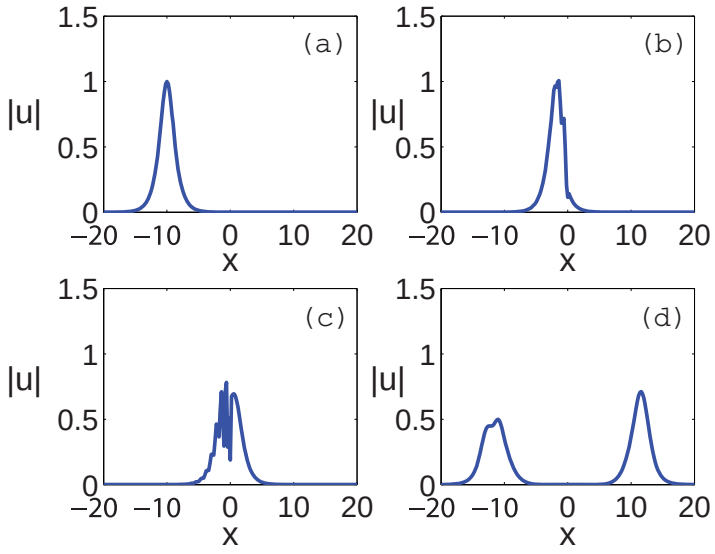

Figure 4.2: Splitting of the soliton ($2-\delta$ potential (P1))

Table 4.2: Transmission and reflection rate, T_q^s and R_q^s, for potential (P2) with parameters $l = 0.05$ and $q = 10v$.

n	v	T_q^s	R_q^s
1	42.9691	0.99874	1.2583×10^{-3}
2	73.6227	0.99923	0.7687×10^{-3}
3	104.776	0.99929	0.7107×10^{-3}
4	136.061	0.99930	0.6950×10^{-3}
5	167.397	0.99931	0.6869×10^{-3}

$t = 0.26743$, and $t = 0.4655$. At the last time, the transmission rate is $T_q^s(v) = 0.9987417$. In contrast, Figure 4.4 shows the splitting of the wave when the resonant condition is not met: $v = \sqrt{(5\pi)^2 + 400}$, $q = 200$, $l = 0.05$ and $dt \approx 2 \times 10^{-4}$. The four panels of Figure 4.4 are the solitary wave at $t = 0, 0.319, 0.479, 0.8$, and the transmission rate is $T_p^s(v) = 0.75$ in the last panel.

Table 4.2 shows the values of R_q^s and T_q^s for $l = 0.05$ and different values of v satisfying the resonant tunneling condition $l = \frac{n\pi}{2\sqrt{v^2-2q}}, n \in \mathbb{Z}$.

4.2.2 Resolution of Outgoing Waves

We identify the transmitted wave to a soliton in the form of (1.4.1) corresponding to the initial condition

$$u(x,0) = Ae^{ivx}\text{sech}(A(x-a_0))$$

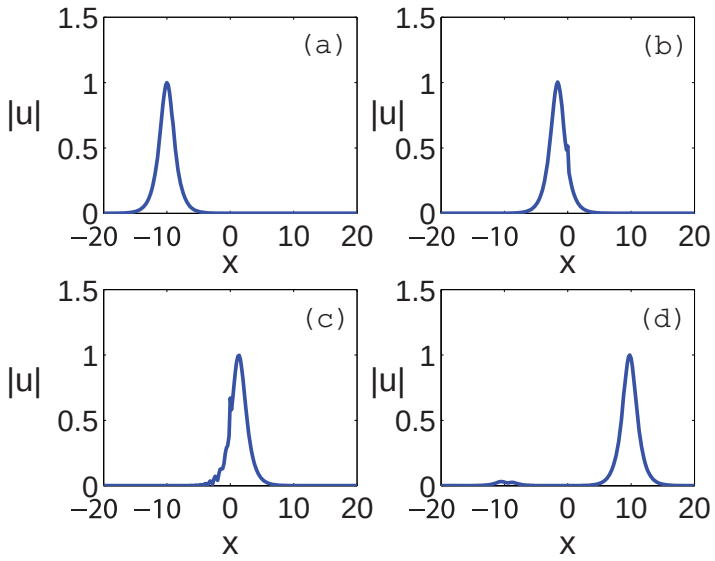

Figure 4.3: Resonant tunneling (box potential (P2))

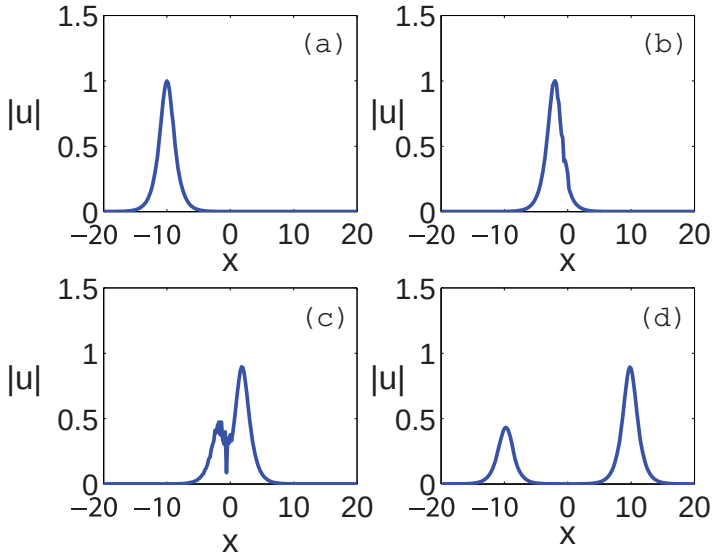

Figure 4.4: Splitting of the soliton (box potential (P2))

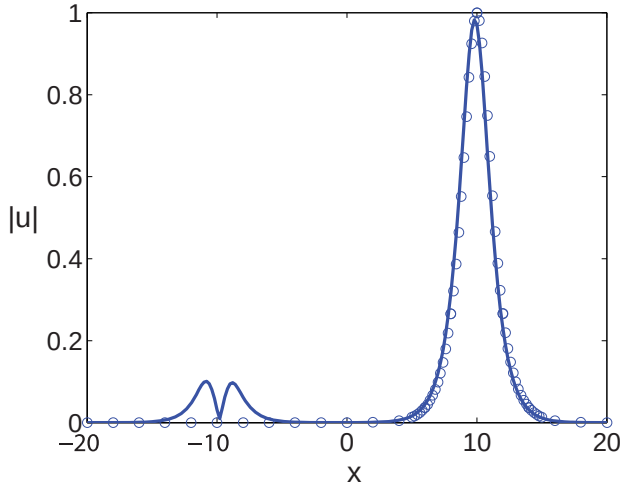

Figure 4.5: Superposition of the transmitted wave to the NLS soliton at time $t_2 = 0.5$; $|u(x,t)|$ is plotted with solid line and $|u_{\phi_1}(x,t)|$ is plotted with circles (2-δ potential (P1)).

but with additional phase shift ϕ_1, namely

$$u_{\phi_1}(x,t) = A\text{sech}(A(x - a_0 - vt))e^{i\phi_1 + ivx + i\frac{(A^2 - v^2)t}{2}} \tag{4.2.3}$$

To find the phase shift, we fix the initial speed v and the time t_1 so that t_1 is large enough for the wave to pass the barriers, and find ϕ_1 that minimizes

$$||u(t_1) - u_{\phi_1}(t_1)||_{L_x^\infty}$$

where $u(x,t_1)$ is the numerical solution.

Denoting t_1 and t_2 the times where the center of the solitary wave is located at $x = 5$ and $x = 10$, respectively, we evaluate the difference

$$e = \max_{t\in[t_1,t_2]} ||u(t) - u_{\phi_1}(t)||_{L_x^2}$$

to show how well the transmitted wave is approximated by the shifted soliton.

Figure 4.5 shows $|u(x,t)|$ (solid line) and $|u_{\phi_1}(x,t)|$ (circle) at $t = t_2$ for the 2-δ potential, using the parameters as in Figure 4.1. We find $e \approx 0.1416$. Figure 4.6 shows the same result at $t = t_2$ for the box potential (P2) with parameters as in Figure 4.3 and we get $e \approx 0.0505$.

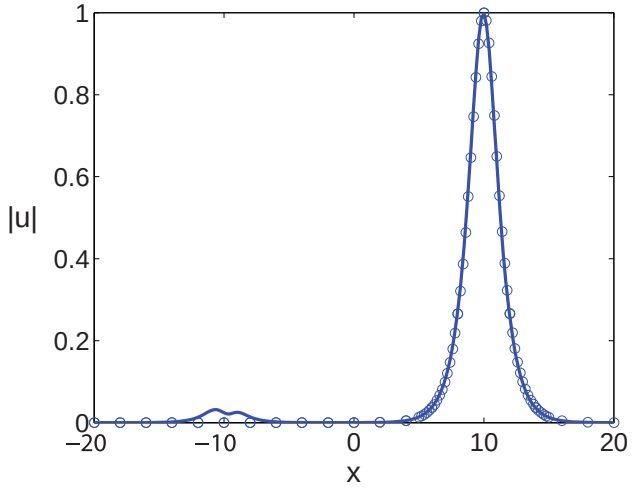

Figure 4.6: Superposition of the transmitted wave to the NLS soliton at time $t_2 = 0.4655$; $|u(x,t)|$ is plotted with solid line and $|u_{\phi_1}(x,t)|$ is plotted with circles (box potential (P2)).

4.2.3 Limiting Value of the Reflection Rates as the Soliton Velocity Increases

The purpose of this section is to further examine the decay of the reflection rate $R_q^s(v)$ in terms of v and check the consistency of our numerics with the theoretical analysis. The estimate (1.4.7) recalled in Section 1 can be seen as an estimate of the fluctuation away from a completely transmitted soliton in the limit of large velocities and long times. The first term of (1.4.7) expresses the algebraic decay in terms of v while the second term is a consequence of the spatial exponential decay of the soliton.

We start with the potential (P1). We fix the parameter $l = 0.05$ (small) and we choose $q = v$. The velocity must then satisfy $v = \frac{(n-1)\pi}{8l}$, $n \in \mathbb{N}$ for the resonant condition to hold. We take $n = 1, 2, 3, 4, 5$. Fig. 4.7 represents the evolution of $R_q^s(v)$ as a function of the center of mass of the soliton (which is equivalent to its evolution versus time) for various values of resonant v. We clearly see its decay as times evolves. We also see that it gets smaller and smaller as the velocity is increased. We confirm these observations by repeating this calculation for different values of l and different values of q. Fig. 4.8 shows a similar behavior in the case of the box potential (P2). In the latter case, $l = 0.05$, $q = 10v$, and the resonant tunneling condition reads $l = \frac{n\pi}{2\sqrt{v^2-2q}}, n \in \mathbb{N}$.

In conclusion, the analysis of our numerical results shows a good qualitative agreement with the theoretical predictions.

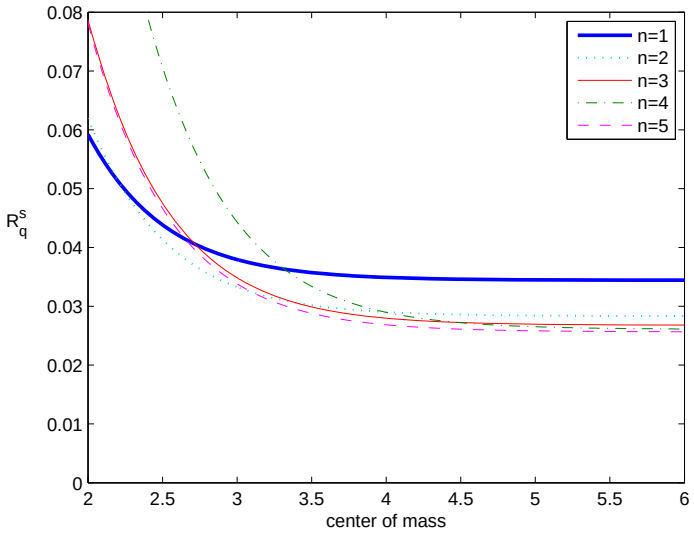

Figure 4.7: Evolution of $R_q^s(v)$ as a function of the position of the center of mass of the soliton for different velocities (2-δ potential (P1)).

4.3 Numerical Method

To integrate numerically equation (1.4.2), we implement the finite element method proposed in the papers of Akrivis et al in [6] and [7] , which was devoted to the study of the structural properties of blow-up solutions the NLS equation. (This method was also used in [33].) We consider an initial condition in the form of solitary wave with phase $\phi_0 = 0$

$$u(x,0) = Ae^{ivx}\text{sech}(A(x-a_0)) \tag{4.3.1}$$

approaching from the left ($a_0 \ll 0$) with velocity v. Without loss of generality, we set $A = 1$. The spatial domain of integration $[-L, L]$ (L is chosen large enough) is discretized with a uniform mesh $-L \leq x_0, x_1, \cdots, x_N \leq L$. The basis for the Galerkin method are the 'hat functions' $\{\psi_1, \psi_2, \cdots, \psi_N\}$ defined as

$$\psi_k(x) = \begin{cases} \frac{1}{h}(x - x_{k-1}), & x_{k-1} < x < x_k, \\ \frac{1}{h}(x_{k+1} - x), & x_k < x < x_{k+1} \\ 0 & \text{otherwise.} \end{cases}$$

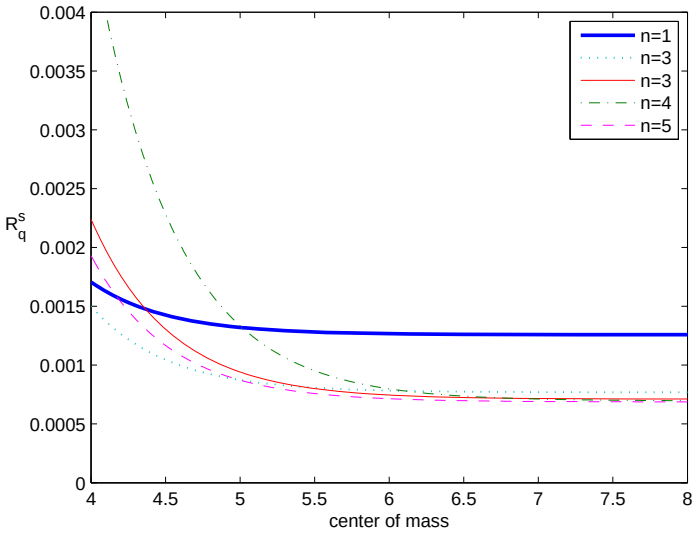

Figure 4.8: Evolution of $R_q^s(v)$ as a function of the position of the center of mass of the soliton for different velocities (box potential (P2)).

and

$$\psi_N(x) = \begin{cases} \frac{1}{h}(x - x_{N-1}), & x_{N-1} < x < x_N, \\ 0 & \text{otherwise.} \end{cases}$$

where $h = 2L/N$, and $k = 1, 2, \ldots, N-1$. The projection of the equation on the elements of the basis gives

$$i\langle u_t, \psi_k\rangle - \frac{1}{2}\langle \partial_x u, \partial_x \psi_k\rangle - q\langle uV, \psi_k\rangle + \langle |u|^2 u, \psi_k\rangle = 0. \tag{4.3.2}$$

Denoting by u_n the approximation of the solution at time $t_n = ndt$, and using a Crank-Nicholson scheme for the time discretization, the system becomes

$$i\langle \frac{u_{n+1} - u_n}{dt}, \psi_k\rangle - \frac{1}{2}\langle \partial_x(\frac{u_{n+1} + u_n}{2}), \partial_x \psi_k\rangle - q\langle (\frac{u_{n+1} + u_n}{2})V, \psi_k\rangle \\ + \langle |\frac{u_{n+1} + u_n}{2}|^2 \frac{u_{n+1} + u_n}{2}, \psi_k\rangle = 0. \tag{4.3.3}$$

or equivalently, denoting $y_n = (u_{n+1} + u_n)/2$:

$$\langle y_n, \psi_k\rangle + i\frac{dt}{4}\langle \partial_x y_n, \partial_x \psi_k\rangle + i\frac{dt}{2} q\langle y_n V, \psi_k\rangle - i\frac{dt}{2}\langle |y_n|^2 y_n, \psi_k\rangle - \langle u_n, \psi_k\rangle = 0. \tag{4.3.4}$$

The nonlinear equation (4.3.4) is solved by iteration. We choose $y_n^0 = u_n$, and y_n^{m+1} is calculated from

$$\langle y_n^{m+1}, \psi_k\rangle + i\frac{dt}{4}\langle \partial_x y_n^{m+1}, \partial_x \psi_k\rangle + i\frac{dt}{2} q\langle y_n^{m+1} V, \psi_k\rangle = i\frac{dt}{2}\langle |y_n^m|^2 y_n^m, \psi_k\rangle + \langle u_n, \psi_k\rangle. \quad (4.3.5)$$

In the implementation of the method, we find that y_n^m typically converges after a few iterations with a precision of 10^{-6}. Rewriting (4.3.5) in a matrix form, it becomes

$$(A + i\frac{dt}{4}K + i\frac{dt}{2}qB)Y = F, \quad (4.3.6)$$

where the $N \times N$ matrices A and K have entries

$$A_{jk} = \langle \psi_j, \psi_k\rangle = \begin{cases} \frac{h}{6}, & \text{k=j-1;} \\ \frac{2h}{3}, & \text{k=j;} \\ \frac{h}{6}, & \text{k=j+1.} \end{cases}$$

$$K_{jk} = \langle \partial_x\psi_j, \partial_x\psi_k\rangle = \begin{cases} -\frac{1}{h}, & \text{k=j-1;} \\ \frac{2}{h}, & \text{k=j;} \\ -\frac{1}{h}, & \text{k=j+1.} \end{cases}$$

Y is the N-vector of components $Y_j = \langle y_n^{m+1}, \psi_j\rangle$, and the right hand side F is the N-vector of components

$$F_j = i\frac{dt}{2}\langle |y_n^m|^2 y_n^m, \psi_j\rangle + \langle u_n, \psi_j\rangle.$$

In the case of the 2-δ potential (P1), the matrix B has the form:

$$B_{jk} = \psi_j(-l)\psi_k(-l) + \psi_j(l)\psi_k(l) = \begin{cases} 1, & \text{when } j = k = \frac{N}{2} + \frac{l}{h}; \\ 1, & \text{when } j = k = \frac{N}{2} - \frac{l}{h}; \\ 0, & \text{otherwise,} \end{cases}$$

where we choose the number of meshes, N, such that $\frac{l}{h}$ is an integer. For the box potential (P2), $B = A\widetilde{B}$, where matrix $\widetilde{B}$ has entries:

$$\widetilde{B}_{jk} = \begin{cases} 1, & \text{when } \frac{N}{2} - \frac{l}{h} \le j = k \le \frac{N}{2} + \frac{l}{h}\ ; \\ 0, & \text{otherwise.} \end{cases}$$

We checked the precision and the convergence properties of our scheme by comparing our numerical solution of the NLS equation (without potential) with exact explicit solutions

(solitons) and calculated that the rate of convergence in $O(h^2 + (dt)^2)$ in terms of the mesh size and time step as proved in [6] (in the absence of potential).

Generally, the NLS equation (1.4.2) with external potential V is invariant under global gauge transformations, which leads to the conservation of mass or charge

$$M = \int |u|^2 dx.$$

Furthermore, since the potential V is time-independent, (1.4.2) is invariant under time-translations, which implies conservation of the energy functional

$$E = \int (\frac{1}{4}|\nabla u|^2 - \frac{1}{2}|u|^4 + V|u|^2)dx.$$

To further check the precision of our calculations, we computed the invariants of the NLS equation, the mass, M, and the energy, E, that takes the form

$$E_{delta} = \int_{\mathbb{R}} (\frac{1}{4}|\nabla u|^2 - \frac{1}{2}|u|^4)dx + q(|u(-l)|^2 + |u(l)|^2)$$

$$E_{box} = \int_{\mathbb{R}} (\frac{1}{4}|\nabla u|^2 - \frac{1}{2}|u|^4)dx + \int_{-l}^{l} q|u(x)|^2 dx$$

for the two examples of potentials we consider. We also performed the computations with different sizes of the domain $[-L, L]$ ($L = 20, 25, 30$). We present our numerical results for $L = 20$, and typically $N = 16000$ mesh points. The initial solution is centered at $a_0 = -10$. For the 2-δ potential (P1), the location of the barriers are at $\pm l$, $l = 0.05$, while the box potential (P2) is located at $[-l, l]$, with $l = 0.05$.

In Table 4.3 and 4.4, we show the value of the mass and energy of the solutions of the NLS equation with potentials (P1) and (P2) respectively. In the former case, the initial velocity is assumed to satisfy $\frac{v}{q} = -\tan(2lv)$ and we choose $v = q = \frac{15\pi}{2}$, and a time step $dt = 1.7 \times 10^{-4}$. In the latter case, v satisfies $2l\sqrt{v^2 - 2q} = n\pi$ and we choose $q = 10v, n = 1, v \approx 42.97$, and $dt \approx 10^{-4}$. Comparing the precision of the calculation with potential (P1) and (P2), we see that the singularities of the 2-δ potential lead to a stiffer problem, and thus less precision is expected.

We also validate our numerical code by reproducing the calculation presented in [33] for one delta potential. Figure 4.9 presents the convergence of the transmission rate $T_q^s(v) = \lim_{t\to\infty} \frac{\int_0^\infty |u(x,t)|^2 dx}{\int_{\mathbb{R}} |u(x,t)|^2 dx}$ to the expected asymptotic value $1/(1 + \alpha^2)$, where $\alpha = \frac{v}{q}$ for the values $\alpha = 0.6, 1, 1.4$.(Figure 2 of [33])

Table 4.3: Conservation of mass and energy (2-δ potential (P1))

	time	M	E_{delta}
Pre-Interaction	0	2.0000	554.8315
Interaction begins	0.3733	2.0000	554.9013
Interaction	0.4242	2.0000	555.1183
Interaction ends	0.4752	2.0000	554.9805
Post-Interaction	0.8486	2.0000	554.8316

Table 4.4: Conservation of mass and energy (box potential (P2))

	time	M	E_{box}
Pre-Interaction	0	2.0000	1.8459×10^3
Interaction begins	0.1860	2.0000	1.8476×10^3
Interaction	0.2325	2.0000	1.8695×10^3
Interaction ends	0.2791	2.0000	1.8478×10^3
Post-Interaction	0.4653	2.0000	1.8459×10^3

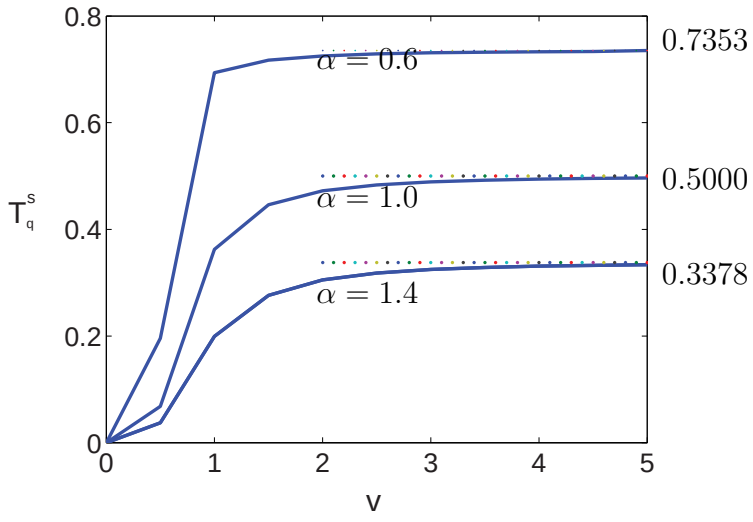

Figure 4.9: Convergence of $T_q^s(v)$ to the expected asymptotic value $1/(1+\alpha^2)$ for $\alpha = \frac{v}{q} = 0.6, 1, 1.4$ as $v \to \infty$.

Bibliography

[1] Abou Salem, W.K., *Solitary wave dynamics in time-dependent potentials*, J. Math. Phys., **49**(2008), 032101.

[2] Abou Salem, W.K., *Effective dynamics of solitons in the presence of rough nonlinear perturbations*, Nonlinearity, **22**(2009), 747–763.

[3] Abou Salem, W.K., Fröhlich, J., and Sigal, I.M., *Collision of fast solitons for the nonlinear Schrödinger equation*, Commun. Math. Phys., **291**(2009), 151–176.

[4] Abou Salem, W.K. and Sulem, C., *Resonance tunneling of fast solitons through potential barriers*, Can. J. Math., **63**(2011), 1201–1219.

[5] Agrawal, G.P., *Nonlinear fiber optics*, Academic Press, San Diego (2006).

[6] Akrivis, G.D., Dougalis, V.A., and Karakashian, O.A., *On fully discrete Galerkin methods of second-order tmporal accuracy for the nonlinear Schrödinger equation*, Numer. Math., **59**(1991), 31–53.

[7] Akrivis, G.D., Dougalis, V.A., Karakashian, O.A., and McKinney, W.R., *Numerical approximation of blow-up of radially symmetric solutions of the nonlinear Schrödinger equation*, SIAM J. Sci. Comput., **25**(2003), 186–212.

[8] Angulo Pava, J., *Nonlinear dispersive equations. Existence and stability of solitary and periodic travelling wave solutions*, Mathematical Surveys and Monographs, 156., Amer. Math. Soc., Providence, RI (2009).

[9] Bronski, J.C. and Jerrard, R.L., *Soliton dynamics in a potential*, Math. Res. Lett., **7**(2000), 329–342.

[10] Cazenave, T., *Semilinear Schrödinger equations*, American Mathematical Society (2003).

[11] Champeaux, S., Laveder, D., Passot, T., and Sulem, P.L., *Remarks on the parallel propagation of small-amplitude dispersive Alfvén waves*, Nonlinear Proc. Geoph., **6**(1999), 169–178.

[12] Colin, M. and Ohta, M., *Stability of solitary waves for derivative nonlinear Schrödinger equation*, Ann. Inst. H. Poincaré, Analyse Non Linéaire., **23**(2006), 753–764.

[13] Colliander, J., Keel, M., Staffilani, G., Takaoka, H., and Tao, T., *A Refined Global Well-Posedness Result for Schrödinger Equations with Derivative*, SIAM J. Math. Anal., **34**(2002), 64–86.

[14] Comech, A., Cuccagna, S., and Pelinovsky, D., *Nonlinear instability of a critical traveling wave in the generalized Kortewegde Vries equation*, SIAM J. Math. Anal., **39**(2007), 1–33.

[15] Comech, A. and Pelinovsky, D., *Purely nonlinear instability of standing waves with minimal energy*, Commun. Pure Appl. Math., **56**(2003), 1565–1607.

[16] Cox, S.M. and Matthews, P.C., *Exponential time differencing for stiff systems*, J. Comput. Phys., **176**(2002), 430–455.

[17] DiFranco, J.C. and Miller, P.D., *The semiclassical modified nonlinear Schrödinger equation I: Modulation theory and spectral analysis*, Physica D, **237**(2008), 947–997.

[18] Dyachenko, S., Newell, A.C., Pushkarev, A., and Zakharov, V.E., *Optical turbulence: weak turbulence, condensates and collapsing filaments in the nonlinear Schrödinger equation*, Physica D, **57**(1992), 96–160.

[19] Fibich, G., Gavish, N., and Wang, X.P., *Singular ring solutions of critical and supercritical nonlinear Schrödinger equations*, Physica D, **231**(2007), 55–86.

[20] Fröhlich, J., Gustafson, S., Jonsson, B.L.G., and Sigal, I.M., *Solitary wave dynamics in an external potential*, Commun. Math. Phys., **250**(2004), 613–642.

[21] Ginibre, J. and Velo, G., *On a class of nonlinear Schrödinger equations. I. The Cauchy problem, general case*, J. Funct. Anal., **32**(1979), 1–32.

[22] Glassey, R.T., *On the blowing up of solutions to the Cauchy problem for nonlinear Schrödinger equations*, J. Math. Phys., **18**(1977), 1794–1797.

[23] Goldman, M.V., Rypdal, K., and Hafizi, B., *Dimensionality and dissipation in Langmuir collapse*, Phys. Fluids., **23**(1980), 945–955.

[24] Grillakis, M., Shatah, J., and Strauss, W., *Stability theory of solitary waves in the presence of symmetry, I*, J. Funct. Anal., **74**(1987), 160–197.

[25] Grillakis, M., Shatah, J., and Strauss, W., *Stability theory of solitary waves in the presence of symmetry, II*, J. Funct. Anal., **94**(1990), 308–348.

[26] Guo, B. and Wu, Y., *Orbital stability of solitary waves for the nonlinear derivative Schrödinger equation*, J. Differ. Equations, **123**(1995), 35–55.

[27] Gustafson, S.J. and Sigal, I.M., *Mathematical concepts of quantum mechanics*, Springer (2011).

[28] Hao, C., *Well-posedness for one-dimensional derivative nonlinear Schrödinger equations*, Commun. Pure Appl. Anal., **6**(2007), 997–1021.

[29] Hayashi, N. and Ozawa, T., *On the derivative nonlinear Schrödinger equation*, Physica D, **55**(1992), 14–36.

[30] Hayashi, N. and Ozawa, T., *Remarks on nonlinear Schrödinger equations in one space dimension*, Diff. Int. Eqs, **7**(1994), 453–461.

[31] Higham, N.J., *Accuracy and stability of numerical algorithms*, volume 94, SIAM, Philadelphia. (1996).

[32] Holmer, J., Marzuola, J., and Zworski, M., *Fast soliton scattering by delta impurities*, Commun. Math. Phys., **274**(2007), 187–216.

[33] Holmer, J., Marzuola, J., and Zworski, M., *Soliton splitting by external delta potentials*, J. Nonlinear Sci., **17**(2007), 349–367.

[34] Holmer, J. and Roudenko, S., *On blow-up solutions to the 3D cubic nonlinear Schrödinger equation*, Appl. Math. Res. Express. AMRX 2007, no. 1, Art. ID abm004, 31 pp.

[35] Holmer, J. and Zworski, M., *Slow soliton interaction with delta impurities*, J. Mod. Dyn., **1**(2007), 689–718.

[36] Holmer, J. and Zworski, M., *Soliton interaction with slowly varying potentials*, Int. Math. Res. Not. IMRN, (2008), Art. ID rnn026, 36pp.

[37] Kassam, A.K. and Trefethen, L.N., *Fourth-order time-stepping for stiff PDEs*, SIAM J. Sci. Comput., **26**(2005), 1214–1233.

[38] Kaup, D.J. and Newell, A.C., *An exact solution for a derivative nonlinear Schrödinger equation*, J. Math. Phys., **19**(1978), 798–801.

[39] Kenig, C.E., Ponce, G., and Vega, L., *Small solutions to nonlinear Schrödinger equations*, Ann. Inst. H. Poincaré, Analyse Non Linéaire, **10**(1993), 255–288.

[40] Kenig, C.E., Ponce, G., and Vega, L., *Smoothing effects and local existence theory for the generalized nonlinear Schrödinger equations*, Invent. Math., **134**(1998), 489–545.

[41] Kierzenka, J. and Shampine, L.F., *A BVP solver based on residual control and the Maltab PSE*, ACM Trans. Math. Software, **27**(2001), 299–316.

[42] Landman, M.J., Papanicolaou, G.C., Sulem, C., and Sulem, P.L., *Rate of blowup for solutions of the nonlinear Schrödinger equation at critical dimension*, Phys. Rev. A, **38**(1988), 3837–3843.

[43] Landman, M.J., Papanicolaou, G.C., Sulem, C., Sulem, P.L., and Wang, X.P., *Stability of isotropic singularities for the nonlinear Schrödinger equation*, Physica D, **47**(1991), 393–415.

[44] Lee, J.h., *Global solvability of the derivative nonlinear Schrödinger equation*, Trans. Amer. Math. Soc., **314**(1989), 107–118.

[45] LeMesurier, B.J., Papanicolaou, G.C., Sulem, C., and Sulem, P.L., *Local structure of the self-focusing singularity of the nonlinear Schrödinger equation*, Physica D, **32**(1988), 210–226.

[46] Lin, J.E. and Strauss, W., *Decay and scattering of solutions of a nonlinear Schrödinger equation*, J. Funct. Anal., **263**(1978), 245–263.

[47] Linares, F. and Ponce, G., *Introduction to nonlinear dispersive equations*, Springer, Berlin (2009).

[48] Lund, J. and Bowers, K.L., *Sinc methods for quadrature and differential equations*, Society for Industrial Mathematics, Philadelphia (1992).

[49] Marzuola, J.L., Raynor, S., and Simpson, G., *A system of ODEs for a perturbation of a minimal mass soliton*, J. Nonlinear Sci., **20**(2010), 425–461.

[50] McLaughlin, D., Papanicolaou, G.C., Sulem, C., and Sulem, P.L., *Focusing singularity of the cubic Schrödinger equation*, Phys. Rev. A, **34**(1986), 1200–1210.

[51] Merle, F., *nonlinear Schrödinger equations with critical power*, Duke Math. J., **69**(1993), 427–454.

[52] Merle, F. and Raphael, P., *On a sharp lower bound on the blow-up rate for the L^2 critical nonlinear Schrödinger equation*, J. Amer. Math. Soc., **19**(2005), 37–90.

[53] Mio, K., Ogino, T., Minami, K., and Takeda, S., *Modified nonlinear Schrödinger equation for Alfvén waves propagating along the magnetic field in cold plasmas*, J. Phys. Soc. Jpn., **41**(1976), 265–271.

[54] Mjølhus, E., *On the modulational instability of hydromagnetic waves parallel to the magnetic field*, J. Plasma Phys., **16**(1976), 321–334.

[55] Moses, J., Malomed, B., and Wise, F., *Self-steepening of ultrashort optical pulses without self-phase-modulation*, Phys. Rev. A, **76**(2007), 1–4.

[56] Ohta, M., *Instability of bound states for abstract nonlinear Schrödinger equations*, J. Funct. Anal., **261**(2011), 90–110.

[57] Ozawa, T., *On the nonlinear Schrödinger equations of derivative type*, Indiana U. Math. J., **45**(1996), 137–163.

[58] Passot, T. and Sulem, P.L., *Multidimensional modulation of Alfvén waves*, Phys. Rev. E, **48**(1993), 2966–2974.

[59] Shampine, L.F., Gladwell, I., and Thompson, S., *Solving ODEs with MATLAB*, Cambridge University Press (2003).

[60] Stenger, F., *A "Sinc-Galerkin" method of solution of boundary value problems*, Math. Comp., **33**(1979), 85–109.

[61] Stenger, F., *Summary of sinc numerical methods*, J. Comput. Appl. Math., **121**(2000), 379–420.

[62] Sulem, C. and Sulem, P.L., *The nonlinear Schrödinger equation: self-focusing and wave collapse*, volume 139, Springer, Berlin (1999).

[63] Tan, S.B. and Zhang, L.H., *On a weak solution of the mixed nonlinear Schrödinger equations*, J. Math. Anal. Appl., **182**(1994), 409–421.

[64] Tsutsumi, M. and Fukuda, I., *On solutions of the derivative nonlinear Schrödinger equation, Existence and uniqueness theorem*, Funkcial. Ekvac., **23**(1980), 259–277.

[65] Tsutsumi, Y., *L^2 solutions for the nonlinear Schrödinger equation and nonlinear groups*, Funkcial. Ekvac., **30**(1987), 115–125.

[66] van Saarloos, W. and Hohenberg, P.C., *Fronts, pulses, sources and sinks in generalized complex Ginzburg-Landau equations*, Physica D, **56**(1992), 303–367.

[67] Vlasov, S.N., Petrishchev, V.A., and Talanov, V.I., *Averaged description of wave beams in linear and nonlinear media (the method of moments)*, Radiophys. Quantum. El., **14**(1971), 1062–1070.

[68] Weinstein, M.I., *Nonlinear Schrödinger equations and sharp interpolation estimates*, Commun. Math. Phys., **87**(1983), 567–576.

[69] Weinstein, M.I., *Modulational stability of ground states of nonlinear Schrödinger equations*, SIAM J. Math. Anal., **16**(1985), 472–491.

[70] Weinstein, M.I., *Lyapunov stability of ground states of nonlinear dispersive evolution equations*, Commun. Pure Appl. Math., **XXXIX**(1986), 51–68.

[71] Zakharov, V.E., *Collapse of Langmuir waves*, Sov. Phys. JETP, **35**(1972), 908–914.

[72] Zettl, A., *Sturm-Liouville theory (Mathematical surveys and monographs)*, American Mathematical Society (2005).